Technische Universität München
Physik Department
Lehrstuhl für Biophysik E22

New model systems for the study of myosin-V mediated transport on biofunctionalized surfaces

Junshan Zhang

Vollständiger Abdruck der von der Fakultät für Physik der Technischen Universität München zur Erlangung des akademischen Grades eines Doktors der Naturwissenschaften genehmigten Dissertation.

Vorsitzender: Univ. Prof. Dr. Manfred Kleber

Prüfer der Dissertation:

1. Univ. Prof. Dr. Matthias Rief
2. Priv.Doz. Dr. Markus Fischer

Die Dissertation wurde am 15. 06. 2004 bei der Technischen Universität München eingereicht und durch die Fakultät für Physik
Am 22. 06. 2004 angenommen.

Table of contents

New model systems for the study of myosin-V mediated transport on biofunctionalized surfaces

Summary

Myosin V, an actin–based processive motor protein, was prepared from chicken brain. Polyclonal and monoclonal antibodies were raised against it. With these proteins several biochemical as well as biophysical assays were developed to test the activity and mobile properties of myosin V. Myosin was grafted onto substrates through arrays of gold dots with well defined distance and through lipid bilayers to test the motility of the motor on the actin transport. A cargo transport assay was introduced to study the stepping motion of the motor which was shown to be stopped by barriers of defined size.

Abbreviations

Ab	:	Antibody
ADP	:	Adenosine Diphosphate
ATP	:	Adenosine Triphosphate
ATPase	:	Adenosine Triphosphatase
BSA	:	Bovine Serum Albumine
DMPC	:	1,2-Dimyristoyl-sn-glyero-3-phosphatidylcholin (di-C14:0)
DMSO	:	Dimehtylsufoxid
DOPC	:	1,2-Dioleoyl-sn-glycero-3-phosphatidylcholin (di-C18:1, cis)
DPPE	:	1,2-Dipalmitoyl-sn-glycero-3-phosphatidylehtanolamin (di-C 16:0)
DTT	:	Dithiotreitol
EDC	:	1-Ethyl-3-(3-dimethylaminopropayl) carbodiimid
EDTA	:	Ehtylendiamitetraacetat
ELISA	:	Enzyme-linked Immunosorbent Assay
EM	:	Electro Microscopy
F-actin	:	Filamentous Actin
F_{ab}, $F_{ab'}$	:	Fragment Antigen binding domain (monovalent)
FM	:	Fluorescent Microscopy
FITC	:	Fluoresceinisothiocyanat
HPLC	:	High performance liquid chromatography
HC	:	Heavy Chain
IgG	:	Immunoglobulin G
KD	:	Kilo-Dalton
*K*m	:	Michaelis Constant
LC	:	Light Chain
LDH	:	Lactate Dehydrogenase
MBS	:	m-Maleimidobenzoyl-N-hydroxysulfosuccinimid Ester
MW	:	Molecule Weight
NAD^+/NADH	:	Nicotinamide Adenine Dinucleotide and its reduced form
PBS	:	Phosphate Buffered Solution

PK	:	Pyruvate Kinase
PLC	:	Preparative layer chromatography
SDS	:	Sodium Dodecyl Sulfate
SDS-PAGE	:	SDS polyacrylamid gel electrophoresis
RT	:	Room Termperature
TCA	:	Trichloris Acid
TLC	:	Thin Layer Chromatography
Tris	:	Trishydroxymethylaminomethan
TRITC	:	Tetramethylrodaminisothiocyanat

1. Introduction

Molecular motors, in particular proteins of the myosin family have attracted tremendous interest in the past decades. Because of its important role in cell motility the interaction between myosin and actin-filament or the regulators have been investigated by a variety of techniques. In 1993, the success of X-Ray structure of the S1 domain of myosin II was a big step which for researches at the molecular level. After that progress made in developing visualization techniques was prompted by fluorescent microscopy, optical tweenzers as well as EM and X-Ray studies at higher resolution.

Among these techniques fluorescent microscopy contributed in a unique way. Using selective labeling techniques, fluorescent dyes Rhodamine and Cy3 do not disturb the native function of myosin or actin filaments. For the fluorescence microscopy either the myosin molecule or the actin filament is labeled by those dyes which allow direct observation of the interaction. The new CCD cameras provide faster response at higher spatial resolution while the laser light source favors a very low background. Thanks to these developments observation at high resolution in real time becomes reality.

Direct observation of actin filament sliding assay showed some interesting difference between the behaviors of myosin V and myosin II. One distinguished characteristic of myosin V is its processivity which means it is able to perform many a steps on the same actin filament without dissociation. Indirect observation by myosin supported actin filament sliding assay indicated this special property. And then the optical tweenzer studies show the discrete steps a single myosin V performed along an actin filament. Recently a fluorescence microscopy study using selectively labeled myosin V revealed the ‘hand-over-hand’ stepping mode. It was the first time for the myosin V molecule to be dynamically observed in real time. Another property of myosin V is its big step size. Earlier studies by EM and the recent FM or optical tweezer study showed that the step size is around 36 nm. This step size enables myosin V to move along actin filament nearly in a strait other than a spiral way. Taking all this evidence together, it is reasonable to reach such a conclusion that myosin V might transport cargo with a single molecule.

Despite of the available knowledge still little is known about the native function of myosin V in vivo. One likely role is short distance transport of organelles where myosin V transfers its cargo to other motor protein such as kinesin. In this work myosin V was studied under the following:

(a) How the myosin V molecule work at a well defined number during the cargo transport is an interesting open question. For this purpose a modified actin sliding assay was introduced in this work. In the cooperation work with Prof. Spatz, a well defined gold dot array was introduced in the actin sliding assay.

(b) To study the behavior of myosin V bound to fluid lipid organelles, a lipid bilayer supported motility assay was performed which allows myosin V diffuse over the surface. For this purpose myosin V was fixed by single-headed monoclonal antibodies F_{ab}-fragment which had been covalently linked to a phospholipids molecule in a lipid bilayer.

(c) The antibodies against myosin V were produced in a cooperation with Prof. Kaspers (Ludiwig-Maxmillian University) and purified. Monoclonal antibodies were assayed and then used for immobilization of myosin V.

(d) Direct observation of cargo transport was accomplished by using small fluorescent latex bead which were linked to the cargo binding domain of myosin V via a monoclonal antibody. The size of the fluorescent latex bead was chosen small enough to bind a single myosin V molecule. The monoclonal antibodies are tested to selectively bind close to the cargo binding domain. The motion of bead coated with myosin V moving along pre-fixed actin filament was recorded and analyzed.

(e) The ATPase activity of myosin V has been studied in related reference and various rates of ATP hydrolysis values have been reported. In this work we make use an ATP recovery system to measure the ATPase activity of myosin V at steady state ATP concentration.

The following work is organized as follows. Chapter 2 is an introduction to some background knowledge about the myosin superfamily, the techniques involved and recent progresses. Materials and methods are described in chapter 3. In chapter 4 results and discussion contains the aspects above mentioned are presented.

2. The history of myosin research

2.1 The myosin superfamily

2.1.1 Overview

The myosin genes found until 2002 have been classified into more than 15 myosin types. Analysis of the myosin gene diversity and difference between myosin subtypes provides hints about its evolution from which an evolutionary tree can be constructed. The tree shows the relation between the myosin motor super-family and other relatives (e.g. G-proteins and kinesin) over a broad variety of structure-function interaction.

For a first rough classification according to function, an individual myosin molecule can be artificially divided into the head (motor domain), neck (regulatory domain) and tail (cargo binding or filament forming domain). However, to simplify the study this division may obscure the fact that the distinct parts of the motor protein interact with each other and the molecule forms a complex machine.

The motor domain is considered to be the major part of the myosin molecule which exhibits a relatively conserved structure. Owing to the progress of various genome projects aiming at the deciphering of the species primary DNA sequences, the list of myosin members is continuously increasing. Functionally, the distinct myosins have been studied with respect to the following aspects:

1. Step Direction.
   Until the finding of the walking direction of myVI, myosins were thought to walk along the same direction: from the pointed (-) end to the barbed (+) end of actin

filament. However, the myVI molecule moves in the reverse direction and this might be responsible for its special role in transport in vivo.

2. Step size
   The average step length of distinct myosin species varies and is a unique property of each myosin member

3. Power Stroke.
   The inner domains involved in force generation undergo conformation change with various displacements depending on different myosin species.

4. Duty Ratio.
   The time that myosin molecule spends attached to the actin during the ATP catalytic cycle relative to the whole cycle time.

5. Kinetics of ATP hydrolysis
   The rate constants of each step in the cross-bridge cycle, in particular the dissociation constants of the reaction products-ADP/Pi, are of prime importance for the overall role of the motor.

6. Processivity
   This term is defined as the average step number a given motor molecule remains bound to an actin filament per diffusion encounter. A high processivity of a motor protein enables itself to walk along its track for a relative long distance without dissociation from the track. Up to date, it is has been found that myosin V, VI, IXb and XI are processive molecules. Myosin II is the typical non-processive motor with low processivity.

7. Sliding velocity
   In a well-defined system in vitro, a given kind of myosin molecule has a characteristic sliding velocity which is measured by motility assays. It is believed to

be controlled by a combination of kinetic and mechanical properties. An extremely wide range (>4000 fold) from 0.015 μm/s (Myosin IX) to70 μm/s (Myosin XI) has been found.

8. Regulation
   It refers both to the regulation of the internal conformational changes in the motor domain and the activation of the motor function (ATPase, power stroke etc.). Regulation may be achieved in several ways: by activation of myosin binding domain on the actin filament regulated by troponin/tropomyosin in the case of muscle derived myosin II or by light chain phosphorylation/dephosphorylation as in the case of myosin II smooth muscle cells, and/or by binding/unbinding as in myosin V. In all cases, Ca^{2+} seems to play a central role as a signaling agent.

2.1.2 Evolution of myosin family members

The evolution tree of motor protein where myosin is involved is illustrated as below.

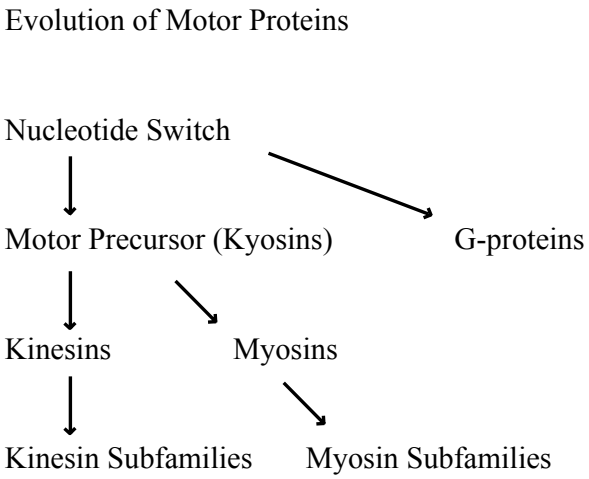

Figure 2.1: Scheme of the evolution tree of motor proteins. The relation between myosin, kinesin and G-protein is indicated (Vale, R. D., 2000).

The scheme shows that myosin and G-protein, two important participants in cell mobility and signal transduction respectively, share a common ancestor. Both of them have weak catalytic activity on their own, be the substrate ATP in the case of myosin, or GTP in the case of G-protein. To compensate for such weak activities, both enzymes require another protein to stimulate their activity. In the case of myosin, this stimulation molecule is F-actin while for G-protein it is GAP (G-protein activating protein). These proteins dramatically increase the ATPase activity several hundred fold. This raises the interesting question of the regulation mechanisms on the molecular level. The comparison of these two types of molecules may lead to a deeper comprehension of the mechanistic functioning of these giant motor machines.

Another comparison of two ATPases, kinesin and myosin, is even more interesting in their stepping motion. Kinesin is a microtubule-based motor protein and performs steps of the tiny size of ~5 nm but resists a high load that is >3 pN. What is more, kinesin is a processive motor meaning it performs several hundred continuous steps along the microtubule before it dissociates.

Within the myosin family, members having similar mobile properties were discovered not a long time ago. Still these findings are exciting. The myosin family has a broad diversity that allows some members to showing a processive walking style similar to that of kinesin, and a variety of step sizes and walking velocities. Along with the accumulation of such knowledge, the hints of direct interaction between kinesin and myosin has been found concerning a shared 8 KD light chain that might has a role in cargo exchanging between the two kind of motor proteins.

Such comparisons are helpful in bringing forward a better overall understanding of the complex network of signaling and motor proteins.

2.2 Progress of myosin studies

The progress of myosin studies over the past three decades is shown in the following scheme (figure 2.2).

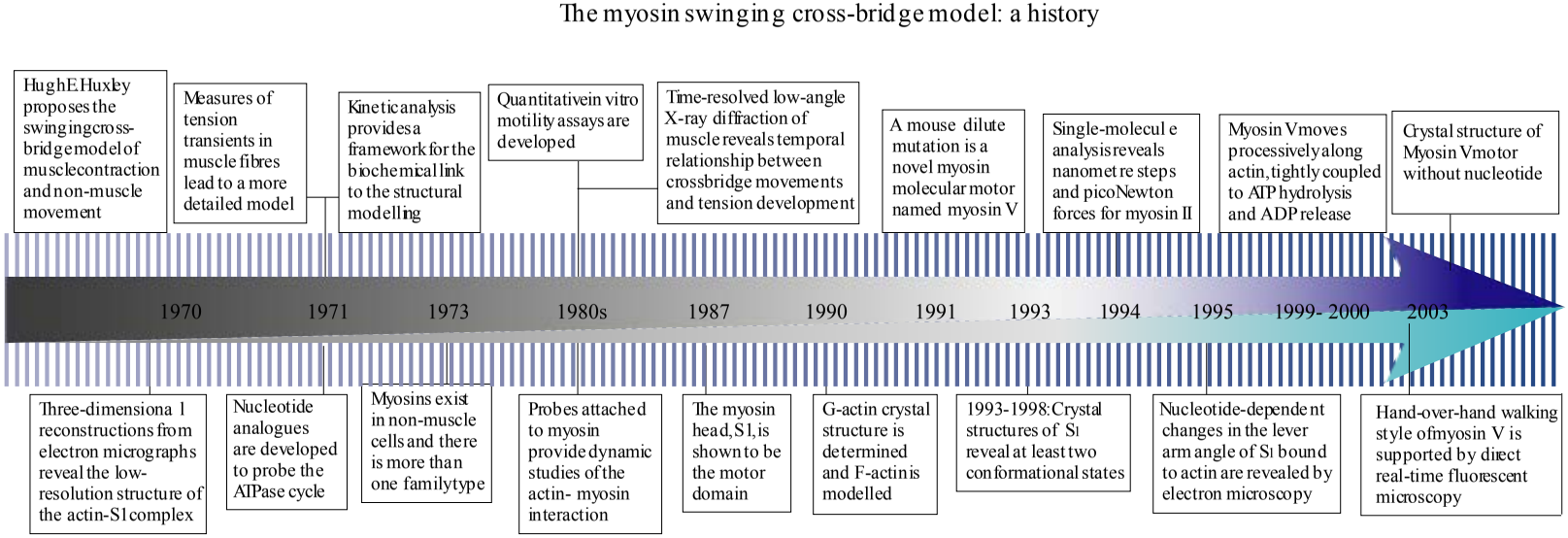

F-actin, filamentous actin; G-actin, monomeric actin; S1, subfragment 1. (This timeline is from J. A. Spudich, 2001 with modification).

Figure 2.2 Progress of myosin studies

2.3 A profile of myosin V

2.3.1 Functional aspects

The earliest genetic information on myosin V was derived from studies of mouse mutants. After that, myosin V encoding gene was found to be expressed in nearly all kinds of cells, from neuron cells to yeast cells. Among mammalian cells, myosin V was found to be particularly abundant in neuron tissues, comprising up to 0.2% of the total protein mass which is close to the amount of another motor protein, kinesin. The roles of myosin V are still under investigation.

Most information on the function of myosin V was obtained by analyzing mutants in mouse and yeast. In the *dilute* mouse functional myosin V is absent. The resulting loss of skin color and neurological disorders are due to defects in melanosome transport in melanocytes and in trafficking of smooth ER in neurons (Wu, 1997). In yeast, myosin V (myo4p) was found to be required for the transport of mRNA to the daughter cell to maintain the mating type (Arn & Macdonald, 1998) while another type of myosin V, myo2p, was found to be involved in vacuolar inheritance and vesicle trafficking associated with exocytosis (Brown, 1997). And there are also hints of a relationship between myosin V and kinesin in yeast where the temperature sensitive mutant (Myo2p66) can be suppressed by the kinesin-like protein SMY1 (Brown, 1997). Absence of myosin V may also be the cause of the Griscelli syndrome, a *dilute* related phenotype in humans (Pastural, 1997).

2.3.2 Structural model and kinetic properties

Endeavors in understanding the interaction between myosin and actin from a general view have been made during several decades. It seemed to be a tough task considering the lack of efficient techniques until recently. The problem of myosin has attracted researchers for a long time. How the overall transport function is regulated and similar questions remain to be answered.

Two kinds of native myosin V molecules have been found in chicken or mouse brain tissue. In the case of the chicken brain myosin Va molecule, it is composed of two identical heavy chains (HC), each consisting of 1829 amino acid residues, and six light chains (LC) in the regulatory domain. The N-terminal part of the HC forms the motor domain, and the regulatory domain is located close to its neck region. The C-terminal part forms a coiled-coil rod exhibiting a globular domain at the end structure which is considered to be the cargo binding domain.

The head domain of myosin V comprises the ATP binding and catalyzing sites as well as the actin binding interface. The breakthroughs on the structural studies on myosin motor domains have been obtained since 1993 by the resolution of the X-ray crystal structure of myosin II motor domain and that of the motor domain complex with various nucleotides, or their analogues (Rayment I. et al., 1993). The X-ray structure of the myosin V motor domain is also recently available (Pierre-Damien Coureux1, 2003).

The regulatory domain of myosin V has become of high interest. It is the region where light chains bind and is thought to be at least partially responsible for the force of the power stroke. The number of bound light chains affects the power stroke and motor processivity. Importantly, this domain can be labeled with fluorescent molecules by light chain exchanging in vitro (J. E. T. Corrie, 1999; Ahmet Yildiz, 2003).

Compared with the other parts, the structure and function of the tail domain of myosin V are largely unknown except that the globular end domain acts as the cargo binding domain. This is due to the lack of an appropriate technique to study the membrane binding protein.

a.

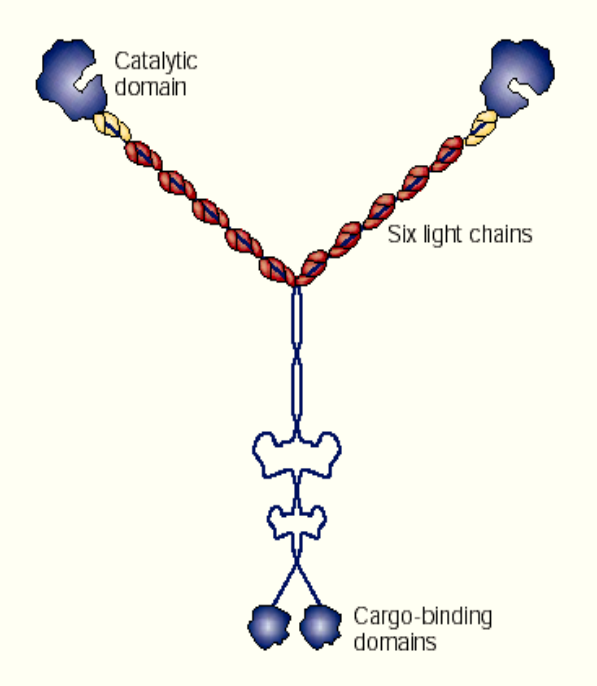

b.

c.

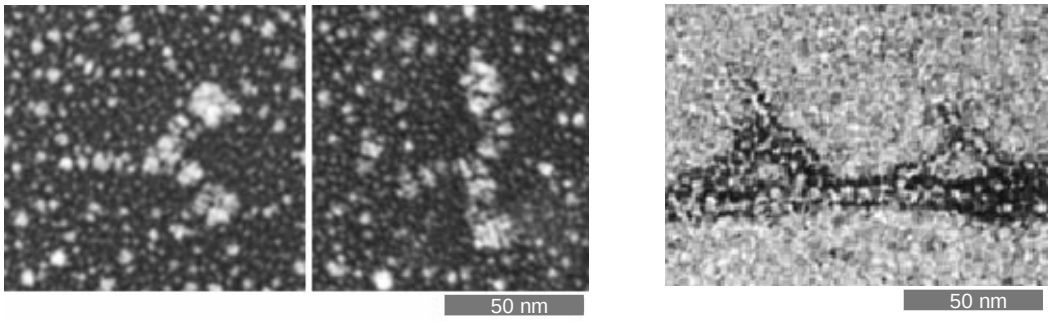

Figure 2.3: Structural model of the myosin V molecule and negative staining pictures of myosin V from electronic microscopy (after Burgess et al., 2001).

Fig. 2.3 summarizes in a model what is known on the structure of myosin V: The group of LCs binds to HCs to stabilize their conformation and is considered to confer a lever arm structure (Figure 2.3a). With electron microscopy by negative staining, the structure of myosin V was visualized as two distinct parts: two identical stalks that indicate the head domains (supported by EM picture data from F-actin myosin V complexes), and a short fragment corresponding to the tail domain. The length of this molecule is ~90 nm (containing head, neck and tail domain, figure 2.3b). A two-headed actin-binding state of

myosin V during which both of its two heads are sitting on a single actin filament was demonstrated by EM. This state is thought to represent the crucial intermediate 'walking' state (figure 2.3.c).

As has been shown, myosin V can bind up to six light chains to the neck domain of HC. To understand the role of these light chains, truncated recombinant HC's were constructed and expressed in baculovirus system (Wang et al., 2000) comprising a series of recombinant HC's containing 3, 2, or 1 LC binding site respectively. The recombinant myosin V and the original myosin purified from tissues differed in velocity in the vitro motility assay. This difference was attributed to the lack of light chains or of proper binding state of LCs.

Comparison of these modified motors by optical tweezers showed that the shortened LC-binding sites also resulted in either a shorter displacement per walking step (24 instead of 36 nm in the case of 4 binding sites), or in a defect walking mode.

As was also shown, the presence of Ca^{2+} ions causes the dissociation of LCs from HCs and results in slower F-actin sliding velocity in motility assay or quenches the sliding completely. But on the other hand, Ca^{2+} is necessary to be present in kinetic assays to activate the ATPase function of myosin V. It acts as an extremely sensitive factor at this point with working concentrations as low as 3.0 μM (Nascimento A.A.C et al., 1996). Without Ca^{2+} little ATPase activity was observed.

2.3.3 Comparison of myosin V with conventional myosin and kinesin, models

When the conventional myosin (myosin II) and kinesin are compared with myosin V, it seems that the differences range from the primary sequence to the structures of distinct subdomains (table 2.1). But still they share some similarities concerning the interior conformation change (figure 2.4) (Ronald D. Vale1, 2000).

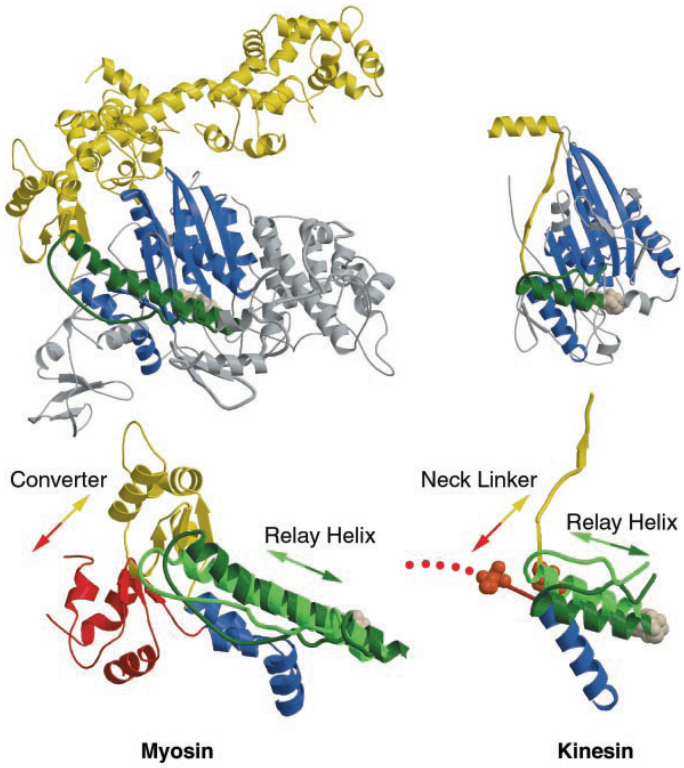

Figure 2.4: Atomic structures of the myosin and kinesin motor domains and conformational changes triggered by the relay helix. The motor domains of smooth muscle myosin and rat conventional kinesin are shown in the upper panels. The common structural elements in the catalytic cores are highlighted in blue, the relay helices and polymer loops are dark green, the mechanical elements [neck linker for kinesin; the converter and lever arm domains for myosin] are yellow, and bound nucleotide is shown as an off-white space-filling model (Ronald D. Vale1, 2000).

Kinesin is another major kind of motor protein which acts on microtubules. It has been uncovered that kinesin is a typical processive motor that could perform several hundreds of steps along the microtubules before dissociation. A comparison of myosin V and kinesin is shown in table 2.1 (Coy, D. L., 1999a; Coy, D. L., 1999b). While performing processive steps, the average step size of ~5 nm for kinesin which is relatively small compared with myosin V's ~36 nm step. But kinesin can resist high load of >3 pN. At such load, myosin V would stall and dissociate from its track. A comparison of these motor proteins is shown in the table.

Table 2.1 Comparison of myosin II, myosin V and kinesin

	Myosin II	Myosin V	Kinesin
Source	Rabbit skeleton muscle	Chicken brain tissue	Expressed in *E.coli*.(recombinant)
Molecular weight (HC + LC)	~480 KD	~560 KD	~78 KD (single headed kinesin)
Number of heavy chains/light chains	2/4	2/~12-13	1/-2
Track	Actin filament	Actin filament	Microtubule
Track sliding velocity in motility assay	~2-3 μm/s	~0.3 μm/s	~0.096 μm/s
Processivity	No	Yes	No
Duty ratio	<0.5	~>0.7	<0.5
Molecule length measured by EM	~100 nm	~90 nm	ND

2.4 The profile of actin

Actin is one of the most conserved eukaryotic proteins. Its polymerization and mechanical behavior are considered to play a critical role in cellular mobility. Recently a mixture of motor protein and F-actin attracts biophysicists by its dynamic properties. Both the processive and nonprocessive motor proteins are assayed in such system in attempt to observe how the distinct kinetics affects certain characteristic biophysical parameters such as viscosity/viscoelasticity.

Myosin motor proteins are ATPases and actin-binding protein. So a very dynamic system could be constructed by using such materials. A long with the depletion of ATP that powers the active interaction with respect to force generation, the system is thought to reach a still state when most or all of the filaments are cross-linked by the motors. The

corresponding changing of the biophysical properties of such a system can be studied by using magnetic tweezers.

A molecular model of G-actin is illustrated in figure 2.5 based on the data from X-ray diffusion experiments. Four sub-domains form two major lobes which are linked by a bound nucleotide molecule and a Ca^{2+} ion that also serve as stabilizers. Polymerization of G-actin requires a threshold actin concentration and the presence of Mg^{2+} and ATP. Due to this, Ca^{2+} at low concentration instead of Mg^{2+} is present in the storage solution to stabilize G-actin and inhibit the spontaneous self-polymerization at the same time.

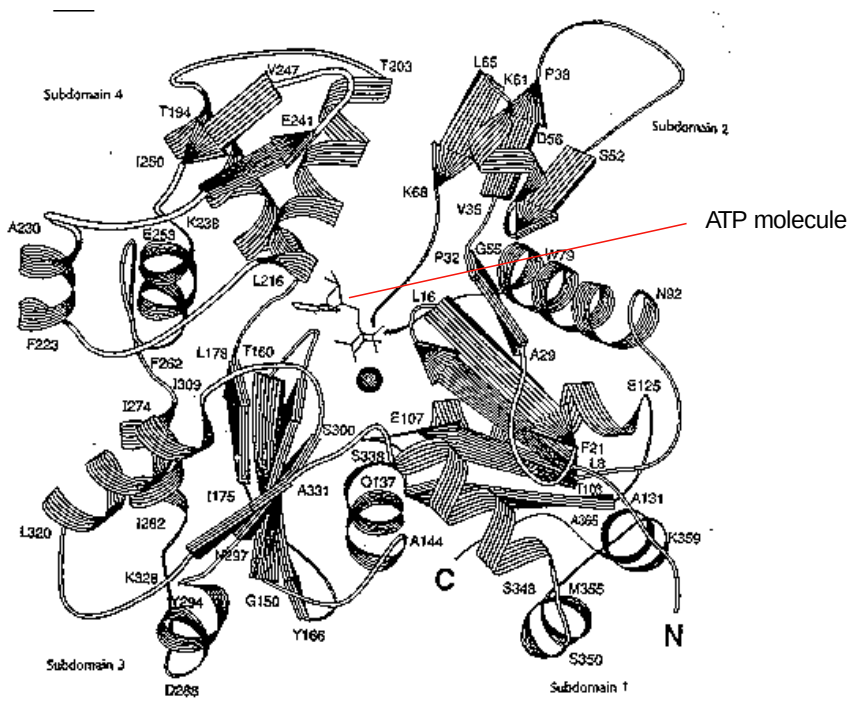

Figure 2.5: A schematic view of globular actin based on X-ray diffraction analysis. An ATP molecule and a calcium ion are indicated in the center of this model. Subdomains 1, 2 and 3, 4 form two lobes folding into a deep cleft. A nucleotide molecule, together with Ca^{2+}, bridges the cleft to form a stable molecule. Actually, without nucleotide, the whole molecule would denature quickly.

Actin polymerization is a self driven process (figure 2.6) where ATP hydrolysis is not necessary. The resulting filament is polarized with two ends showing different on/off kinetics: under steady state conditions one end with net dissociation of actin monomers, also call the minus end (-), and the other with a net binding reaction which is therefore growing, also called the plus end end' (+). The terms "barbed end" for the plus end, and "pointed end" for the minus end are derived from electron microscopic appearance of an actin filament which was fully decorated with S1 domains of myosin II.

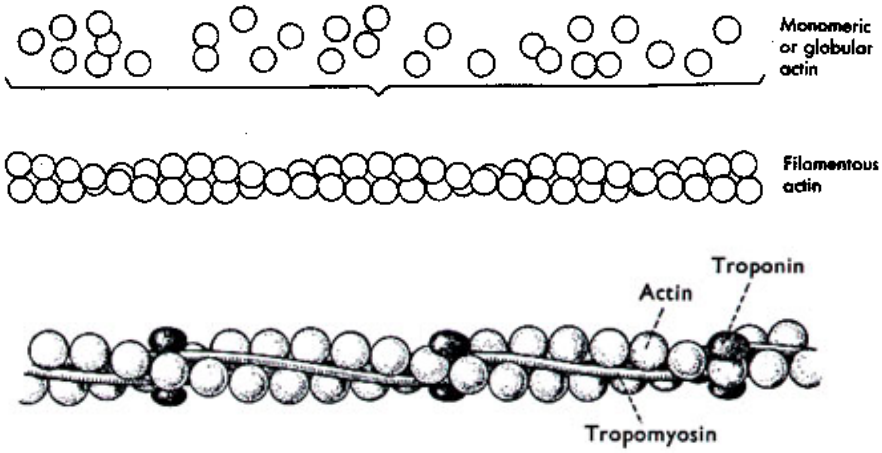

Figure 2.6: Actin polymerization is a self-driven process. Besides appropriate pH adjusted by buffer, ions and ATP as well as the concentration of G-actin play critical roles in polymerization.

Actin binding proteins are involved both in the structural and the functional aspects of cellular skeleton. A well studied model is the muscle functional unit - the sarcomere - which is responsible for force generation in muscle tissue.

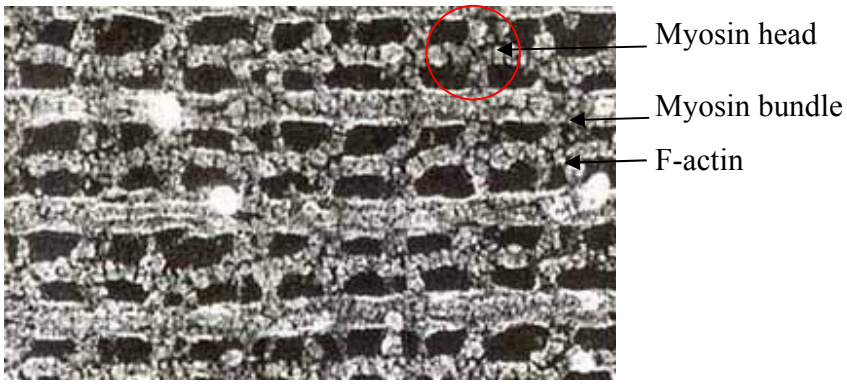

Figure 2.7: the structure of actomyosin in the cross-striated muscle system. Myosin heads appear as cross-bridges in the illustration obtained by negative staining electron microscopy (Bagshaw, 1993).

2.5 Progress of the study on myosin V-actin interaction

Myosin V was found and named as a new member of the myosin family in 1991. After that, continuous achievements were obtained from a broad variety of subjects ranging from biochemical to biophysical studies. A broader connection with other interesting objects is in expected to be discovered.

2.5.1 Sources of myosin V

There are two sources of myosin V available for various experiments. In the earlier period, the myosin molecules were purified from either chicken or mouse brain tissue. These samples differ in the fraction of bound light chains and in the kinetic properties (Cheney et al., 1993; Espindola et al., 2001; De La Cruz et al., 2000a). Historically the studies of those myosin V materials led to the discovery of the processivity of this motor molecule (Mehta, A. D., 1999a). However the native myosin V species from other source do not necessarily behave as a processive motor, as has been found with both *Saccharomyces cerevisiae* myosin V homologs that appear to be weakly processive or non-processive (Reck-Peterson et al., 2000b). This demonstrates a hint of the significance

of mechanical, kinetic and functional differences among related members of the same myosin class.

In order to obtain higher yields and more options for modifications, DNA-recombination techniques have been used to express myosin V or its subdomains. The most successful preparation has been obtained from a baculovirus expression system. Compared with the previous methods based on classical preparation techniques, this method is flexible in allowing a variety of modification such as molecule replacement, generation of protein chimera, truncation of specific binding domain (De La Cruz, 1999; De La Cruz, 2000a, De La Cruz, 2000b; Trybus, 1999; Moore, 2001) and other advantages such as: a) over-expression in insect system; b) flexible ways varying the structure base on a; c) indirect methods by constructing knock-out mutants et al.

Optimal spatial or temporal resolution of observation was achieved when these preparation techniques were applied in combination. Breakthroughs have been obtained in the recent biophysical studies where the labeling of single myosin V molecule is done with recombinant light chains. In this case, myosin V maintains processivity while being specifically labeled (J. E. T. Corrie, 1999; Ahmet Yildiz, 2003).

2.5.2 Biophysical techniques

2.5.2.1 Gliding filament assay

The gliding filament assay was introduced in 1986 (Kron and Spudich, 1986). It allows the observation of fluorescent polymer tracks (actin filaments on myosin; microtubules on kinesin) moving upon an array of surface-fixed motors. The difference of the gliding velocity of myosin II and V provided for the first time evidences that myosin V is processive. (Mehta et al., 1999a; Uyeda et al., 1990; De La Cruz et al., 1999; Moore et al., 2000). Also this assay indicated the difference between the native myosin V purified from brain tissue and recombinant myosin V subdomains. The native myosin V could support continuous actin sliding even if applied at an extremely low density such as 0.05-2.7 molecules/μm^2 (Mehta, 1999a; Mehta, 2001); in contrast the recombinant myosin

could sustain the actin sliding but required methylcellulose to restrict actin filament diffusion (Wang et al., 2000).

2.5.2.2 Optical tweezers

Two types of optical tweezers set-up have been applied to demonstrate the processivity of myosin V molecule. In the dual bead set-up laser traps capture two beads attached at each end of a single actin filament (Finer et al., 1994; Mehta et al., 1998). The filament is then stretched to tension and moved close to the surface decorated sparsely with myosin molecules (Figure 2.8).

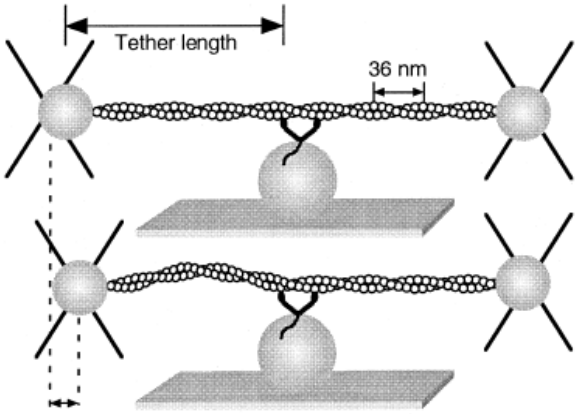

Figure 2.8: A dual-bead set up used in optical tweezers assay (Ronal S. Rock et al., 2000).

A different experimental geometry was introduced in the later studies (Rief M., 2000): The motor was attached to polystyrene beads at low density, which were then trapped and moved near surface-mounted actin tracks (Block et al., 1990; Kuo and Sheetz, 1993; Svoboda et al., 1993). These experiments used a force clamp technique (Visscher and Block, 1998; Visscher et al., 1999), in which a feedback circuit positions the trap to maintain system tension at a programmed level. This scheme prevents motor stalling and dissociation due to prohibitive optical load (Figure 2.9).

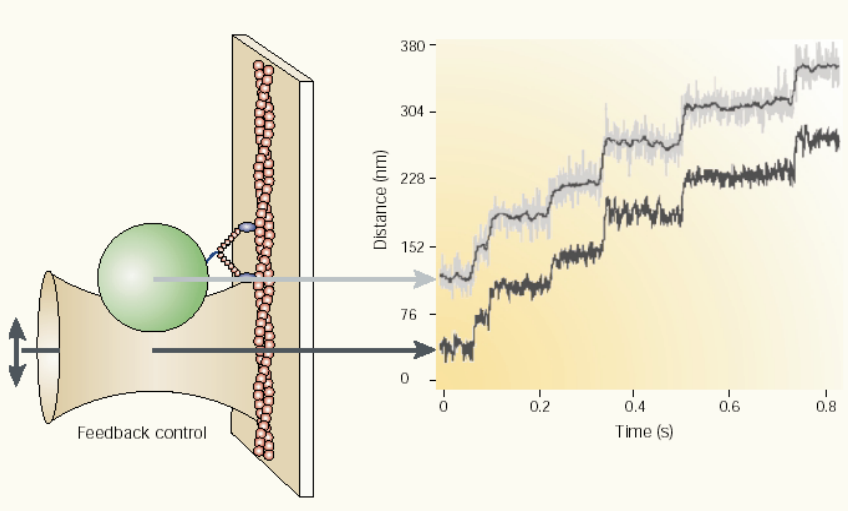

Figure 2.9: Modified optical tweezers set-up (Rief M., 2000). A single polystyrene bead is decorated with low density of myosin V and the motion of the bead is controlled by a force clamp technique (Visscher and Block, 1998; Visscher et al., 1999).

These above techniques provided interesting results on the cargo transport properties as well as in the studies on the kinetic mechanism of processive motors. During the step-wise movement of myosin V-cargo complexes, the cargo was determinated to be transported in regular ~36 nm steps shown in the stair-like position distribution indicating that the cargo binding domain of the molecule follows the same motion (Rief M., 2000). By varying the load, the force properties of the motor was investigated. As was shown, myosin V could resist a load of ~1 pN above which it stalls and dissociates from its track (Rief M., 2000).

2.5.2.3 Fluorescence microscopy

An excellent technique which can be used in vivo and in real time to study the behavior of myosin V is fluorescence microscopy (FM). It benefits from the development of the microscopy and detection sensor devices as well as from specific fluorescent labeling techniques.

As a prerequisite of FM, specific labeling is critical. An impressive strategy using labeled light chains and light chain exchanging has been successfully implemented. The conformation of light chains wrapped around the myosin II heavy chain is illustrated in figure 2.10a. Rodamine molecule was activated to form a bifunctional rhodamine reagent (BR±I_2) (figure 2.6b) which is subsequently used in cross-linking the the four pairs of cysteine residues introduced by recombinant techniques into the light chain. Thus the motion of light-chain-domain tilting and twisting could be investigated (Corrie J.E.T., 1999)

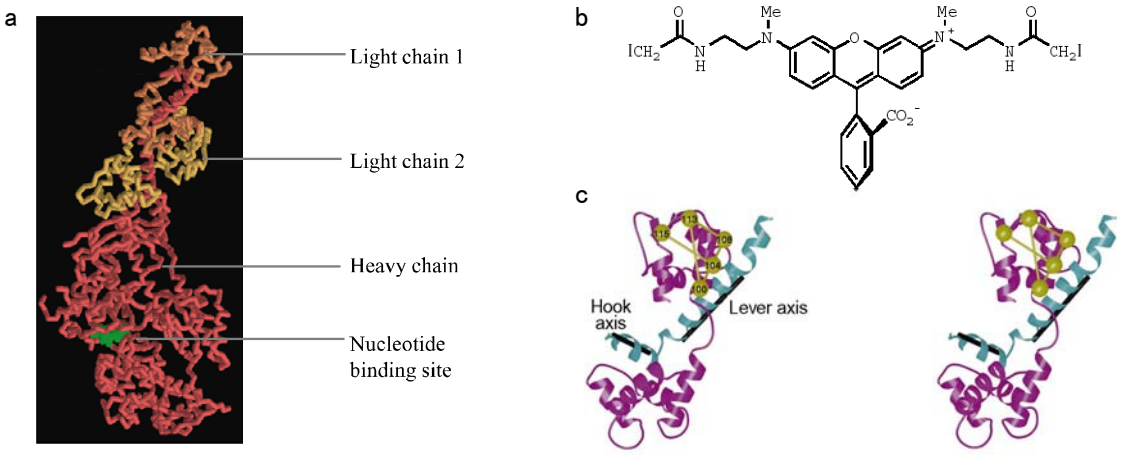

Figure 2.10: a. Relative positon of myosin II heavy chain and light chains. b. Structure of bifunctional rhodamine reagent (BR±I_2). c. Stereo pair of the regulatory light chain (RLC) region of the myosin head, showing the RLC (magenta), the lever and hook axes (black), part of the myosin heavy chain (blue) and the four pairs of cysteine residues that were crosslinked by bifunctional rhodamine (green spheres and rods). This figure is taken from Corrie J.E.T., 1999, page 425.

Two distinct processive stepping models, the inch-worm and the hand-over-hand models, have been proposed to explain myosin V's motion. To simplify the step mechanism, all of the intermediate substeps are ignored in those models. In summary, these models differ mainly in the translocation mechanism of the trailing head. In the inchworm model, each step occurs by the coordinated translocation of both of its heads. Logically the inch-worm

model introduces more instability than the hand-over-hand model (Joseph N. Forkey, 2003; Ahmet Yildiz, 2003).

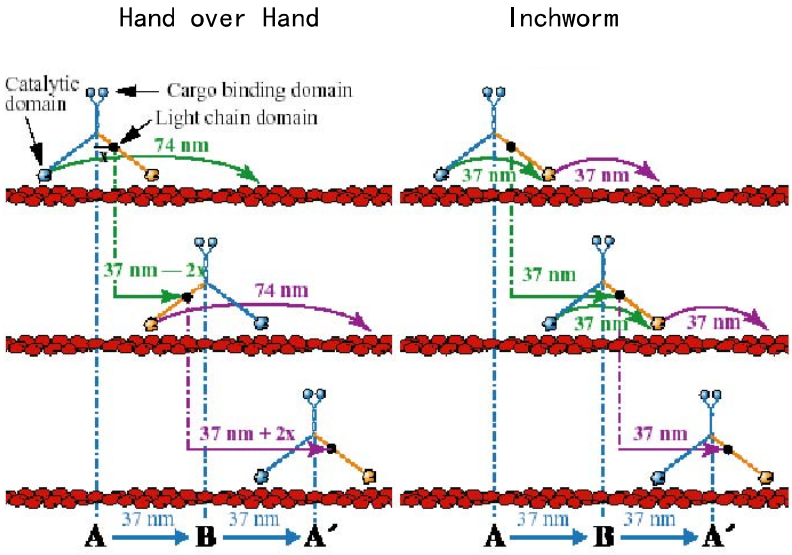

Figure 2.11: Two models of processive stepping. The hand-over-hand model (left) supposes that the stalk moves ~37 nm and the trailing head moves ~74 nm while the leading head stays where it binds. According to the inchworm walking style (right), both the stalk and the trailing head move the same distance, ~37 nm (This figure is from Ahmet Yildiz et al., 2003).

Recent investigation by a single-molecule fluorescent polarization technique showed the lever arm rotation of the calmodulin-binding domain in myosin V. This evidence supported the hand-over-hand model. And further evidence came from fluorescence micrography performed on moving motors labelled by a single fluorophore in a variety of well-defined positions (Ahmet Yildiz, 2003). Under an ultra-high spatial (<1.5 nm) and temporal (0.5 s) resolution, the distinct labeled lever arm domains exhibited various displacements during a chemomechanical cycle (figure 2.8). The step size derivation varies from ~37 nm to ~74 nm depending on the distance between the dye and the midpoint of the two heads - the closer the dye molecule located to the midpoint, the closer the translocation distance got to ~37 nm; in contrast, the further it located the end

of head the translocation distance got to ~74 nm. This result strongly supports the hand-over-hand stepping model (Joseph N. Forkey, 2003; Ahmet Yildiz et al., 2003).

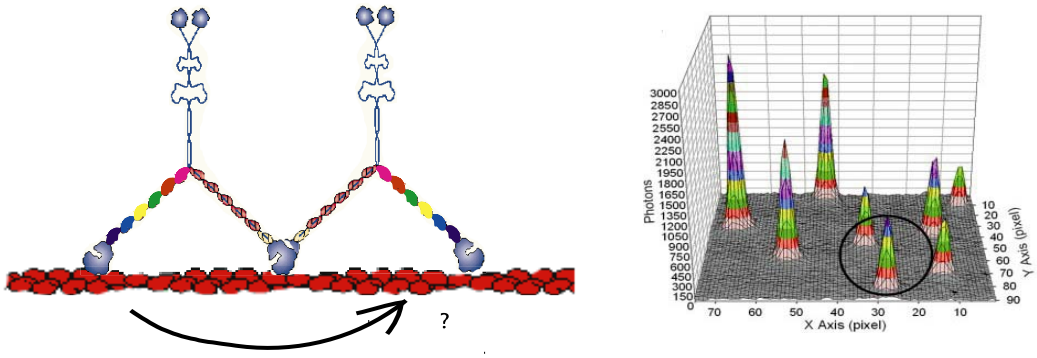

Figure 2.12: Fluorescent labeled myosin molecules performing hand over hand motion (left); integration of fluorescent signal results in varying peak density (right, from Ahmet Yildiz et al., 2003).

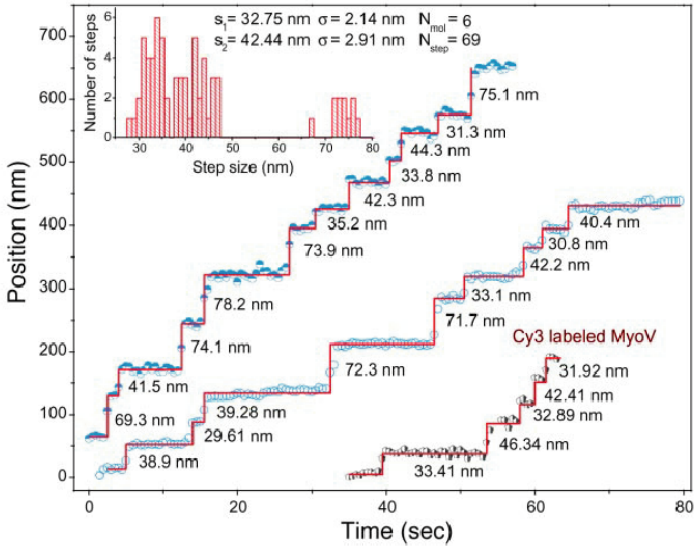

Figure 2.13 Stepping traces of three different myosin V molecules displaying alternating 42-33 steps, and histogram of a total of six myosin V's taking 69 steps. These step sizes indicate that the dye is 2 to 3 nm from the center of mass along the direction of motion. The bottom right trace is for a Cy3-labeled myosin V, whereas the other two are for BR-labeled myosin V's (from Ahmet Yildiz et al., 2003).

3. Materials and Methods
3.1 Chemicals and Buffers

1. Motility assay buffer: pH = 7.4

Prepare 10 × buffer stock; degas prior to use; store at 4 °C.

Imidazole:	25 mM
$MgCl_2$:	4 mM
KCl:	25 mM
EGTA:	1 mM
DTT:	1 mM

2. Actin polymerization buffer (F-Buffer): pH = 7.5

Prepare 10 × buffer stock; aliquot and store at -20 °C; the same requirement is applied on G-buffer.

Tris.Cl:	2 mM
MgCl:	2 mM
KCl:	100 mM
DTT:	0.2 mM
$CaCl_2$:	0.2 mM
ATP:	0.5 mM

3. G-actin storage buffer (G-Buffer): pH = 8.0

Tris.Cl:	2 mM
$CaCl_2$:	0.2 mM
DTT:	0.2 mM
ATP:	0.2 mM
NaN_3:	0.05%

4. ATPase assay buffer/solution:

ATP regeneration system:

H_2O:	842 µl
Motility assay buffer (10 ×):	200 µl
DTT (1M):	4 µl
ATP (0.5 M):	4 µl
F-actins (20 mM):	800 µl
$CaCl_2$ (100 mM):	20 µl
Camodulin (1 mg/ml):	40 µl
NADH (10 mM):	40 µl
Pyruvate (20 mM):	40 µl
Total volume:	2 ml

(Mix well before the addition of following enzymes.)

Enzyme solutions:

Lactic Dehydrogenase (1 unit/µl):	2 units/ml
Pyruvate Kinase (1unit/µl):	2 units/ml
Myosin V (1mg/ml):	3 µl

Mix well and pipette 500 µl mixtures to corvette.

5. Myosin II (myosin II, S1, HMM) preparation buffer:

Myosin buffer I: pH 7.4

KCl	600 mM
KH_2PO_4	50 mM
DTT	2 mM
Azide	0.02%

Myosin buffer II: pH 7.4

KCl	3.0 M
Na_2HPO_4	5 mM
DTT	2 mM
NaN_3	0,05 %

Myosin buffer III: pH 7.4

NaCl	40 mM
Na_2HPO_4	5 mM
DTT	2 mM
NaN_3	0,02 %

6. Buffers for the preparation of myosin V:

S500 buffer: pH = 8.0; 1.0 litter

Adjust pH with 10 M NaOH to pH8.0 before addition of DTT. Cool it down to 4 °C

HEPES:	10 mM
NaCl:	60 mM
$MgCl_2$:	5 mM
EGTA-Acid:	2 mM
ATP:	0.5 mM
DTT:	2 mM

TMAE Buffer: pH = 7.5; 500 ml

Triethanolamide:	20 mM
EGTA-Na:	2 mM
DTT:	2 mM

NaCl solution:	4.0 M
100 ml	(23.376 g/100 ml)

Homogenization buffer: pH = 7.7;
500 ml (For 100 chicks)

HEPES:	40 mM
EDTA-Na:	2 mM
Pefabloc:	59 mg
Benzamidine:	79 mg
Aprotinin:	2 mg
DTT:	2 mM
ATP:	0.5 mM

Adjust pH to pH 7.7 with 1 M NaOH; degas the solution prior to addition of DTT; Pefabioc, Benzamide, and Aprotinin should be added just before use.

Washing buffer: pH = 7.2 250 ml

HEPES:	20 mM
EDTA-Acid:	0.5 mM
EGTA-Acid:	0.5 mM
DTT:	0.5 mM

Degas the solution just before use.

6. Buffer for purification of antibodies:

Binding buffer: pH=7.2;

Tris.Cl	50 mM

Elution buffer: pH=2.7

sodium citrate	50 mM

F_{ab} reduction buffer: pH=4.5

Citrate	50 mM
NaCl	100 mM
Borate	100 mM
EDTA	2 mM
DTT	20 mM

This buffer is intensively degassed prior to addition of DTT.

7. Broad Range Mr. Standard (Dalton):
(Bio-Rad product)

Myosin	200,000
Phosphorylase	116,250
β-galactosidase	97,400
BSA	66,200
Ovalbumin	45,000
Carbonic anhydrase	31,000
Soybean trypsin inhibitor	21,500
Lysozyme	14,400
Aprotinin	6,500

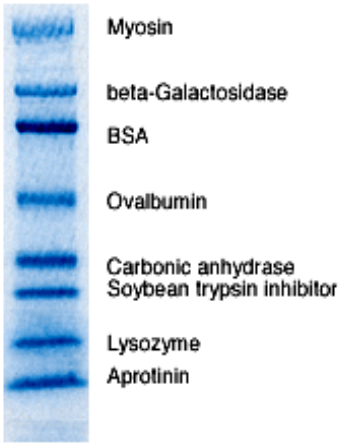

3.2.1 Preparation of HMM (Heavy Meromyosin) from myosin II

Myosin II was prepared from rabbit skeleton muscle according to (Margossian S.S., 1982) and stored at -20 °C in the presence of Glycerol at 50%.
The preparation of HMM followed the procedures below.

- Myosin was dialyzed over night against high salt myosin buffer I:
- Then the concentration of the solution was examined by UV spectroscope at 280 nm. The absorbance coefficient of myosin was known to be 0,53 cm^2 /mg. In a typical experiment, the concentration of myosin was calculated to be ~6.1 mg/ml.
- The solution wase then diluted by 1:10 with myosin buffer II, a condition under which myosin precipitated. After that, the solution was centrifuged at 35.000 × g, 4 °C using a JA 10 rotor.
- The pellet was collected and resuspended with 8 ml myosin buffer II containing 3 M KCl. The mixture was then homogenized using a 10 ml homogenizer.
- This solution was then centrifuged for 30 min at 43.000 × g, 4°C using a Ti50 rotor. The insoluble fraction was sedimented to pellet and discarded.

  Enzymatic digestion

- TLCK treated α-Chymotrypsin was added to 50 µg/ml and the mixture incubated 10 min at room temperature. To stop the reaction, PMSF was added to a final concentration of 0.5 mM.
- The mixture was then dialyzed overnight against myosin buffer III
- During dialysis against this buffer, the intact myosin molecules aggregate and become insoluble.
- After dialysis, the solution was ultra-centrifuged for 1 hr at 35.000×g, 4°C. The supernatants are pooled and the concentration of HMM was determinated to be 3.6 mg/ml with an extinction coefficiency of 0.5 cm^2/mg.

The HMM solution was kept at -80°C in presence of 35% sucrose.

3.2.2 S1 subfragment of myosin II

50 ml of rabbit muscle myosin solution at a concentration of ~8 mg/ml (containing 50% glycerol) was dialyzed against 6 L of myosin buffer I

Myosin was proteolyzed with α- chymotrypsin at a ratio of 3.33 µg α- chymotrypsin per mg of myosin. The mixture was incubated for 10 min at 25 °C before PMSF added to 50 µM to stop the reaction.

The mixture was then dialyzed against buffer containing lower NaCl concentration of 40 mM and centrifuged at 40.000 × g, at 4 °C using a Ti 45 rotor.

According to the adsorption using an absorption coefficiency of A 280 = 0,75 cm^2 /mg the concentration of S1 was estimated to be 2.14 mg/ml in a total volume of 45 ml.

3.2.3 NEM (*N*-ethylmaleimide) treated HMM

HMM was prepared as described above and DTT and NEM (*N*-ethylmaleimide) solution were prepared freshly. The starting concentration of HMM was examined to be 5.8 mg/ml and then the solution dialyzed over night against myosin buffer III.

The dialyzed solution was then centrifuged for 1 hr at 36.000×g, 4 °C by using a Ti50 rotor.

NEM was prepared as 100 mM stock solution. This solution was added up to a final concentration of 1 mM and the mixture vortexed and incubated for 45 min at room temperature. DTT was then added to a final concentration of 10 mM to stop the reaction. Subsequently the solution was dialyzed against myosin III buffer over night. As the final step, the solution was ultracentrifuge again for 1 hr at 34.000 rpm at 4°C using a Ti50 rotor. The resulted pellet was discarded.

For storage, sucrose was added to 35% and DTT was added up to 10 mM to this solution. Aliquots were stored at -80°C.

3.2.4 NEM treated S1

The concentration of S1 solution was determinated to be 3.8 mg/ml by spectroscope under UV 280 using an absorption coeffieciency of 0,53 cm^2 /mg. The buffer was exchanged against sodium-phosphate buffer by using a 5 ml Hitrap desalting column. The volume was adjusted to 5 ml with the same buffer. Fresh NEM was dissolved in distilled H_2O to 0.1 M (12.7 mg/ml) that was used as stock solution. 50 µl of freshly prepared 100 mM NEM solution was added into 5 ml S1 solution, and the mixture was incubated at room temperature for 45 min. Fresh DTT solution (stock concentration was 1.0 M) was added to a final concentration of 10 mM to quench the reaction. The subsequent purification of NEM-S1 was performed with a Mono-Q column on a HPLC system.

Firstly, a buffer change was performed using a Hitrap column (Amersham product) again with TMAE buffer, pH 8.0 as the elution buffer. At this step, the excess NEM and DTT were largely removed.
The eluted fractions are loaded onto a pre-equilibrated Mono-Q column. After washing, a linear sodium concentration gradient from 200-750 mM was applied to elute the NEM-S1 sample.

The fractions containing NEM-S1 were determinated by SDS-PAGE. After the fractions are pooled the buffer was changed into 1× motility assay buffer, pH7.4. The storage condition was the same as that used for myosin.

As seen from SDS-PAGE the S1 solution was normally contaminated by HMM and LMM resulting from the enzymatic digestion where native myosin was used. Because HMM, S1 or NEM-S1 have very similar affinity for actin in the absence of ATP, the denatured or partially denatured HMM could cause severe problems in our experiments where the size of the actin binding protein matters. For this reason, a high purity of NEM-S1 was required.

During this preparation, the Hitrap desalting column other than traditional dialysis was routinely used to facilitate a quick bench work.

3.3 Myosin V

3.3.1 Buffer used in the preparation of myosin V

Homogenization buffer: pH = 7.7; 500 ml (For 100 chicks)		Adjust pH with 1 M NaOH; degas the solution prior to addition of DTT; Pefabloc, Benzamidine, and Aprotinin are the last reagents to be added;
HEPES:	20 mM	
EDTA-Na:	1 mM	
Pefabioc:	59 mg	
Benzamide:	79 mg	
Aprotinin:	2 mg	
DTT:	1 mM	
ATP:	0.5 mM	

NaCl solution:	4.0 M, 100 ml	NaCl:	600 mM
		$MgCl_2$:	5 mM
S500 buffer: pH = 8.0; 1 L		EGTA-Acid:	1 mM
HEPES:	20 mM	ATP:	0.5 mM

DTT: 2 mM
Adjust pH with 10 M NaOH to pH8.0 before addition of DTT. Cool it down to 4 °C

Washing buffer: pH = 7.2; 250 ml
Degas the solution just before use.
HEPES: 20 mM
EDTA-Acid: 0.5 mM
EGTA-Acid: 0.5 mM
DTT: 1 mM

TMAE Buffer: pH = 7.5; 500 ml
Triethanolamide: 20 mM
EGTA-Na: 2 mM
DTT: 1 mM

3.3.2 Preparation of myosin V

Since myosin V is relatively abundant in neural tissue, we took 1 day old chick brain as starting material for the preparation. Routine preparations from 100 chicken brain typically resulted in ~0.5-1.0 mg myosin V (>95% purity). The procedure was in principle based on the method described by R. Cheney (Cheney et al., 1993; Cheney et al., 1998). The following modifications were made:

A different mixture of protease inhibitors was added to the homogenization buffer, namely Pefabloc, 120 mg/L; Benzamidine, 79 mg/L; Aprotinin, 2 mg/L. A higher centrifugation speed was chosen in the co-precipitation step (40.000 × g). The ion exchange chromatography was performed on a mono Q column that has a higher protein capacity and a broader compatibility for the applied pH range.

Preparation of the purification of chicken brain myosin Va

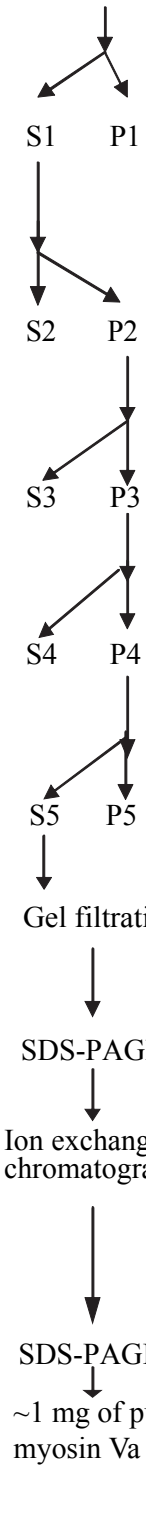

Prepare 150 chick brains (~140 g brain tissue)
Homogenize in 4 volumes of homogenization buffer; e.g. mix 45 ml buffer with each 10 brains (10 strokes with a Potter-Elvejhem homogenizer at ~ 300 rpm).

Centrifuge 40 min at 32,500 × g, 4°C; combine the supernatants.

Add NaCl, 4 M, to attain a final concentration of 600 mM and mix gently to allow myosin V, organelles and actin precipitate for 1 hour on ice.

Centrifuge 40 min at 40,000 × g, 4°C

Collect pellets and resuspend them in 45 ml of washing buffer, then add 5 ml 10% Triton X-100. Homogenize the pellet as before.

Centrifuge 20 min at 40,000 × g to collect myosin V-actin pellet.

Rinse pellet with 25 ml washing buffer to remove residual detergent.

Centrifuge 20 min at 40,000 × g.

Solubilize BM-V from the rinsed pellet with 4-5 ml of S-500 buffer containing 10 mM ATP.

Centrifuge for 30 min at 140,000 × g to sediment F-actin and associated proteins

Load supernatant on a 1.5 × 75 cm S-500 gel filtration column and run overnight (or ~ 10 hours, depending on flow rate) using S-500 Buffer at 4°C.

Analyze fractions by SDS-PAGE (with the given column, the myosin-V-containing fraction appears at around 85 ml.)

Pool fractions containing BM-V and dilute into 2 volumes of TMAE Buffer to decrease ion strength.

Load onto a 1 ml Mono-Q ready-to-use column equilibriumed with TMAE buffer, wash and elute with a 250-750 mM NaCl gradient in TMAE buffer.

Analyze eluted fractions by SDS-PAGE.

Pool fractions containing myosin V.
Concentrate the sample to ~2 mg/ml in storage buffer and aliquot the sample and then store at -80°C.

The following specifications were found to be optimal to obtain good yields.

In the solubilization step, 5 ml S-500 buffer containing 10 mM ATP was used. After ultracentrifugation the supernatant was at once loaded onto the S-500 GF column. An over night elution was performed by setting the flow rate to 15 ml/h, collector speed to 12 min/tube. The actual fraction size was measured to be ~1.5 ml/tube instead of the setting volume of 3 ml/tube. The decreased flow rate was caused by the resistance of the gel filtration column. Alternatively, the gel filtration could be performed without a pump in our specified set-up. Compared with the pump-powered gel filtration, gravity was more reliable to achieve a steady flow rate in GF (gel-filtration) where a high flow rate is not required. Fractions eluted from the gel filtration (GF) column were sampled and analyzed by SDS-PAGE. Myosin V was found to be eluted starting from ~85 to 105 ml, in a peak volume of ~15-25 ml. These fractions were then analyzed by SDS-PAGE (figure 3.1) to determinate the distribution of the myosin V sample (figure 3.2).

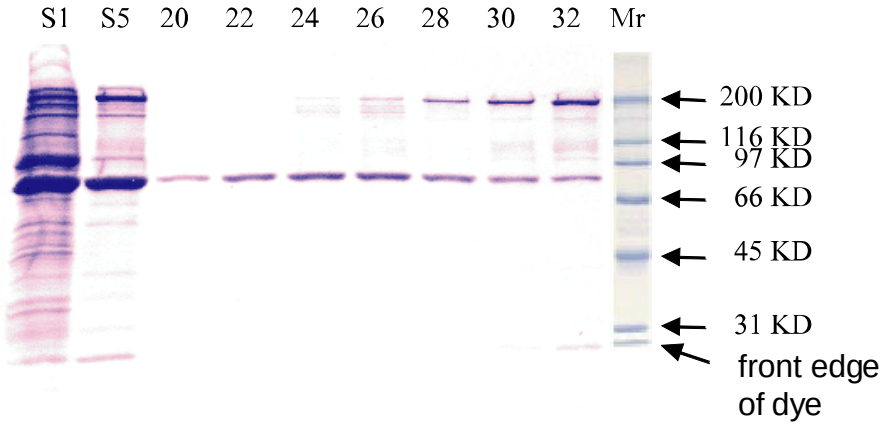

Figure 3.1: Samples taken from myosin V preparation steps were analyzed by SDS-PAGE. (Fraction number was taken from one of the preparation).

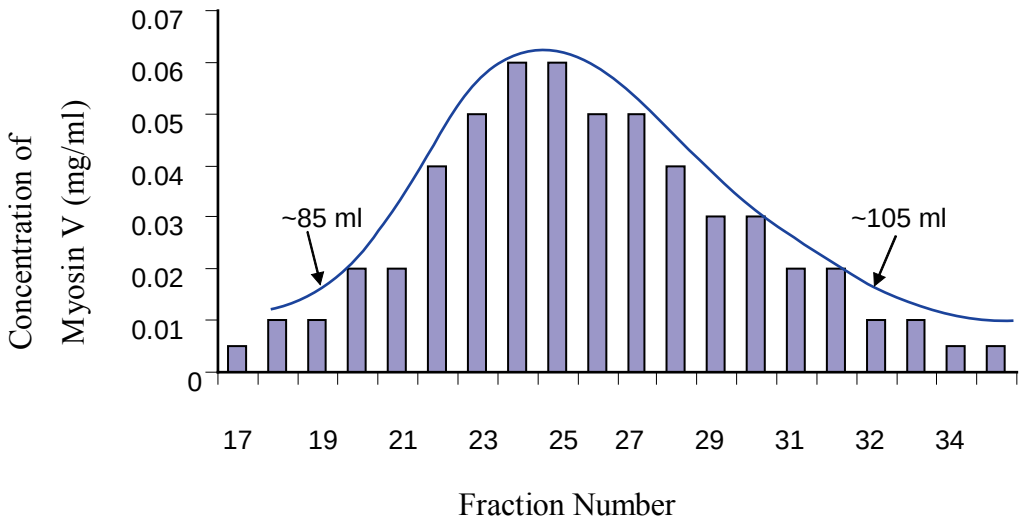

Figure 3.2: The distribution of the myosin V in the eluted fractions (fraction size was ~1.5 ml).

Fractions containing myosin V were pooled and mixed with 2 volumes of TMAE buffer (NaCl free) to decrease the ion strength prior to the ion exchange chromatography. The column was thoroughly equilibrated before the sample was loaded at a rate of 1 ml/min by using a pump with a working volume of 5 ml (here, a 50 ml super loop is the better alternative).
After the washing step, elution was performed at a flow rate of 0.75 ml/min with a linear gradient of 250-750 mM NaCl. Under these conditions, myosin V was eluted around 500 mM NaCl. This step dramatically reduces the sample volume from ~60 ml to ~1.5 ml.

The eluted sample is then analyzed by SDS-PAGE. Myosin V demonstrates a band immigrates at the position of ~200 KD and another band at position <31 KD. They are considered to be the heavy chain and light chains. According to databank, myosin V is consisting of two identical heavy chains (HC, ~200 KD) and about 12-14 light chains (LC, ~15 KD) with 6 LCs binding to each head domain and a 9 KD light chain binding to the tail domain. In this result, the LCs has been separated.

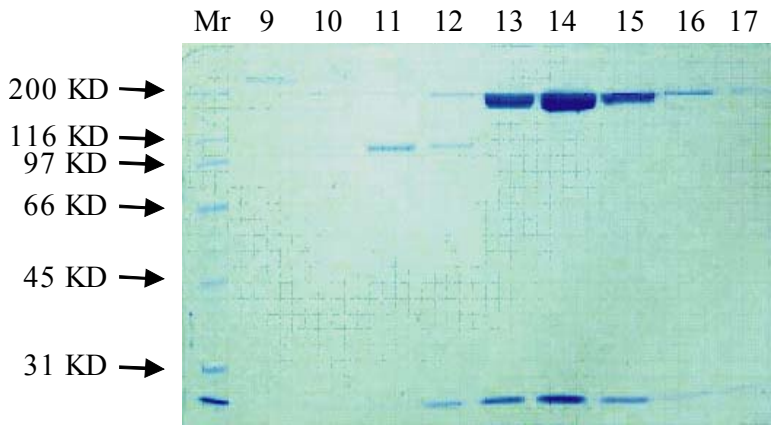

Figure 3.3: Elution from ion exchange column. 5µl samples were taken from each fraction and analyzed by SDS-PAGE. The purity of myosin V was >95 % (Fraction Nr. 13, 14 and 15)

TMAE buffer was replaced by storage buffer using a Centricon tube (cutting molecular weight of 50 kD). The Centricon tube contains an embedded filter of distinct pore size which retains proteins above a defined molecular weight. For instance, a tube with a cutting molecular weight of 50 KD allow > 90-95% of molecules which have MW ⩾50 KD to be retained. It allows also making use of centrifugation in purposes such as quick buffer exchanging, or protein concentration. Compared with dialysis, such a procedure takes much less time so that the stability of the myosin V is better maintained.

A key step in the preparation of myosin V is the coprecipitation of myosin V and organelle in presence of salts, e.g. NaCl. Myosin V is believed to bind those organelles which haven not been characterized well yet. However, as far as the preparation procedure concerns, such a coprecipitation is advantageous.

We found that it is optimal to use 1× assay buffer containing 10 mM DTT, 2 mM ATP, 35% sucrose and an excess concentration of calmodulin (~1 mg/ml). Storage over 6 months does not result in remarkable loss of activity, or detectable degeneration when checked by SDS-PAGE. Small aliquot around 5 µl or even less volume is recommended

for long-term storage. Normally storage of a protein at higher concentrations facilitates its stability. As far as myosin V is concerned, it is normally stored at 1~2 mg/ml (or 1.8~3.2 μM). Figure 3.4 shows the effects from the storage on the integrity of myosin V over a time of 5 month.

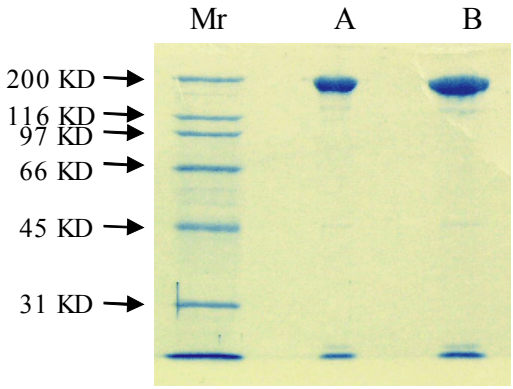

Figure 3.4: After 5 months of storage, the stability of myosin V was checked by SDS-PAGE. The inspection of the band shows that there is no detectable degeneration due to storage. A, B represents 2.5 μg, 5 μg sample respectively.

3.3.3 ATPase Assay

Myosin V is a special ATPase that hydrolyzes ATP and converts the chemical energy into mechanical motion just like the other members of myosin superfamily. Here we implemented an enzyme-coupled ATPase assay to study the ATPase function of myosin V under steady state ATP concentration. One aim is to investigate its ATPase activity under various concentration of F-actin which serves as a stimulator. Another aim is to study the effect of ions, e.g. Mg^{2+}, Ca^{2+}, on the ATPase activity of myosin V molecules. Besides these purposes, the ATPase test provides a reference for other applications such as magnetic tweezers study.

The following protocal was applied: myosin V was incubated with ATP in the presence of F-actin together with phosphoenoepyruvate, pyruvate kinase, NADH and L-lactic-dehydrogenase to convert the ADP produced back into ATP to keep ATP at a constant

concentration. Because the inhibition of the myosin ATPase by ADP is minimized by this reaction, the ATPase function of myosin is measure under optimal conditions.

The reactions concerned in this assay are as follows. Firstly, one ATP molecule is hydrolyzed by myosin V generating an ADP molecule. The ADP generated is converted back into ATP by the action of Pyruvate Kinase using PEP as a substrate. Subsequently, NADH is oxidized into NAD^+ by Pyruvate catalyzed by L-lactic-dehydrogenase. The reaction is monitored at 340 nm by spectroscopy (refer to the absorption curve of NADH and NAD^+). The decay rate of absorption reveals the ATPase activity of myosin molecules.

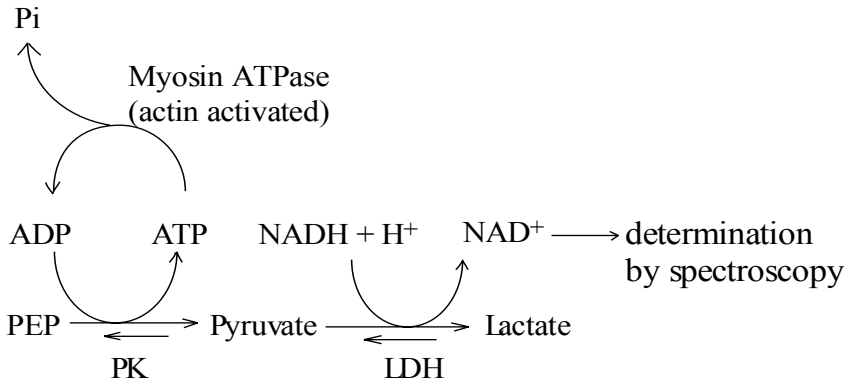

Note: LDH: L-Lactic Dehydrogenase; PK: Pyruvate Kinase
PEP: Phosphoenoepyruvate

Figure 3.5: A brief scheme of reaction involved in NADH coupled ATPase assay

Procedure of ATPase assay:

F-actin is prepared as a stock solution of 20 μM (see chapter 3.5.1) and diluted to 2 × working concentration with 1 × assay buffer. In order remove the possible bubbles in the F-actin gel during the measurement, F-actin is sonicated for 1 min and stabilized by an equal concentration of phalloidin.

Ca^{2+} is added up to a final concentration of 1.0-2.0 mM from a stock solution of 100 mM of $CaCl_2$. A control reaction without Ca^{2+} is performed.

The substrates, phosphoenoepyruvate and NADH, are diluted to 2 × working concentration (1 × working concentration: PEP, 10 μM; NADH 1 μM) in 1ml 1 × assay buffer (used for 4 test tubes).

ATP is diluted to 2 mM from a stock solution of 100 mM;

In 250 μl of the above mixture, myosin V is dissolved at ~10 pM from a 0.5 mg/ml stock. PK, LDH and $CaCl_2$ are then added and the solution is mixed quickly and thoroughly by vortexing.

250 μl F-actin solutions is mixed with an equal volume of the above solution and mixed thoroughly prior to observation under 340 nm by absorption spectroscopy.

The reaction mixture is transferred to a 500 μl cuvette and a time scan of the absorption 340 nm is recorded for 5 min at room temperature.

In summary, the final reaction mixture contains ATP, 1 mM; actin, 10 μM; myosin V, 5 pM; Ca^{2+}, ~1 mM; 1 × motility assay buffer. The actin versus myosin molar ratio is 200: 1. A control reaction is performed under the same conditions but without Ca^{2+}.

Note:
The mixing of F-actin and myosin is the last step prior to spectroscopy because the denatured molecule available in the sample crosslink the actin filament and then disturb the diffusion of the components.

The procedure for HMM ATPase assay is the same except the concentration of ATP and actin/myosin molar ratios.

The basic reactions of the ATPase assay are presented in figure 3.6.

a.

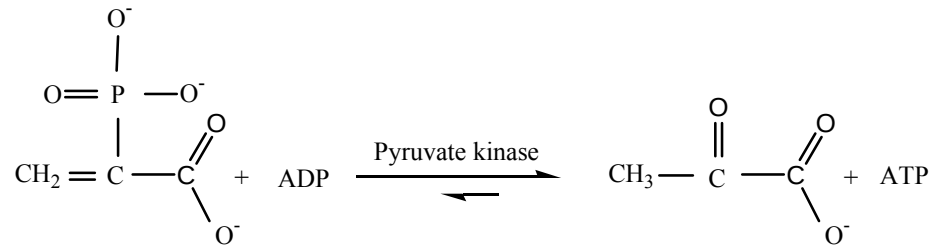

Phosphoenolpyruvate Pyruvate

b.

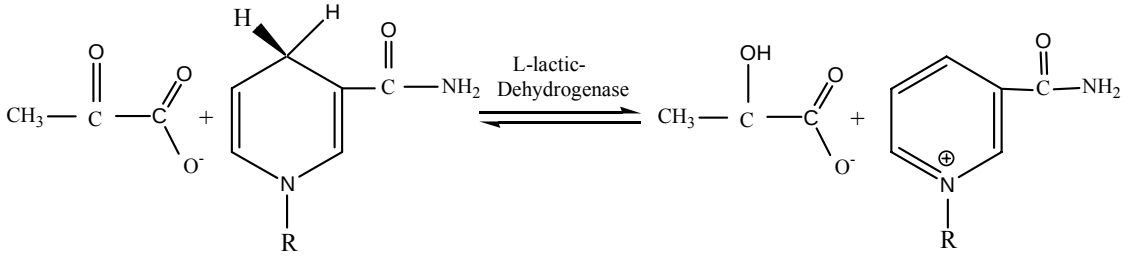

Pyruvate NADH Lactate NAD^+

c.

$$ATP \xrightarrow{\text{Myosin V + F-actin + } Ca^{2+}} ADP + P_i$$

Figure 3.6: Chemical reactions involved in the NADH coupled ATPase assay

3.4 Preparation of polyclonal/monoclonal anti-myosin V antibodies

Antibodies provide a very helpful tool in protein analysis. They enable the specific detection of specific proteins, the analysis of protein distribution and the determination of the molecular structure. The anti-myosin antibodies provide information on the myosin V-actin interaction and thus facilitate various experiments.

3.4.1 Polyclonal antibodies

Polyclonal anti-myosin V antibodies were prepared from immunized rabbits and subsequently purified from anti serum.

Antibodies were purified from antiserum by affinity chromatography over a protein A-Sepharose FF column, 5 × 0.5 cm containing 2 ml medium (Amershan-Pharmacia Product) according to the procedure recommended by the manufactory company.

1. Equilibrate protein A column with 5 volumes of binding buffer (50 mM Tris.Cl, pH 7.2);
2. Load antiserum on column at a flow rate of 5 ml/min, or allow antiserum flow through column by gravity;
3. Wash the column with 3 volumes of binding buffer; discard the flow-through;
4. Elute the antibody using elution buffer (50 mM sodium citrate, pH 3.5 or 2.7, depending on the subtype of antibody);
5. Analyze the eluted fractions by SDS-PAGE and pool those samples containing antibody.
6. Adjust pH to 7.2 since antibody is more stable in neutral environment.
7. Add NaN_3 to a final concentration of 0.02% and then keep antibody solution on ice. Under these conditions antibodies could be kept safely for a few months. For a longer storage, e.g. a few years, it is recommended to aliquot the antibody sample and then keep them at -20 or -80°C.

This procedure was used for polyclonal as well as monoclonal antibodies.
After elution, the antibodies were sampled and assayed by SDS-PAGE electrophoresis. As shown in figure 3.8, the antibody was found at 50 KD and >200 KD under reducing and non-reducing conditions respectively. The purity of the sample was > 95% and free from BSA. The abundance of antibody in different antiserum varies between different preparation. Typically, we obtain a yield around 10 mg from a 100 ml antiserum culture.

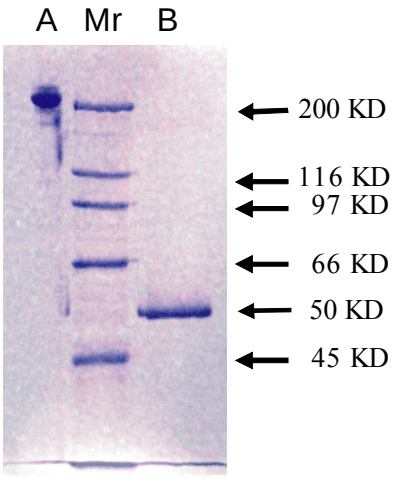

Figure 3.7: SD-PAGE of purified polyclonal antibodies from one liter of antiserum. A. Non-reducing condition; B, reducing condition. Mr. Molecular mass markers (light chains are not contained in this gel.

3.4.2 Monoclonal antibodies

Five monoclonal antibody - producing cell lines were selected out and cultured. The corresponding monoclonal antibodies were then purified and assayed by a variety of immunochemical techniques including ELISA, Western-blotting, neural cell staining et al. A collection of results is shown in table 3.1.

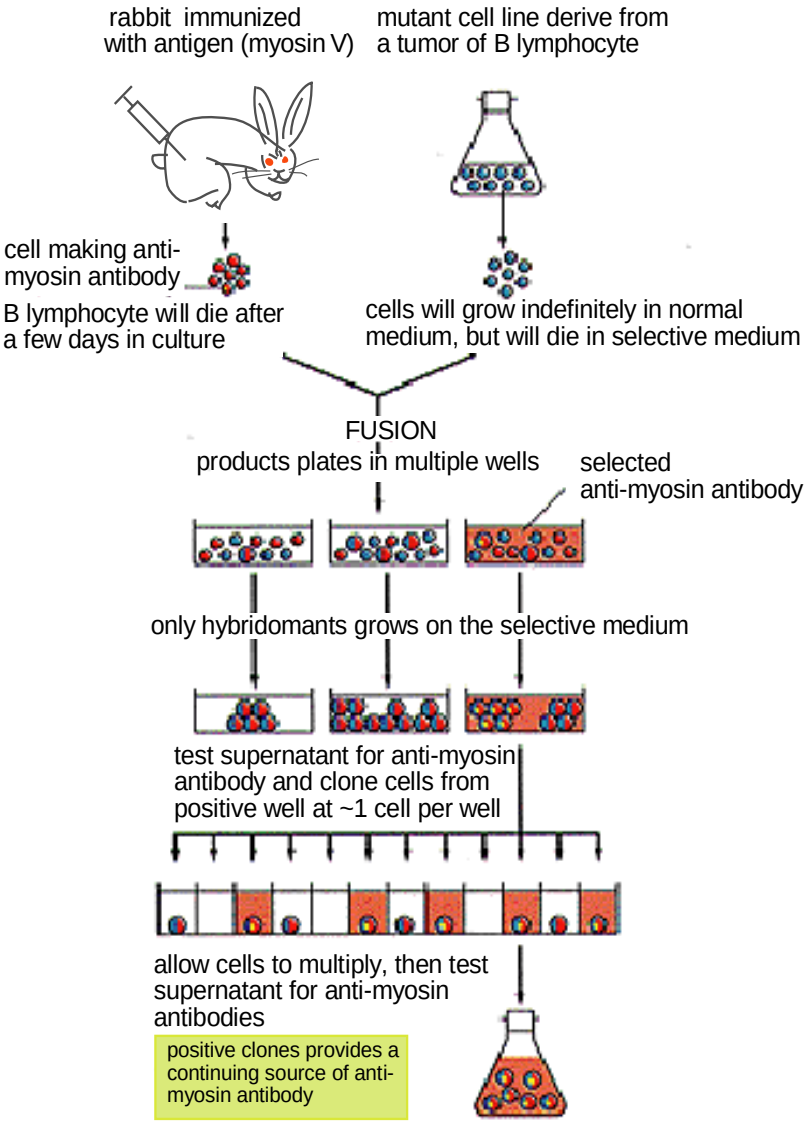

Figure 3.8: Immunization of rabbit and mice. The preparation of the serum from rabbit blood and the production of lymphocyte from mouse spleens was done in the laboratory of Prof. Kaspers at LMU (Ludwig-Maximilians-University of Muenchen). Purification and characterization was done in E22, Physik Dept. of TUM.

Characterization of Monoclonal Antibodies against Chick Brain Myosin V

Nr.	mAB	Ig Isotype	Western Blot	Immunostain*) (rat nerve cells)	Immunostain*) (chicken HD11)	ATPase	Motility Assay
1	5F5	IgG 2a	+++	+	+++	+	+
2	11H4	IgG 2a	+++	+	+++	+	+
3	13E11	IgG2b	+	+	+	+	+
4	15C3	IgG 2a	+++	++	+	+	+
5	15H8	IgG1	+++	+	++	+	+

*) here, intensity was judged in comparison to polyclonal anti-myosin-V-antibodies, set as ++++

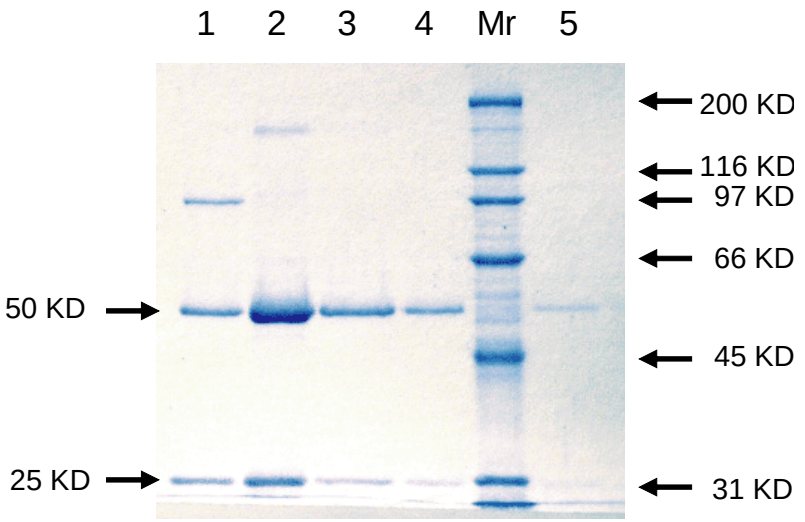

Figure 3.9: Purified monoclonal antibodies (ranging from Nr.1 to Nr. 5) analyzed by SDS-PAGE under reducing condition. Two major bands migrates ~ 50 and 25 KD.

The results show that antibodies are reduced into two fragments with molecule weight of ~50 KD (standing for heavy chains) and ~25 KD (light chains) respectively.

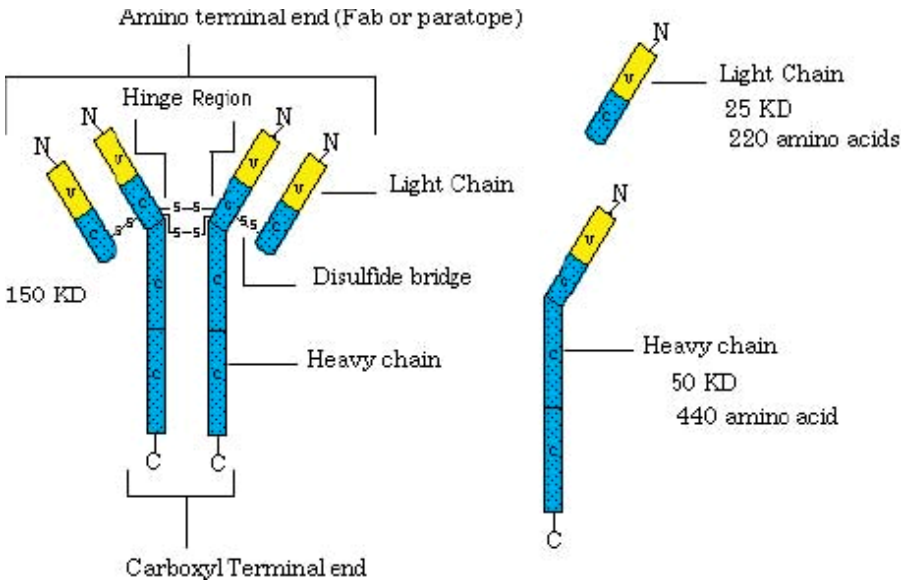

Figure 3.10: Schematic representation of IgG molecular structure. In a SDS-PAGE, IgG migrate at 150 KD or higher in non-reducing condition or in reducing condition under

such condition the heavy chains and light chains dissociated and migrated at the ~50 and 25 KD position, respectively.

3.4.3 Preparation and purification of F_{ab}

Pepsin splits antibodies at the carboxyl-terminal side of the disulfide bonds that hold the two heavy chains together. The $F(ab')_2$ fragment should be 105 KD on an SDS-PAGE gel under non-reducing conditions. The enzymatic digestion results in a fragmentation of the Fc part and then those small peptide pieces are removed by Gel Filtration. For this purpose a prepacked Sephadex G-25 desalting column was used.

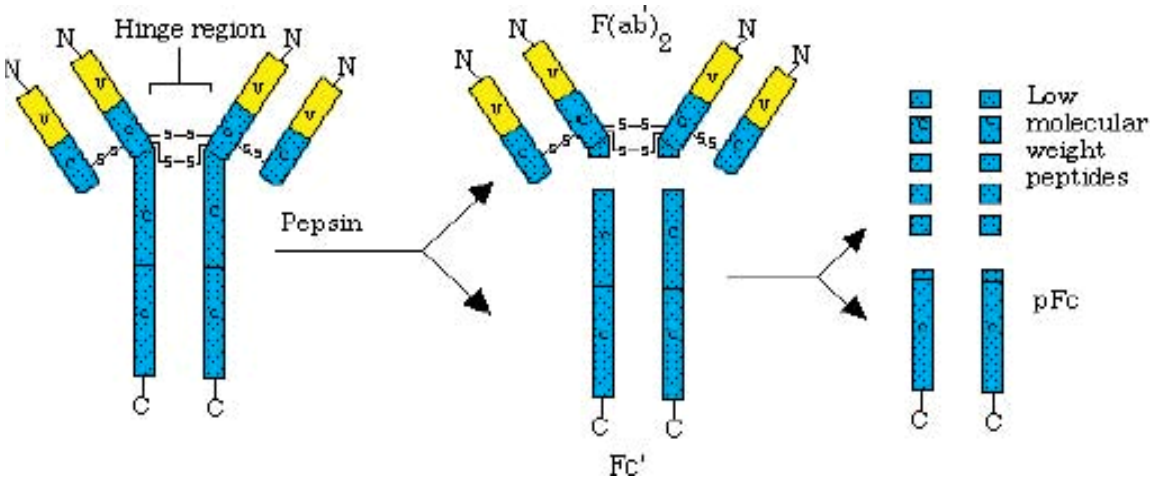

Figure 3.11: Enzymatic digestion of antibody with pepsin results in separated F(ab')2 and Fc. And Fc fragment is normally further digested into small pieces in a prolonged reaction.

Preparation of $F(ab')_2$ by pepsin digestion

1. Monoclonal antibody was concentrated to 6 mg/ml with a Microcon tube, with a cutting molecular weight of 50 KD.
2. The immobilized pepsin was purchased as lyophilized powder (Sigma product). It was hydrated, washed and filtered several times to remove any stabilizers that probably inhibit the enzyme activity.

3. Digestion of antibody 15H8 was performed at 37 °C, in a shaking incubator to keep the resin well mixed. 0.3 ml of hydrated pepsin resin (~ 2 unit of pepsin) was mixted with ~2 mg antibody. The digestion buffer consisted of 100 mM Sodium Citrate, pH3.5.
4. The digested peptide fragments were analyzed by SDS-PAGE analysis. After digestion, the undigested IgG immigrates at 150 KD fraction, $F(ab')_2$ 105 KD, while the Fc fragment was extensively degraded into small pieces.

5. Purification of the digested product. The mixture was filtered to remove the immobilized pepsin, and then IgG and Fc fragments were removed by a protein A funtionized column. As the last step, the flow-through from the protein A column is collected and concentrated to 0.5 ml before a GF chromatography by using Sephadex G25.

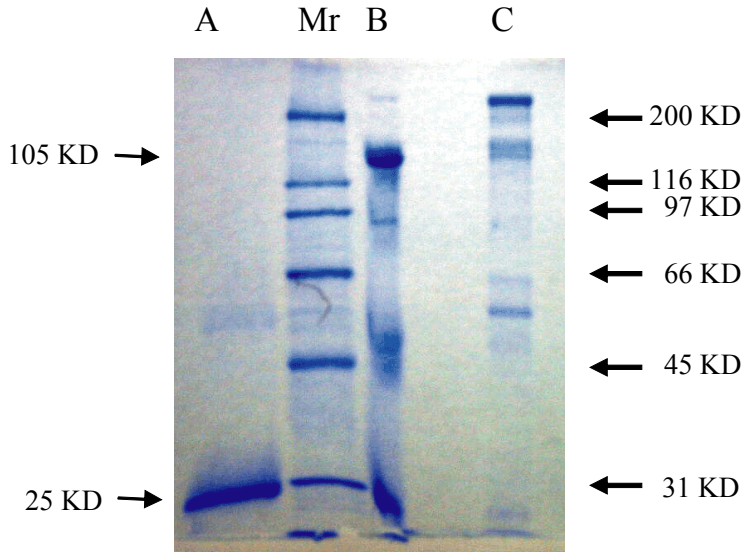

Figure 3.12: SDS-PAGE analysis of $F(ab')_2$ and intact Ab Nr. 5. A, $F(ab')_2$ under reducing condition; B, $F(ab')_2$ no reducing condition; C, intact antibody under no reducing condition.

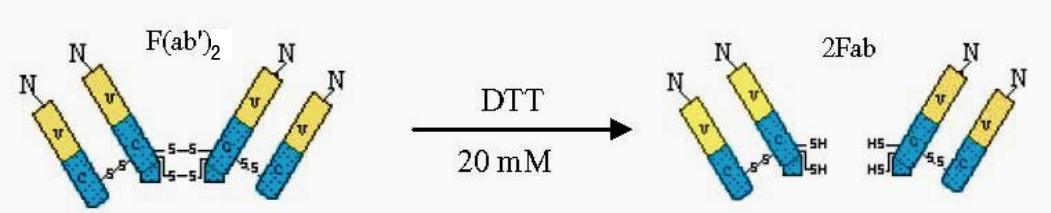

Figure 3.13: Selective reduction of $F(ab')_2$ with DTT results in free -SH groups at the carboxyl terminal end of F_{ab}.

Procedure of F_{ab} purification:

The $F(ab')_2$ is treated with a reductive buffer under Argon atmosphere:
DTT, 20 mM; NaCl, 100 mM; Borate, 100 mM; Citrate, 50 mM; EDTA, 2 mM; pH 4.5.
This buffer is intensively degassed prior to addition of DTT.

After incubation at room temperature for 90 min, the reduced F_{ab} is purified by gel filtration chromatography with Sephadex G25 by using coupling buffer.

As even traces of remaining DTT could disturb the subsequent reaction, the elution fraction must be cut sharply. Here we used a desalting column containing 5 ml medium of Sephadex G25 (Pharmacia Product). The sample volume was adjusted to 0.5 ml by using a Centricon tube before passage through the column.

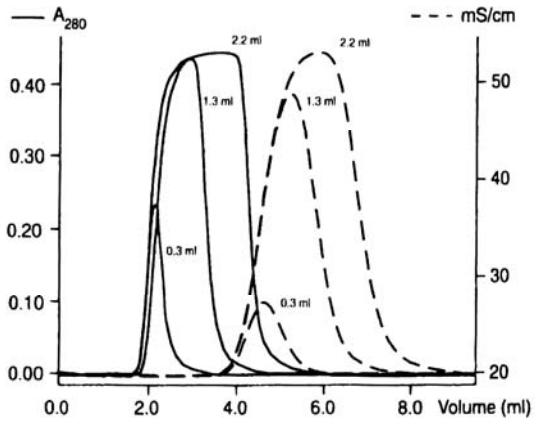

Figure 3.14: The effect of different sample volumes on the HiTrap Desalting column using a syringe for sample injection.

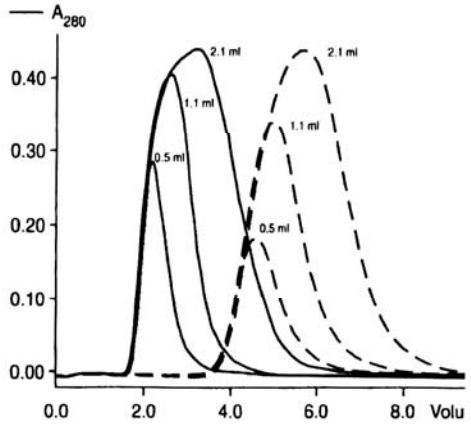

Figure 3.15: The effect of different sample volumes on the HiTrap Desalting column using tubing loops for sample injection.

The effects of sample volumes and instruments for injection in buffer changing procedures are shown in figure 3.14 and 3.15. To confirm such effects, the following control experiment was performed. The BSA solution at a concentration of 1 mg/ml was used for test. And the distribution in the eluted fractions is analyzed by SDS-PAGE. This result provides a reference for the buffer changing step where F_{ab} is concerned.

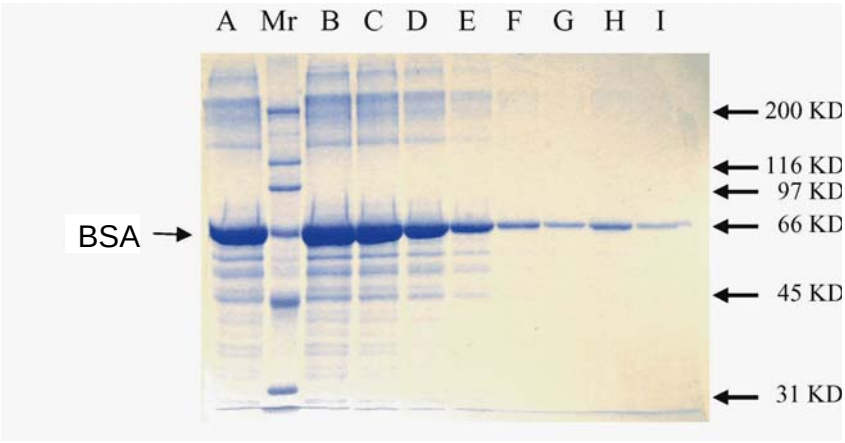

Figure 3.16: SDS-PAGE analysis of eluted fractions. A, 0-135 µl; B, 135-270 µl; C, 270-405 µl; D, 405-540 µl; E, 540-675 µl; F, 675-810 µl; G, 810-945 µl; H, 945-1080 µl; I, 1080-1215 µl; Loaded sample was 300 µl BSA solution, 1 mg/ml.

As shown, BSA sample was found in the very beginning eluted fractions, 0-135 µl or even earlier (Data not shown). The BSA concentration peak is estimated to appear at 250 µl. In actual purification in the case of F_{ab} fraction A-D were pooled and used for subsequent reactions. The dilution factor was ~1.5.

3.5.1 Actin

Actin was prepared from rabbit muscles according to Pardee and Spudich with an additional gel filtration step (S-300 HR column). For a stable storage of G-actin, Actin is kept in a G-buffer where ATP and Ca^{2+} instead of Mg^{2+}, as stabilizers. ATP could help the stability of Actin where Ca^{2+} prevents self-polymerization. A typical reaction system as follow routinely results in a good preparation of F-actin from a G-actin 5 µM, (125 µl) was as follows:

H_2O:	89 µl
F-Buffer 10 ×:	12.5 µl
G-actin (5 µM):	17.5 µl (26.25 µg)
Phalloidin-Rhodamine (1 mM):	6 µl
Total volume:	125 µl

Note: The reaction substrates are added into a 0.5 ml Eppendorf tube in the order indicated. Phalloidin-Rhodamine solution is added at the end and was carefully pipetted under the surface of the solution which was well mixed. Then the solution is either kept at room temperature for 2 hours or overnight and was protected from light with a piece of Aluminum foil. From our experience better actin integrity could be obtained by doing so.

3.5.2 Silicon/glass based gold array

In an example the structure of a gold array based on a silicon slide is shown schematically in figure 3.18 and 3.19. Here gold dots are arranged in rings. The border of the ring consists of three layers of gold dots with a diameter of 5 nm and a regular distance of 60 nm between the dots. We used two kinds of arrangement of the defined rings where the diameter of the ring is set to 1.5 or 2.5 μm while the distance between the gold dots ring is 2.5 or 1.5 μm respectively.

With these parameters, it is easy to deduce the number of gold dot in a ring with a diameter of 1.5 μm to ~730 by application of the equation of $N=2\pi r/d$ where r is the radius of the dot and d is the distance in between gold dot. The size of the gold dot and that of these ligands bound to them are compared in table 3.3.

Table 3.3: A comparison of sizes of ligands and gold dot

	Molecule Weight (KD)	Estimation of Size
Gold dot	/	5 nm (diameter)
G-actin	42	~3.3 ×5.6 ×5.0 nm *[1]
Proten A	42	~3.3 ×5.6 ×5.0 nm*[2]
Antibody (IgG)	150	~5 × 4 × 9 nm*[3]
F_{ab} fragment	50	~3 × 4 ×8 nm*[4]
Myosin V	~560	~4 × 4 × 90 nm*[5]

*1 Kabsch, 1990; *2 estimated by *1; *3 estimated by *4; *4 M. Egger, 1990; *5, Burgess et al., 2001.

As the comparison the size of a single gold dot is 5 nm is so small that it probably interacts only with a single molecule such as antibodies, or myosin. The interaction between a gold dot and a peptide ligand could be hydrophobic interaction. In figure 3.18, the back side of the gold array/silicon is shown. The gold dot array locates in the center of the silicon surface with a size of 20 × 20 µm. To locate the array area by microscopic observation, several scratches are marked on the backside. In the center of the red cycle there is the gold array and at the right side is an orientation mark. These marks are very helpful in the actual handling with a reverse microscope.

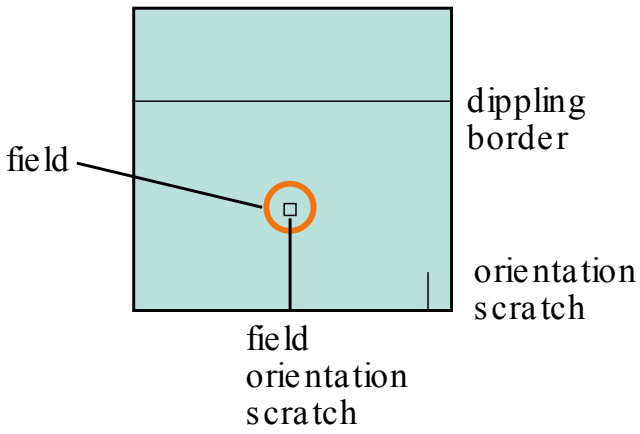

Figure 3.18: The backside of a silicon chip with a gold array.

In figure 3.19, the scheme of array is illustrated. There are two different sizes with respect to the ring diameter and the space size of the rings. This size is critical as it provides a well-defined ligand binding pattern. The total possible binding sites over the surface is decided by the distance parameters (a, b, c and d).

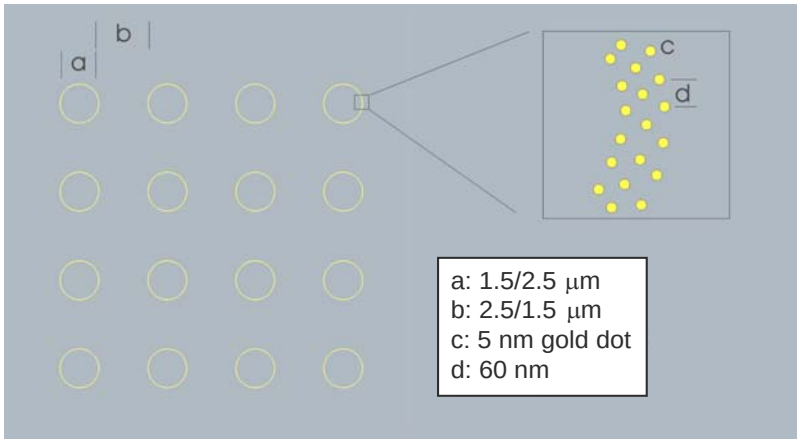

Figure 3.19: A well defined gold dot array on a silicon base (Jaquce, 2003).

3.5.3 Lipid monolayer

Preparation of fluid bilayer membrane-coated glass slides

1. Small Unilamellar Vesicles (SUV's; diameter < 100nm) 100-200 µmol with e.g. DMPC or SOPC.

2. Clean the glassewares by sonifying with Hellmanex and water and rinse thoroughly with millipore water in between (1 × H + 10 × water; 1 × H + 10 × water; 1 × water + 10 × water; 1 × water + 1 × water at least). Afterwards dry them overnight in the vacuum chamber.

3. Coat the glasses for 1.5 to 2 hours by flushing the clean and dry glasses with the SUV solution.

4. Wash the still adhered vesicles away by flushing them with buffer at high speed.

(This work was contributed by Christian Daniel, E22)

3.5.4 Fluid vesicle decorated by F_{ab}

The procedure to construct a lipid bilayers coupled with F_{ab} consisted of the following steps:

1. Lipid molecule activation and purification
2. Preparation of F_{ab} in reduced state
3. Construction of lipid monolayer on a cover glass
4. Preparation of lipid vesicle
5. Coupling reaction between vesicles and F_{ab}
6. Lipid vesicle-F_{ab} forms the second layer by diffusion over the monolayer.

In figure 3.22, a schematic structure of the lipid molecule coupled with a F_{ab} fragment is shown. The estimated size of the molecule is indicated. (Ph.D thesis of Martin Egger)

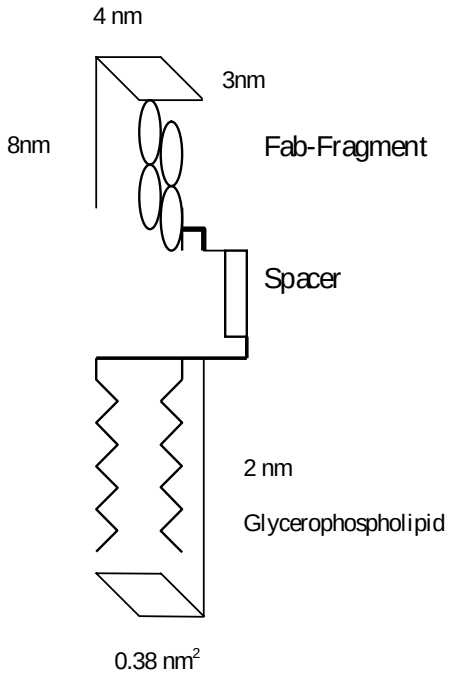

Figure 3.20: Schematic structure of a lipid molecule decorated with F_{ab} with approximated size indicated (this figure is from the Ph.D thesis of Martin Egger).

3.5.4.1DPPE activation:

1. Dissolve 10 µmol DPPE (~6.9 mg) in 6 ml $CHCl_3/CH_3OH$ (9:1; V:V), add 20 µmol of dry triethanolamine (2.7 µl) to keep amino groups deprotonated.
2. Dissolve 12 µmol MBS, or MPB in 500 µl $CHCl_3/CH_3OH$ solution and pipette it into the lipid solution.
3. Stir at room temperature in Argon atmosphere for 5 hours.
4. After the reaction is completed, dry the solution by N_2 stream and put it into vacuum overnight.
5. Take up the residue in 1 ml chloroform and extract one time with PBS buffer (pH 7.5), then twice with degassed H_2O.
6. Further purification by PLC (preparative layer chromatography) on silica gel with chloroform/methanol/acetic acid/H2O (60:50:1:4 V: V) as running solvent, with a spot of DPPE as control.
7. Scratch UV-visible band (UV 256 nm) moving ahead of DPPE from plate, put this on top of a small silica column, and elute with 12 ml Chloroform/Methanol (9:1).
8. Evaporate with help of N_2 stream to complete dryness and then freeze-dry at -20 ℃.
9. Take up the residue in as much chloroform as to reach a calculated final concentration of 10 mM; store aliquots in glass ampoules at -20 ℃.
10. Check purity and identity of the activated lipid by TLC and spraying reagents

a) Phosphate (molybdenum)
b) Free amino groups (ninhydrin)

TLC analysis of activated DPPE
Running solution: Chloroform: methanol: water (65:25:4, v: v: v)
The TLC plate was firstly cleaned in the running solution and then dried with warm air.

Drop 1 µl DPPE (dissolved in chloroform at a concentration of 1 mg/ml) solution and mark the position.
And then immerse the bottom of the slide into TLC solution. Keep the TLC device from open air. Allow the front reach a height 0.5 cm from the end of the slide and then stop it

by drying with warm air.

Spray the detection reagent onto the silica gel layer and dry it after that.

For phosphate group detection, molybdenum acid solution was used for spraying and then the slide was dried and heated by an air heater until phosphate containing dot turns blue.

For free amino group detection, ninhydrin solution (in butanol) was used and the procedure was the same as for the determination of the phosphate group detection.

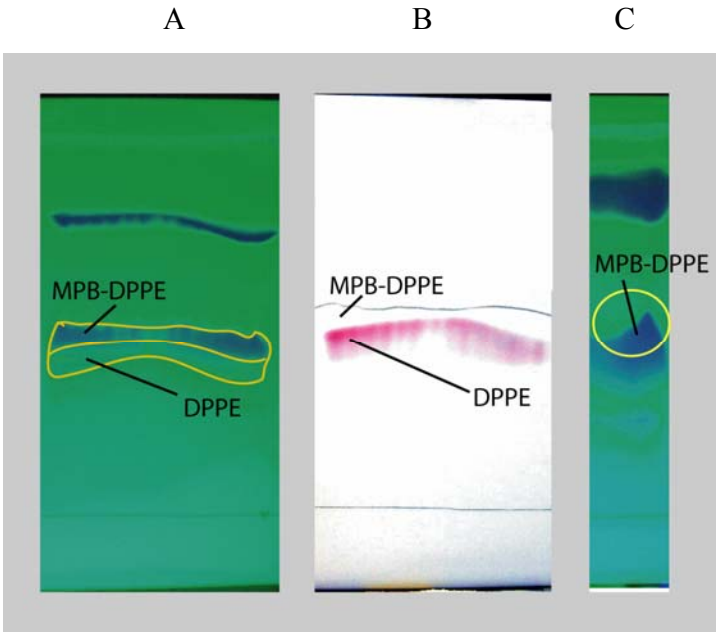

Figure 3.21: The resolution of activated DPPE (MPB-DPPE) (A) and DPPE on PLC plates. These photos were taken at UV 256 nm illustration which visualized the lipd bands in dark blue. Picture B shows the distribution of the free amino groups of DPPE after nihydrin spraying. From the comparison of photo A and B, one could find that the DPPE fraction trailed directly to the MPB-DPPE fraction but was not visible under UV 256 nm. With respect to such a distribution, the dark blue area in the yellow cycle (photo C) was taken for further purification

In figure 3.21, the resolution of activated DPPE by MPB is illustrated in a PLC. The purified MPB-DPPE is analyzed by TLC in figure 3.21.

In the PLC, the difference in moving velocity betweenMPB-DPPE and DPPE was small so that intensive care must be taken to assure the purity of MPB-DPPE.

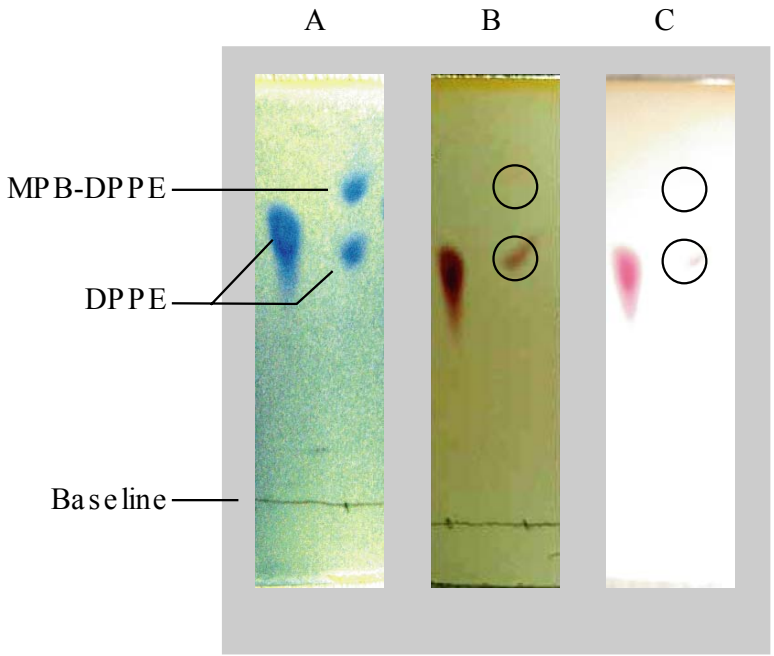

Figure 3.22. Phosphate group (A) and free amino group (B): substrate from reaction mixture; C: Purified MPB-DPPE) detection revealing that DPPE was removed during purification steps.

3.5.4.2 Incorporation of activated DPPE into lipid vesicles coupling of F_{ab}

About 1.2 mg of MPB-DPPE obtained by the procedure described above was dissolved in chloroform to a concentration of 0.1 mg/ml. Matrix lipid, DMPC dissolved in chloroform at a calculation of 0.1 mg/ml was mixed with MPB-DPPE at a ratio of 8:1. And then the

mixture was evaporated in N_2 stream in room temperature and further dried under vacuum at -40 ℃.

Conjugation buffer (0.01 M HEPES, 150mM NaCl, pH=8.0) was added to the dried lipid mixture followed by a 2 hours incubation under Argon protection at 37 ℃. Then the mixture was sonicated until it became clear. This procedure takes a few minutes at 25 mA, 25% pulse. The mean size of vesicles obtained by in this way was estimated to be ~50 nm. This vesicle solution was used for conjugation for the coupling of F_{ab}-fragment prepared as described below. The total lipid concentration in the final solution was 3 mM.

The $F(ab')_2$ fragments were split into monovalent $F_{ab'}$ fragments by selective reduction:

1. ~ 2 mg $F(_{ab'})_2$ was dissolved in 0.1 M citrate buffer containing 100 mM NaCl, 2 mM EDTA at pH 4.8. The final concentration was 10 -20 mg/ml (~200 µl).
2. A freshly prepared DTT solution of 1 M was added (in dropwise) under slight stirring up to a final concentration of 20 mM DTT, and the reaction vessel was flooded with argon.
3. After a reaction time of 90 min at room temperature, the solution containing the F_{ab} fragments (~250 µl) was loaded on a 5 ml Hitrap column equilibrated by coupling buffer, and the first 0.5 ml of eluted sample (containing ~1.5 mg F_{ab}) was added directly to the vesicle suspension.
4. The mixture was incubated under condition stirring for 6 hours under protection of Argon at 30 ℃.
5. To make the vesicle visible, a small portion of Bobityl labeled DPPE (used at 0.5%) could be added to the lipid mixture before the reaction.

Note:
Freshly reduced F_{ab} was also used for deposition on gold arrays. The free -SH groups of the F_{ab} fragments undergo a strong interaction with gold particles by forming S-Au bonds.

3.5.4.3 Oberservation F-actin bound to fluid lipid bilayer

Different from the flow cell used in normal motility assay, the observation of lipid bilayers supported motility assay needs special reservoir as shown in figure 3.25

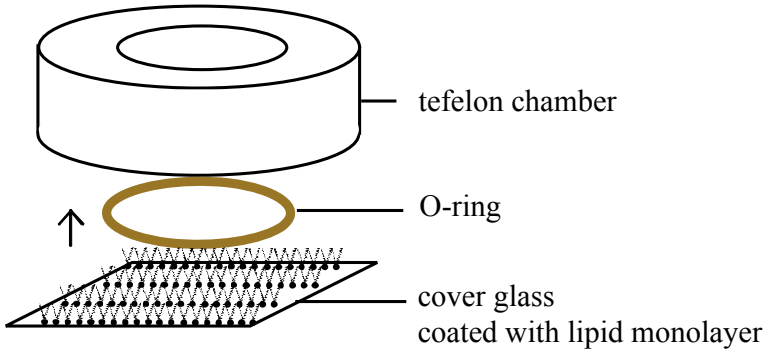

Figure 3.23. This set-up contains a reservoir with working volume of ~0.5 ml. At the bottom, a rubber O ring is used to seal the reservoir together with cover glass coated with lipid monolayer.

First the cell was assembled by using the reservoir, O ring and a piece of lipid monolayer coated cover glass and then tightened and incubated with 0.5 ml motility assay buffer. Then the F_{ab}-vesicle solution was added directly into the cell. After a few minutes of incubation, the homogeneity of the film was checked by observation under microscope.

BSA at a concentration of 0.1 mg/ml was added to the formed lipid bilayers to prevent the unspecific binding of actin filament. Buffer changing was performed after each addition of new solution to remove excess reaction substrates.

Myosin V was diluted from stock solution with 1 × motility assay buffer at a concentration of ~0.01-1 µg/ml and added to the cell. After an incubation of 5 minutes, excess myosin V molecules are removed by intensive rinsing with buffer.

F-actin was diluted to 5 pM from a phalloidin stabilized stock solution of 5 mM in 1 × motility assay buffer and then added into the solution. The mixture was incubated for

another 5 minutes. During this incubation, the cell was transferred to the microscope for observation of F-actin binding.

ATP (0.5-1 mM) was added as the last step. Upon the addition of ATP, actin filament was observed to move spontaneously.

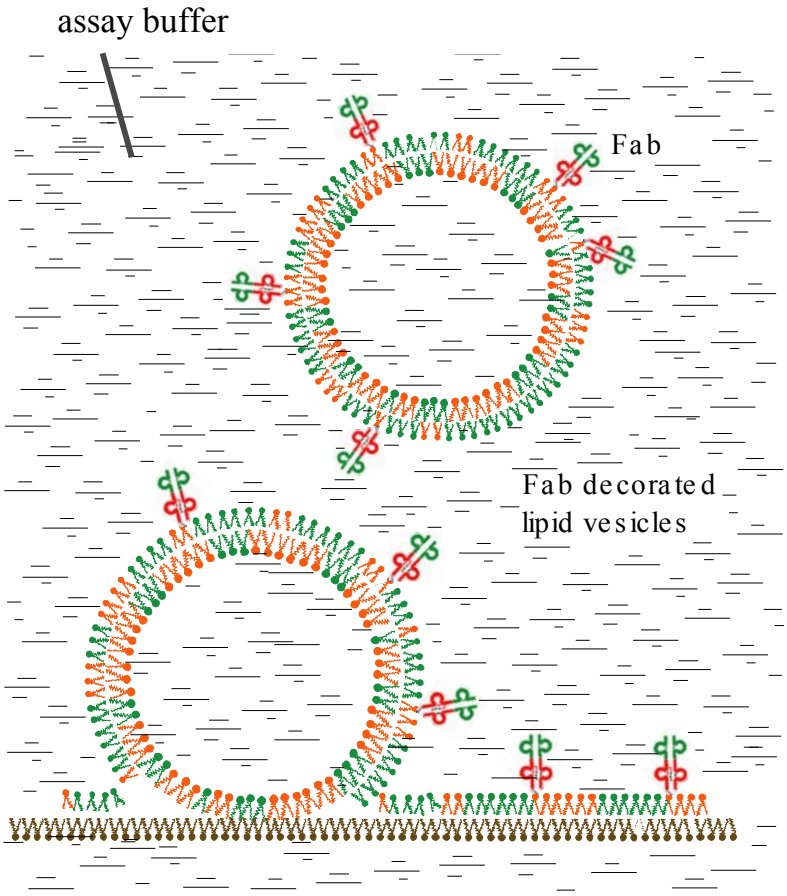

Figure 3.24: Schematic illustration of the fusion of F_{ab} decorated lipid vesicles after deposition on lipid monolayer. The orange part of the vesicle indicates the MPB-DPPE while the green part indicates DMPC that was used as matrix. The brown layer shows the lipid monolayer that was consisting of SOPC and DMPC at a ratio of 1:1.

3.6 Fluorescence microscopy

A schematic view of the fluorescence microscopy is shown in figure 3.27. In the following the details of the set-up comprising the microscope set, the light-filter system and the data processing unit is described.

The microscope (Axiovert 200 Zeiss Overkochen) is either equipped with a 100 × or 63× oil objective (plan-Neofluar).

The light source is provided by an Atto Arc 2 (100 W, Osram). These samples are stained either by Tetramethylrodaminisothiocyanat (TRITC; excitation peak 540-545 nm, emission peak 570-573 nm) or by Fluoresceinisothiocyanat (FITC; excitation peak 495 nm, emission 513 nm). For observation band pass filters of 546 ± 12 nm for TRITC or 450-490 nm for FITC were used.

The data processing unit consists of a fast image grabbing device-CCD camera (Orca ER, Hamamatsu; Herrsching), that could collect images of size of 672 × 512 pixel at rate of 10-25 pictures/s and a personal computer (2 Pentium III 850, 512 MB RAM, 4 Maxtor 80 G hard disk in 4+0 raid array, et al.) that could support a continuous data transfer rate ⩾ 24 MB/s.

The software for data processing was developed by VC++ 5.0 and named ‘open box’. It was designed for Windows NT 4.0 and compatible with later Windows operating system (Keller M., 2003; Schilling J., 2003).

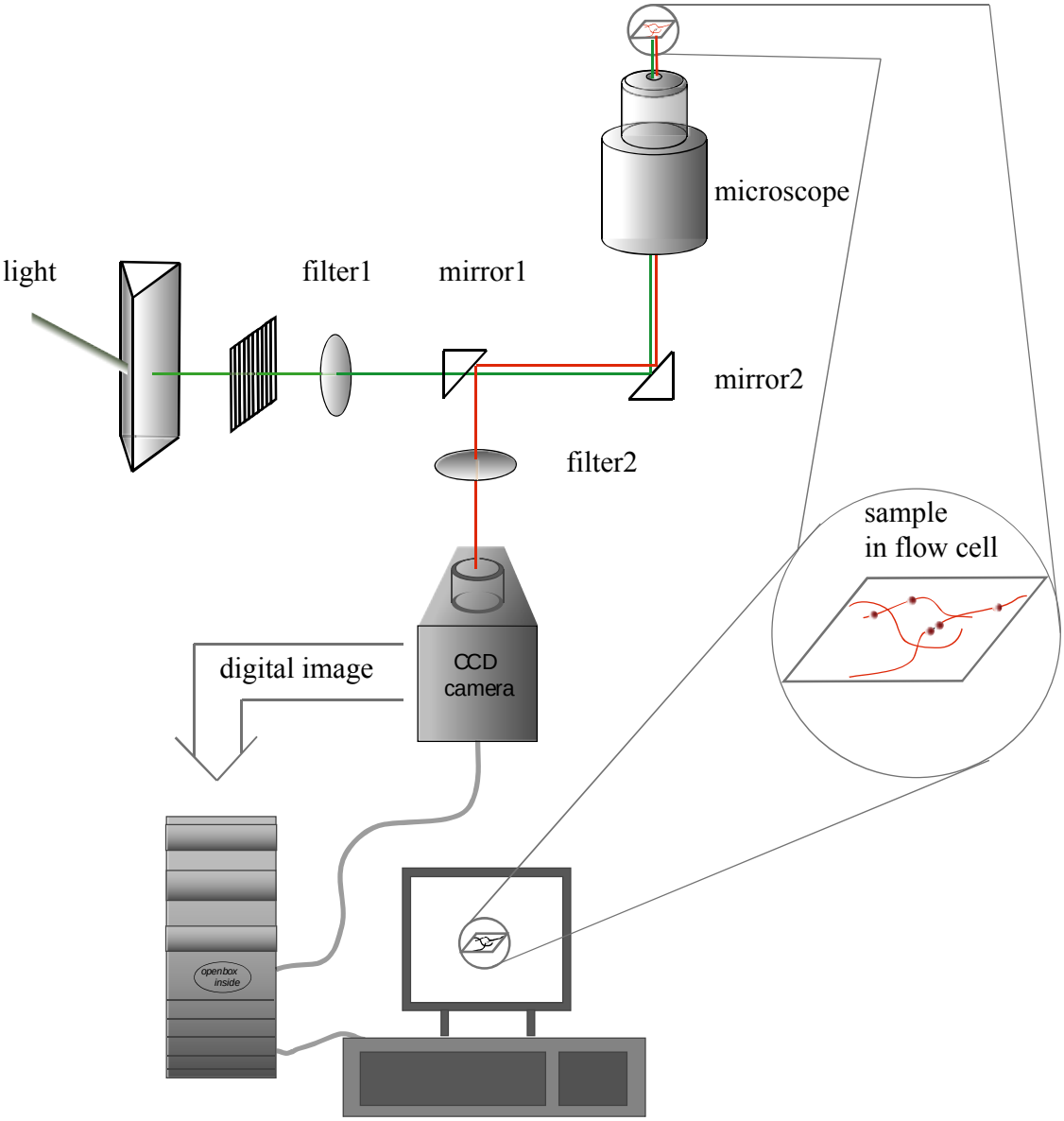

Figure 3.25: Schematic view of the fluorescence microscopy set-up.

4 Results and discussions

4. 1 ATPase tests

4.1.1 ATPase assay with heavy-meromyosin II (HMM)

A series of control experiments were done to compare the ATPase activity of HMM under various actin versus HMM ratios and ATP concentration. The moler ratio of actin versus HMM varied from 50:1 (figure 4.1 a, b) to 100:1 (figure 4.1, c, d, e) while the ATP concentration varied from 10 to 1.0 mM (figure 4.1 a to e).

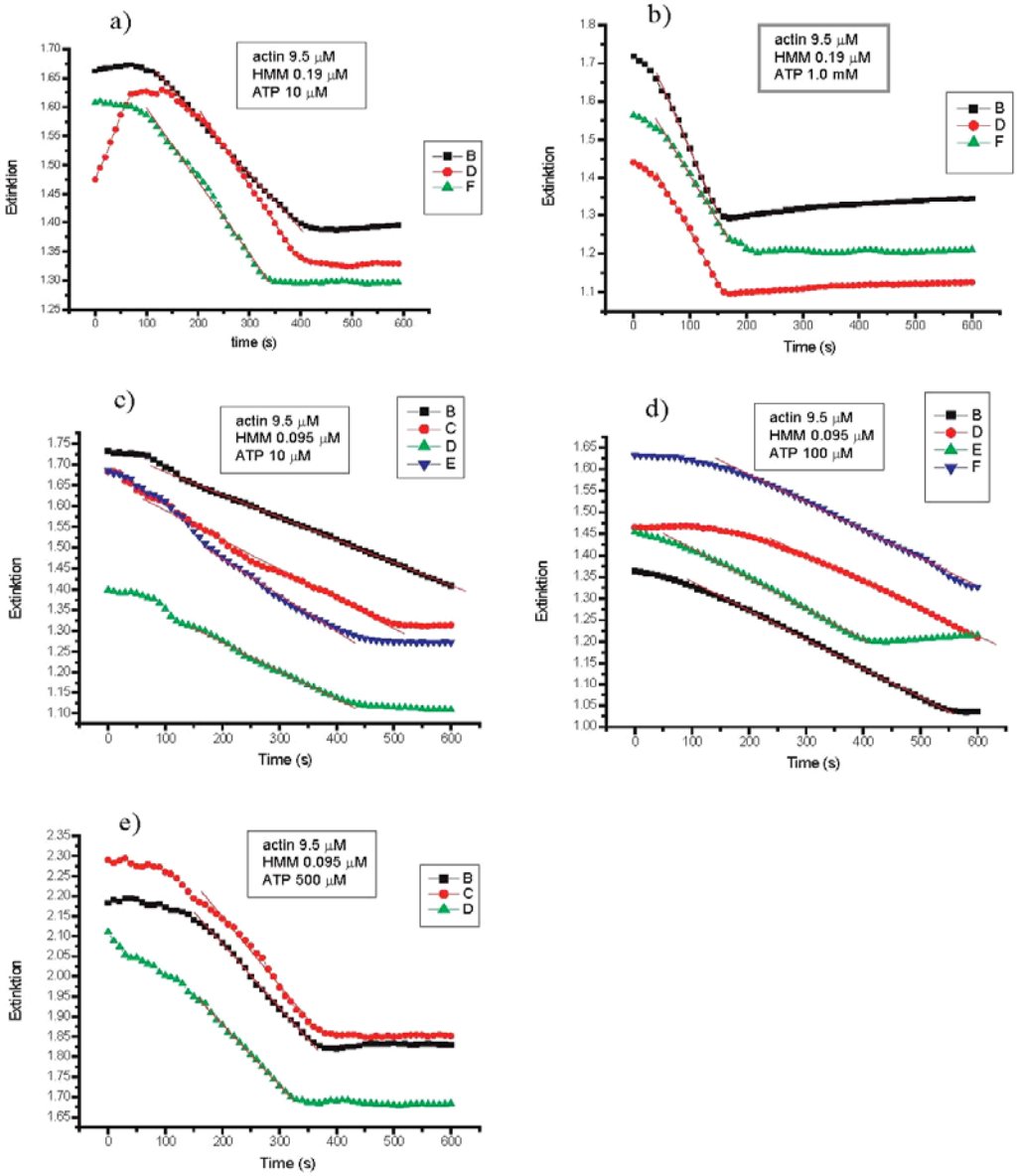

Figure 4.1: ATPase assay with HMM.

The results are summarized in table 4.1. It is seen that the optimimal concentration of ATP is ≥500 μM and of the actin/HMM moler ratio ≥100: 1.

Table 4.1: Results from HMM by using NADH coupled ATPase assay

Actin (μM)	HMM (μM)	Actin/HMM Molar ratio	ATP (μM)	K_{cat} (s^{-1})
9.5	0.19	50 :1	10	1.0
9.5	0.19	100 : 1	1000	2.4
9.5	0.095	100 : 1	10	1.10
9.5	0.095	100 : 1	100	1.12
9.5	0.095	100 : 1	500	2.71

4.1.2 ATPase test with myosin V:

The condition for the assay for myosin V is the same of those for the control experiments with HMM. The molar ratio of actin versus myosin V was 200: 1, the ATP concentration was 1 mM and the Ca^{2+} concentration 1 mM.

The turn-over rate found for myosin V is measured to be ~ 7 ATP.$head^{-1}$.s^{-1}. This value is close to the values reported in the literature which range from 3.3 (Trybus et al., 1999) to 12-15 $head^{-1}$ ATP.s^{-1} (De La Cruz et al., 1999). Comparable results were found for single bead transport test based on fluorescent microscopy. In this test the ATPase activity is determined from the velocity of single myosin V coupled to bead a value of ~4.5 ATP. $head^{-1}$. s^{-1} was found by motility assay according to the velocity which is ~ 300 nm.s^{-1}.

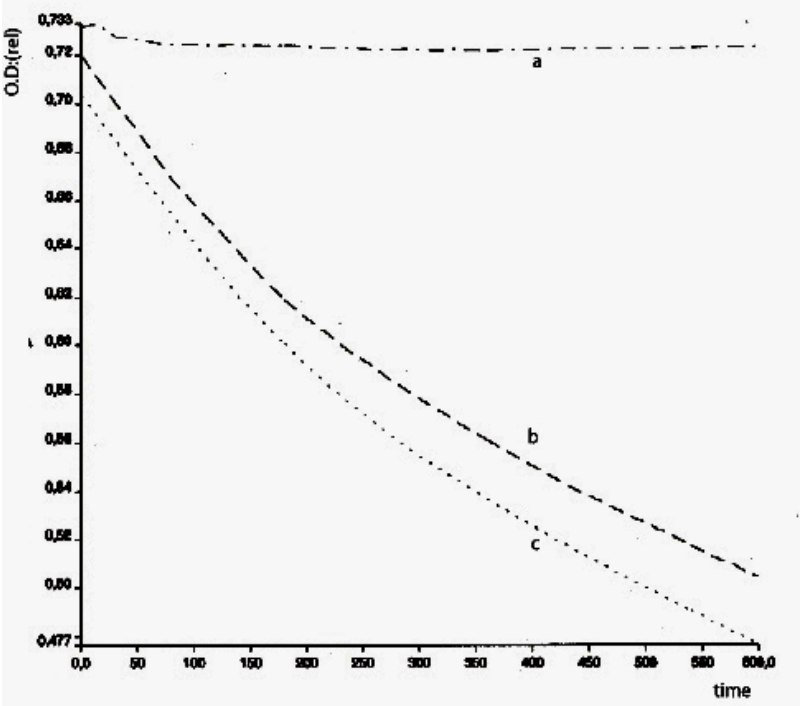

a) ATP-turnover number: 0.02 s^{-1}
actin/myosin V = 100; Ca^{2+} free
b) ATP-turnover number: 7.4 s^{-1}
actin/myosin V = 100; Ca^{2+} 1 mM
c) ATP-turnover number: 6.7 s^{-1}
actin/myosin V = 200; Ca^{2+} 1 mM

Figure 4.2: ATPase assay with myosin V. a), ATPase assay in absence of Ca^{2+}; b), c), ATPase assay in presence of Ca^{2+} at actin/myosin ratios between 100 and 200.

Ca^{2+} dependence:

An important result is the finding that the ATPase function of myosin V is strongly regulated by Ca^{2+}, as shown in figure 4.2. It agrees with previous reports (Homma, K., 2000) When Ca^{2+} is absent, myosin V exhibits little ATPase activity (~0.02 $head^{-1}$ $ATP.s^{-1}$). The ATPase activity increases by a factor of 300 to a value of ~7 $head^{-1}$ $ATP.s^{-1}$

after addition of Ca^{2+} between 3.0 µM -1.0 mM (Figure 4.3). The molecule mechanism of the effect is largely unknown but it is likely that the Ca^{2+} causes dissociation of light chains (LCs) from the heavy chain (HC) of myosin V. Cosedimentation showed that the fraction of the dissociated LCs is estimated to be ~27-32% (or 1.3 CaM per heavy chain) (Nascimento A.A.C et al., 1996) at 1 mM of Ca^{2+}.

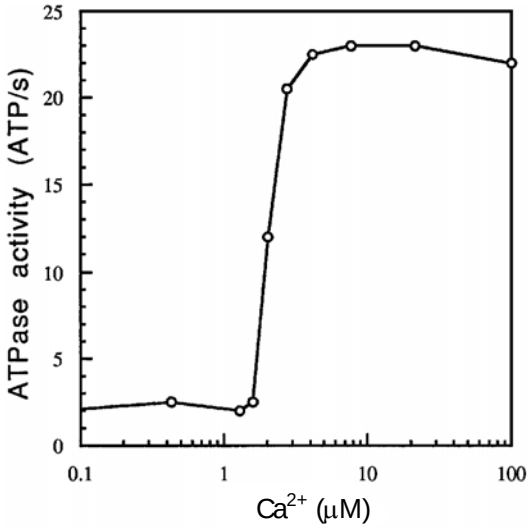

Figure 4.3: Ca^{2+} in the µM range stimulates the actin-activated ATPase activity of myosin V. It seems that Ca^{2+} has a strong effect on the ATPase activity within a narrow concentration range from ~1 µM to 3 µM. The half maximum activation is 1.8 µM (this figure is from Nascimento A.A.C et al., 1996).

The effect of Ca^{2+} seems to be contradictory between the results of the ATPase test and the motility assay where the presence of Ca^{2+} leads to a slower sliding rate or even suppression of actin sliding (Cheney et al., 1993). Concerning this effect, the dissociation of LCs seems to hinder their strict regulation on the HCs. Without this regulation, the HC appears to recover its strong ATPase activity. In the presence of excess calmodulin, the suppressed actin sliding could be restored by LC dissociation caused by Ca^{2+} (Cheney et al., 1993).

An interesting question is the relationship between LC binding, power stroke and ATPase. It appears that the partial dissociation of LCs from HC leads to higher ATPase activity but umcomplete power stroke function. Recent studies showed that the number of the bound LCs on the HC affects the processivity of myosin V. Studies of the recombinant myosin V containing a truncated neck domain which consists of one (De La Cruz et al., 1999, De La Cruz et al., 2000a, De La Cruz et al., 2000b) or two (Trybus et al., 1999) instead of six LC binding domains (Wang et al., 2000) showed the walking process is impeded. The mutation containing four LC binding domains maintains processivity but a shortened step size of ~24 nm while the mutation containing two LC binding domains is not processive. This highlights the importance role of LC for the regulation of the processive behavior of the myosin V molecule.

In this ATPase assay, the ADP is generated by ATP hydrolysis by myosin V and converted back into ATP by phosphoenopyruvate with the effect that the ADP inhibition is minimized. ADP is a strong inhibitor of ATPase activity of myosin V. In the ATP catalytic cycle, the ADP dissociation is the limiting rate that is around 11.5-14.5 s^{-1} even when myosin is bound to actin filament (Trybus et al., 1999; Wang et al., 2000). Compared to ATP hydrolysis rate >250-750 s^{-1} and P_i release rate >250 s^{-1} the ADP releasing step is extremely slow. This kinetic adaptation of myosin V facilitates a high duty ratio (~>0.7) under physiological conditions (high actin concentration) that is required by processive myosin.

Due to the inhibition by the product ADP, the ATPase activity of myosin V decreases sharply as the ADP accumulates. The skeletal myosin is less sensitive with respect to an inhibition. In the ATP/F-actin/myosin mixture, skeletal myosin might cause ATP depletion while myosin V does not. As found in separated experiments attempting to construct a dynamic interaction system consisting of skeletal myosin and actin filament, the system undergoes an increase of viscosity due to ATP depletion caused by the myosin II ATPase activity. While in the case of myosin V, such a transition was only observed with the help from other ATPase-Apyrase which hydrolyzes ADP as well.

4. 2 Detection of the binding sites of anti-myosin V antibody

The determination of the binding sites of anti-myosin V antibody on myosin V molecule was one of the major questions of the work. For this study five distinct monoclonal antibodies available. This analysis was done by combination of proteolysis enzymatic digestion and western blotting techniques.

First the myosin V molecule is digested intensively and then the resulted fragments are separated according to their molecule weight by SDS-PAGE. The selectional proteolysis enzymes were chosen based on the evaluation on the primary sequence of myosin V (which is obtained from protein data bank).

Since Myosin V is composed of two identical HCs and ~14 light chains. The quesiones to be answered by binding site detection are:

- whether or not the binding site is located in the light chains?
- provided the binding sites are located at the HCs where is the domain located?

The following showes the primary sequence of Chicken brain myosin Va with thrombin cleavage sites highlighted. (The data is from protein databank swiss-port; the cleavage site information is from the enzyme provider)

SQ SEQUENCE 1829 AA; 212381 MW; 0538B278DFC09F6E CRC64;

The sequence of myosin-Va:

MAASELYTKY ARVWIPDPEE VWKSAELLKD YKPGDKVLQL RLEEGKDLEY[50] CLDPKTKELP
PLRNPDILVG ENDLTALSYL HEPAVLHNLK VRFIDSKLIY[100] TYCGIVLVAI NPYEQLPIYG
EDIINAYSGQ NMGDMDPHIF AVAEEAYKQM[150] ARDERNQSII VSGESGAGKT VSAKYAMRYF
ATVSGSASEA NVEEKVLASN[200] PIMESIGNAK TTRNDNSSRF GKYIEIGFDK RYRIIGANMR
TYLLEKSRVV[250] FQAEEERNYH IFYQLCASAA LPEFKTLRLG NANYFHYTKQ GGSPVIDGID[300]
DAKEMVNTRQ ACTLLGISDS YQMGIFRILA GILHLGNVEF ASRDSDSCAI[350] PPKHDPLTIF
CDLMGVDYEE MAHWLCHRKL ATATETYIKP ISKLHAINAR[400] DALAKHIYAN LFNWIVDHVN
KALHSTVKQH SFIGVLDIYG FETFEINSFE[450] QFCINYANEK LQQQFNMHVF KLEQEEYMKE
QIPWTLIDFY DNQPCINLIE[500] AKMGVLDLLD EECKMPKGSD DTWAQKLYNT HLNKCALFEK
PRLSNKAFII[550] KHFADKVEYQ CEGFLEKNKD TVYEEQIKVL KSSKKFKLLP ELFQDEEKAI[600]
SPTSATPSGR VPLSRTPVKP AKARPGQTSK EHKKTVGHQF RNSLHLLMET[650] LNATTPHYVR
CIKPNDFKFP FTFDEKRAVQ QLRACGVLET IRISAAGFPS[700] RWTYQEFFSR YRVLMKQKDV
LSDRKQTCKN VLEKLILDKD KYQFGKTKIF[750] FRAGQVAYLE KIRADKLRAA CIRIQKTIRG
WLMRKKYMRM RRAAITIQRY[800] VRGHQARCYA TFLRRTRAAI IIQKFQRMYV VRKRYQCMRD
ATIALQALLR[850] GYLVRNKYQM MLREHKSIII QKHVRGWLAR VHYHRTLKAI VYLQCCYRRM[900]
MAKRELKKLK IEARSVERYK KLHIGLENKI MQLQRKIDEQ NKEYKSLLEK MNNLEITYST
ETEKLRSDVE RLRMSEEEAK NATNRVLSLQ EEIAKLRKEL[1000] HQTQTEKKTI EEWADKYKHE
TEQLVSELKE QNTLLKTEKE ELNRRIHDQA[1050] KEITETMEKK LVEETKQLEL DLNDERLRYQ
NLLNEFSRLE ERYDDLKDEM[1100] NLMVSIPKPG HKRTDSTHSS NESEYTFSSE ITEAEDLPLR
MEEPSEKKAP[1150] LDMSLFLKLQ KRVTELEQEK QSLQDELDRK EEQALRAKAK EEERPPIRGA[1200]
ELEYESLKRQ ELESENKKLK NELNELQKAL TETRAPEVTA PGAPAYRVLL[1250] DQLTSVSEEL
EVRKEEVLIL RSQLVSQKEA IQPKEDKNTM TDSTILLEDV[1300] QKMKDKGEIA QAYIGLKETN
RLLESQLQSQ KKSHENELES LRGEIQSLKE[1350] ENNRQQQLLA QNLQLPPEAR IEASLQHEIT
RLTNENLDLM EQLEKQDKTV[1400] RKLKKQLKVF AKKIGELEVG QMENISPGQI IDEPIRPVNI
PRKEKDFQGM[1450] LEYKKEDEQK LVKNLILELK PRGVAVNLIP GLPAYILFMC VRHADYLNDD[1500]
QKVRSLLTST INGIKKVLKK RGDDFETVSF WLSNTCRFLH CLKQYSGEEG[1550] FMKHNTPRQN
EHCLTNFDLA EYRQVLSDLA IQIYQQLVRV LENILQPMIV[1600] SGMLEHETIQ GVSGVKPTGL
RKRTSSIADE GTYTLDSIIR QLNSFHSVMC[1650] QHGMDPELIK QVVKQMFYII GAVTLNNLLL
RKDMCSWSKG MQIRYNVSQL[1700] EEWLRDKNLM NSGAKETLEP LIQAAQLLQV KKKTDEDAEA
ICSMCNALTT[1750] AQIVKVLNLY TPVNEFEERV LVSFIRTIQL RLRDRKDSPQ LLMDAKHIFP[1800]
VTFPFNPSSL ALETIQIPAS LGLGFISRV[1829]

The primary sequence of myosin V contains several thrombin cleavage sites (table 4.2) It is seen that though not all of them are expected to support efficient proteolysis digestion due to various reasons, e.g. the distinct secondary structures, the proteolysis condition/the efficiency of the proteolysis digestion etc. An evaluation of the cleavage sites based on a length analysis after an extanded digestion test. An estimation of the size is shown.

Table 4.2: List of peptide length variety resulted from partial digestion from thrombin (highlighted numbers indicate the most suspected cleavage site)

	1	779	801	850	875	1198	1342	1412	1472	1829
1	-	779	801	850	875	**1198**	**1342**	**1412**	**1472**	1829
779		-	22	71	96	394	563	633	693	1050
801			-	49	74	388	541	**611**	671	1028
850				-	25	348	492	562	**622**	979
875					-	323	467	537	**597**	954
1198						-	144	214	274	631
1342							-	70	130	487
1412								-	60	417
1472									-	347
1829										-

Myosin V is selectively digested by thrombin (50 mM Tris/HCl buffer, pH 8.3) at a ratio of myosin V: thrombin of 50:1 (μg/μg) at 37 °C for 2 hours, and then analyzed by SDS-PAGE.

The result shows two predominant bands one at 150 KD and the other at 65 KD. The 150 KD is not very sharp so that it is possible that it could consist of a population of several bands of similar molecular weight.

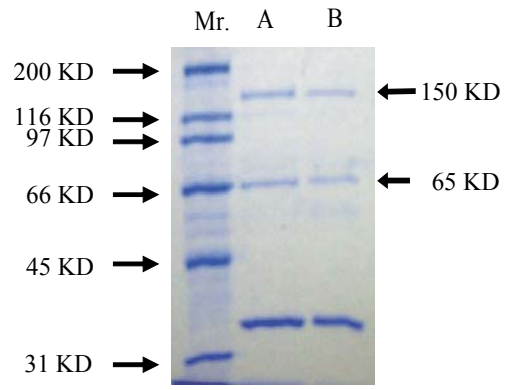

Figure 4.4: A, B, Myosin V digested by thrombin shows two predominant bands that migrate around 150 KD, 65 KD respectively. A, B stand for the myosin V samples digested in parallel.

Subsequently Western blotting is performed by using a polyclonal antibody and 5 distinct monoclonal antibodies shown in fig 4.4. All of the monoclonal antibodies recognize the two major bands, indicating that there should be an overlapping part between the fragments of 150 KD and 65 KD. Based on the average molecule weight of amino acid residues which is 110 Dalton, the peptides ranging from amino acid residues 1-1134, 1-1342, 1-1412 or 1-1472 are suspected to account for the ~150 KD fragment, and 801-1412, 850-1472 or 875-1472 for the ~65 KD fragment.

Figure 4.5: the possible cleavage sites within the myosin V heavy chain peptide.
The monoclonal antibody binding sites are attributed to the binding sites located between residues 801-1472 (~5 KD). We assume that there is a hot-spot of antigenicity since all the available antibodies tested recognized this relatively narrow region. To explore the binding sites at a higher resolution the following experiments were performed.

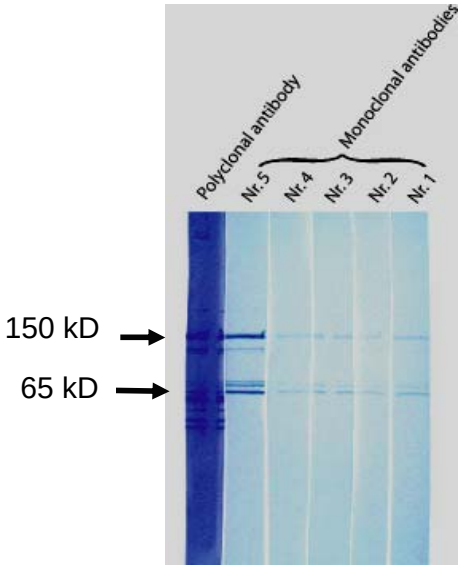

Figure 4.6: Western blotting using five distinct monoclonal antibodies against myosin V.

As shown in the figure 4.6, the multi-clonal antibody recognizes much more peptide debris distributing over a wide molecule weight range. There are several major reasons for the difference between multiclonal and monoclonal antibodies tests: firstly, the proteolysis digestion by thrombin results in a mixture of a wide range of molecule weights; secondly, the multiclonal antibody is composed of a mixture of distinct immuno-globular proteins each containing distinct antigen recognizing sites. A third reason is that due to the sensitivity of western blotting that is at the level of ~10 ng, there are bands which are invisible by normal commass light blue staining but visible in western blotting test.

To further exploit the monoclonal antibody binding site in myosin V HC, calpain is employed for proteolysis digestion. Calpain is very useful in the selective digestion because of the presence singular specific cleavage sites within the myosin V HC domain located between amino acid residues 1131-1141 (Alexandra A. C. Nascimento, 1996).

The activity of calpain is strongly regulated by Ca^{2+} ions, and sensitive to oxidative environments. (Ref) EGTA, DTT should be always present in the storage buffer to keep

the enzyme stable and Ca^{2+} is only added in the digestion mixture just before use. Ion strength plays a critical role in digestion and here a preferable concentration of 100-200 mM of KCl is used according to reference (Ref). Calpain digestion is performed with a ratio of myosin: calpain = 20: 1 (w/w). A variety of incubation time ranging from 5 to 15 min was tested.

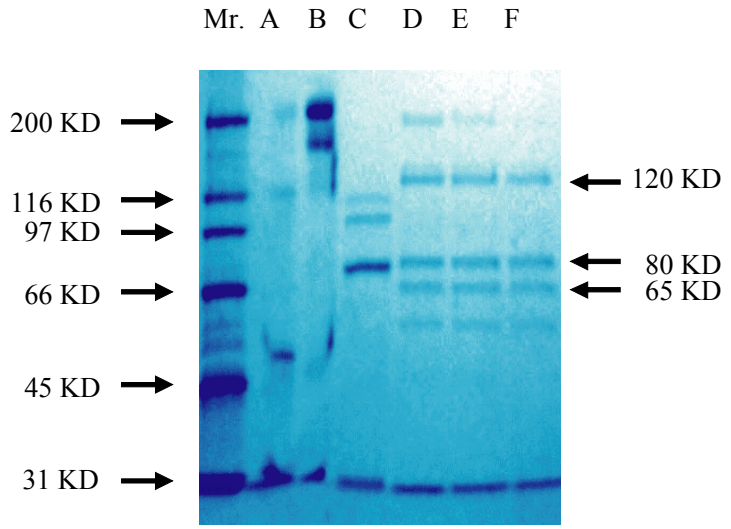

Figure 4.7: Proteolysis digestion of myosin V by calpain. A), reduced Ab; B), native Ab; C), calpain; D, E, F, myosin V digested after 5, 10 and 15 min of incubation.

The resulted fragments' size agrees with those in reference (Nascimento, A. A. C., 1996). The well separated 65 and 80 kD fragments correspond to the head and the tail domain of myosin V molecule respectively. The 120 KD band represents an intermediate fragment which is further digested resulting in a 65 KD fragment and smaller peptide fragments. To prepare the proteolysis digestion samples for western blotting, the incubation time is prolong to 30 min and the 120 KD bands become invisible (Data not shown). After digestion, the mixture is treated for SDS-PAGE electrophoresis and then tested by western blotting using monoclonal antibody Nr. 4 and Nr.5. Those two monoclonal antibodies are chosen out based on the ATPase assay and an antibody affinity test. More tests are to be done to detect the binding sites of the rest monoclonal antibody.

The subsequent western blotting test reveals that only the 80 KD band is positive which means that the tail domain of myosin V molecule contains the antibody binding sites for both monoclonal antibody Nr.4 and Nr. 5. As this region of myosin V is considered to act as cargo binding domain, those two monoclonal antibodies are selected for further investigation of cargo binding domain studies.

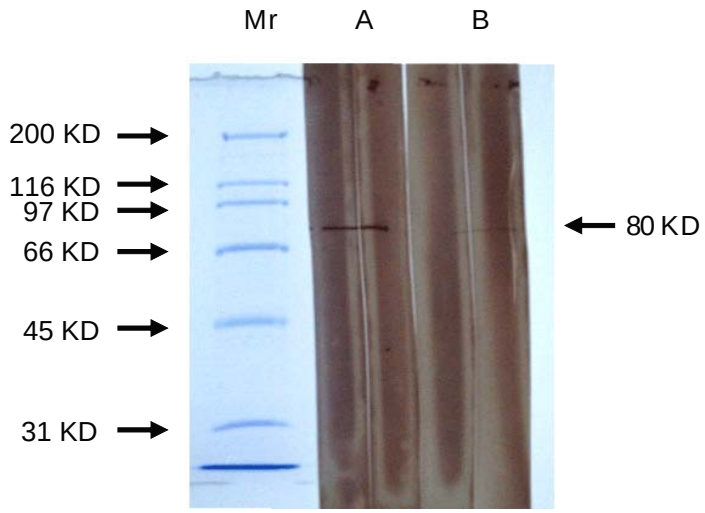

Figure 4.8: Western blotting test result manifests that the band recognized by monoclonal antibodies Nr.4 (A), 5 (B) appears to be peptide of 80 KD.

The cleavage site of calpain is shown schematically in figure 4.9. From the combination of figure 4.5 and 4.9, we conclude that the antibody binding region is deduced to be between amino acid residues 1136-1472.

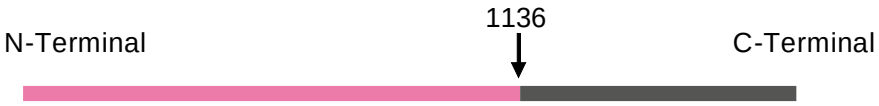

Figure 4.9: Scheme of the calpain cleavage site in the myosin V HC.

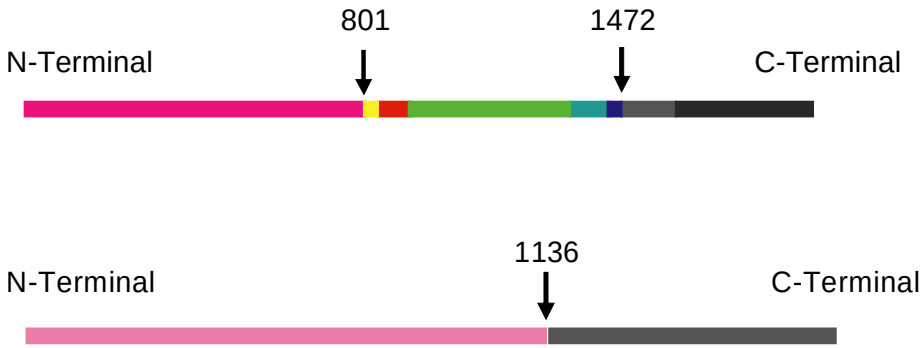

Figure 4.10: Combination of schemes of thrombin and calpain cleavage sites in the myosin V HC.

To further study the antibody binding sites in the heavy chain of myosin V, several methods were employed. Firstly, some other proteolysis enzymes e.g pepsin is recruited for proteolysis digestion to get smaller fragment while maintaining the antibody affinity and then the positive fragment could be separated by proper means (e.g SDS-PAGE, 2D electrophoresis, affinity chromatography, HPLC et al) and then tested by mass spectroscopy (MS) and peptide sequencing. Mass spectroscopy is a powerful tool for this purpose because of its high accuracy which allow it detect the location of the fragment from the molecule weight. The peptide sequencing provide the primary sequence of the first 5-15 amino acid residues (for instance) from the N-terminal or from the C-terminal. Thus the MS technique and the peptide micro-sequencing could be bundled to give more accurate antibody binding information. In this work, we tried peptide sequencing to detect the N-terminal amino acid residues sequence. However, in our experiment the smaller fragment resulted from thrombin digestion could not be assayed by MS for some reasons unknown. Perhaps the N-terminal of this peptide is protected by some modification of amino acid residues that protect it from the hydrolysis in the sequencing machine. The detail is under investigation and is expected to be solved in a further study. As we expect, the detection of the binding site of the monoclonal antibody is necessary for future applications.

4.3 Invitro motility assays and evaluations

4.3.1 Conventional Motility assays with myosin V

The conventional motility assay is based on a experimental set up to test the motor activity of myosin and to study the interaction between myosin and actin in real time (Kron and Spudich, 1986). The working principle of a conventional motility assay can be summarized as follow: first, myosin is immobilized on a proper surface, e.g. glass, nitrocellulose, and then actin filaments are introduced into the system so that on the surface actin and myosin form a two dimensional network which allows observation through fluorescent microscopy. The substrate is then deposited in the measuring chamber. It is a convenient set up allowing the investigation of the influence of various factors such as regulatory proteins, inhibitors and so on. Before other techniques are introduced to the study of molecular motors, e.g. optical tweezers, an apparatus give unprecedented accurate measurements of a single step or even of the substep size level, motility assay served as the main functional test of myosin.

Concerning the binding of myosin to the surface, various interaction forces between the protein and the solid surface may be involved. As far as myosin is concerned, we make use of the hydrophobic properties which force the molecule to bind to the surface of nitrocellulose via their tail domains. Successful applications started back in 1998 or even earlier. After binding to nitrocellulose surface under a high concentration of salt, myosin demonstrates to be active after the excess salt is removed.

In motility assays, each motor protein or motor protein sub-domain exhibits a distinct sliding velocity which partially reflects its properties (table 1.1). For a given kind of myosin, such an actin sliding velocity could be affected by a variety of factors such as motor density, ATP concentration, ion strength, concentration of special ions e.g. Mg^{2+}, Ca^{2+} and many more. The key property of myosin, the ability to perform power stroke could be directly studied through microscopy, which has a distinct advantage of this assay. As a basic analytical approach, motility assays have been routinely performed to test the activity evaluation of myosin preparations.

The rigor heads in the denatured myosin molecules that lack the capacity of generating power stroke could be determinated indirectly in such a test. As they bind to the actin filaments without dissociation in the presence of ATP molecules, it results in that the heads hinder the sliding movement of the actin filament. This phenomenon is apparent in the sliding motion as it severely disturbs the normal sliding motion (figure 4.11).

Figure 4.11: the rigor heads in denatured myosin molecules hinter the sliding motion of actin filaments. In the two rows of pictures, two actin filaments were found to rotate around a point which indicated the location of a rigor head.

In the motility assay, myosin V differs from myosin II, or HMM in the density that is necessarily required to continuously support F-actin sliding. The applied myosin V concentration could be decreased to 50 ng/ml or 100 pM, while the threshold concentration of HMM or myosin II is 100 fold higher (at ~5 μg/ml). When myosin V is applied at a concentration around 5 μg/ml, or 10 nM, the actin filamenats became shredded into small pieces immediately after ATP addition, a phenomenon that has rarely been demonstrated for the case of myosin II or HMM.

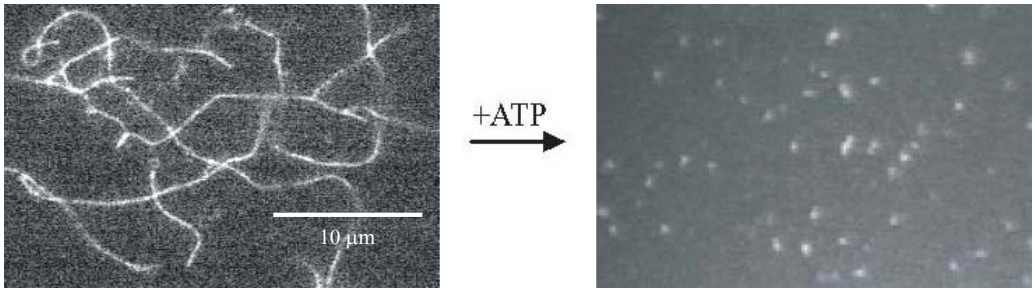

Figure 4.12: When myosin V is applied at a concentration ≥ 5 μg/ml, the actin filaments were shredded into small pieces by myosin V simultaneously upon ATP addition.

In our experiments, fragmentation of actin filament during motility assays seemed to be inevitable when a nitrocellulose-functionalized surface was used. Long filaments existed only over a short period of time for about a few minutes, before they broke or were shredded into short pieces. After an incubation of ~10 minutes, only short filaments were found. A typical breaking event is shown in fig.4.13. Presumably it is the cooperation of a group of myosin V binding to the same filament that should be responsible for the fragmentation. As shown in fig. 4.13, an actin filament with a length of ~12 μm breaks into shorter pieces which have various length ranging from ~2 μm to ~8 μm which is within the range of persistence length of F-actin.

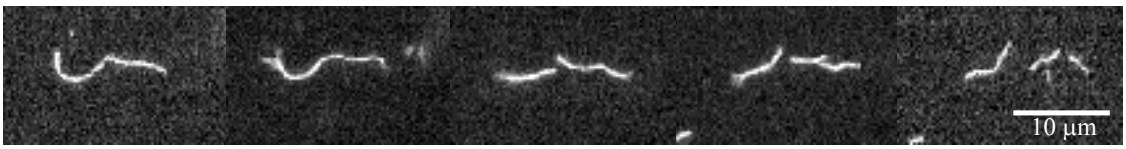

Figure 4.13: A typical break event of an actin filament in a myosin V supported motility assay is illustrated.

Though the myosin V molecule is bound to the solid surface by its tail domain, it does not necessarily mean that it is tightly fixed. The whole molecule of myosin V is estimated to have a length of ~100 nm (according to data from EM) and can thus myosin molecule

probably maintain flexibility in the adsorbed state. This allows the head domain to adapt to the correct orientation towards actin filaments and to perform power strokes.

Single double-headed motor supported motility could be performed by decreasing the density of myosin V on the nitrocellulose surface to an appropriate level. The minimum myosin V concentration depends on the length of F-actin filaments. In the case of a mean length of 10 μm, a minimum concentration of myosin V of ~0.1 μg/ml or 16 nM was found to enable single motor motility measurement.

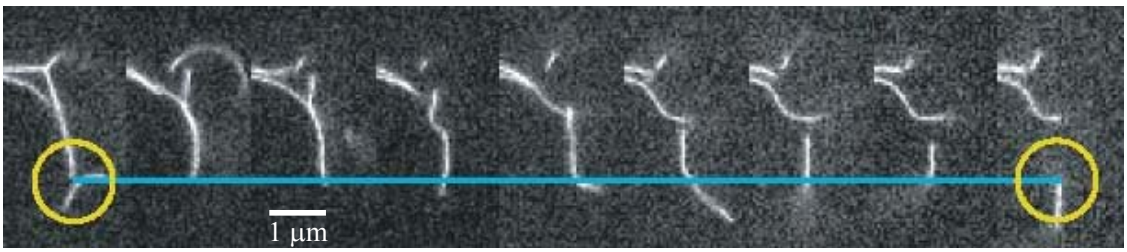

Figure 4.14: F-actin could move along its whole length, indicating that the motor protein can continuously propel F-actin from the binding end towards the barbed end.

In such a motility assay, one could occasionally observe moving actin filaments rotating around a fixed point where they were apparently immobilized by a pre-fixed myosin molecule. In some events, F-actin could move the whole length of itself, indicating that the motor continuously propelled F-actin from the bound end towards barbed end. The sliding of actin driven by a single motor provides strong evidence for the processivity of myosin V. A nonprocessive myosin, e.g. HMM, or myosin II, fails to support motility of F-actin at concentration below 5 μg/ml.

4.3.2 Motility assay using beads coated with myosin V

4.3.2.1 Beads moving on immobilized actin filament

In order to study the function of myosin V as transporter of cargo, it is necessary to reverse the arrangement of the motility assay. Latex beads of various sizes (ranging from 40 nm to 1 μm) have been utilized for this microscopic study. Myosin V molecule is

coupled to the beads either unspecifically by direct interaction due to the hydrophobic effect or by indirect means via antibody-antigen. It is assumed that in all of the above coupling schemes the myosin V binds to the bead by its cargo binding site.

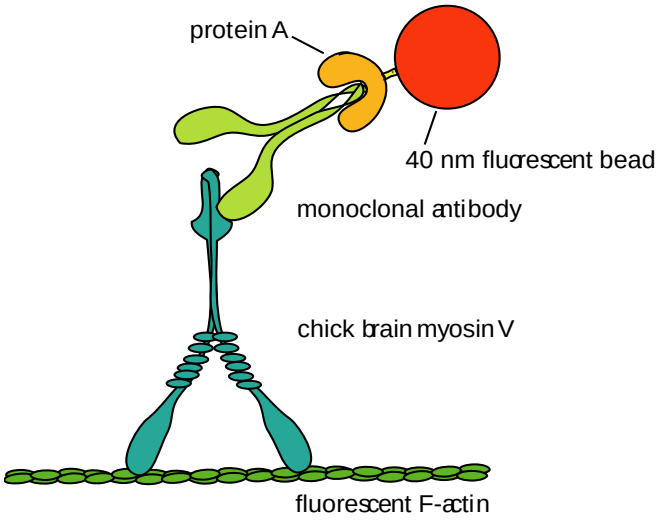

Figure 4.15 Scheme of a 40 nm fluorescent bead binding to myosin V via protein A and anti-myosin V monoclonal antibody.

It should be pointed out here that the size of the beads matters because of the fact the smaller the bead is the fewer molecules can be coupled to it. Considering the size of the myosin V molecule (~90 nm in length), a 40 nm bead could bind to a sub-domain of it. At an optimal ratio of bead versus myosin molecule, single beads decorated with single myosin molecule could be obtained.

In this work, 40 nm latex beads with active groups (carboxyl groups) for covalent coupling of protein via peptid bands were applied. The latex beads were first coated with protein A to bind antibodies against myosin V. The procedure is described in detail in chapter 3.2.3. The resultant antibody/ bead complex may bind more than one myosin V molecule because one antibody molecule contains two antigen binding sites (Fv). This possibility depends on both conformation of the interfaces of the antibody and myosin V molecules. The applied ratio of antibody versus myosin V could be another factor.

The whole set-up of the flow cell is illustrated in Fig. 7 of Materials and Methods Section. For a control binding of F-actin to substrate we used NEM-treated HMM which binds F-actin specifically and irreversibly even in the presence of ATP. The experimental procedure was as follows:

•First the nitrocellulose coated surface is incubated with NEM-HMM to produce discrete F-actin supporting sites over the surface. For this purpose, NEM-HMM is dissolved in washing buffer which contains a high salt concentration that facilitates the protein to interact with the surface by hydrophobic interaction. After incubation the excess NEM-HMM is removed by pure washing buffer.

•Rhodamine-phalloidin labeled F-actin is then added to the flow cell. Some F-actins diffuse from the bulk to reach the surface, and are immobilized by the prefixed NEM-HMM. The NEM-HMM concentration is ~50 µg/ml, as much as in conventional motility assay.

•The 40-nm beads coated with myosin V are prepared according to the Material and Methods Section 3.2.3 and applied in the flow cell and incubated a few minutes with the cover slip side facing down (to prevent accumulation of excess beads sinking to the surface due to gravity). After that the excess beads are removed by rinsing with ATP free assay buffer. By microscopic observation it is verified that the area of interest stays in focus.

•The bound myosin-V coated beads respond quickly to the addition of ATP and start to move along the actin filament. The motion of the bead is recorded by CCD camera and analyzed.

The specific interaction between antibody and myosin V improves the signal/noise ratio in our set up (as shown in Figure 4.16).

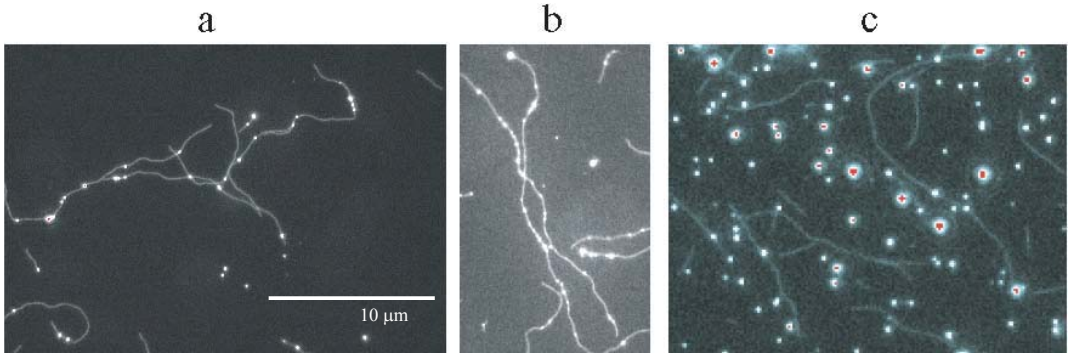

Figure 4.16: Demonstration of the specific binding of myosin-V-coated beads to F-Actin by fluorescence microscopy: NEM-treated HMM is bound to nitrocellulose-coated glass slide which is then blocked against further binding of proteins by BSA. F-actin was labeled and stabilized with Rhodamine-Phalloidin and then bound irreversibly to the NEM-HMM. Finally the beads were added. The beads were also labeled by Rhodamine. a, b: Myosin V was bound indirectly through specific monoclonal antibodies to the beads; only few beads did not bind to F-acitn. c. The beads did also bind when myosin V was directly coated on the bead by hydrophobic interaction but this resulted in predominantly unspecific binding.

Observation of the motion of the bead shows a variety of interesting aspects as describted below: By controlling the mole ratio of myosin V to the beads it is possible to generate beads carrying a single myosin V molecule. The motion of a bead is thus expected to reflect that of a single motor. Our set-up does not allow observing that weak fluorescence from a single fluorescent molecule. On the other hand, the latex bead exhibits a large number of fluorophores and gives strong enough signals to observe the motion.

4.3.2.2 Some additional observations:

The binding of F-actin to NEM-HMM is insensitive to high ion strength. F-actin diffused through the bulk and contacted the NEM-HMM layer randomly. Binding might start from any part of the filament that was caught by immobilized NEM-HMM by chance. The fixed part prolonged until the whole filament lay over the surface. Occasionally, F-actin formed crossed 2D network as shown in the same figure.

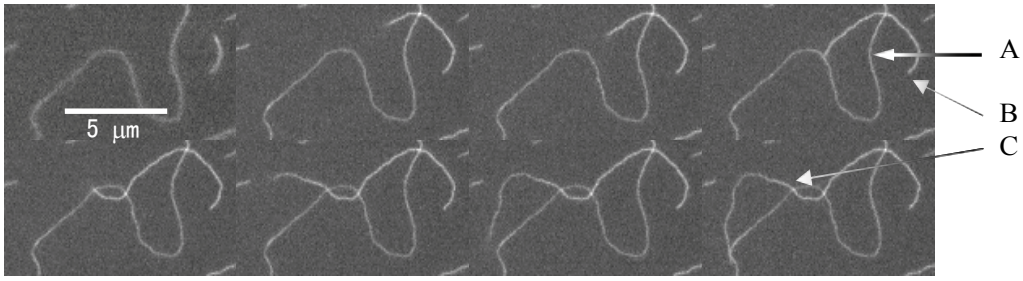

Figure 4.17: Actin filaments labeled by rhodamine are bound to the surface of the bottom of the flow cell. It is seen that filaments crossed occasionally. A, B show the early period of the binding process. First a single filament binds over the nitrocellulose surface, then another actin filament contacts the surface and be caught by NEM-HMM and crosses the first one (figure C). The pictures were taken with a 100 × objective.

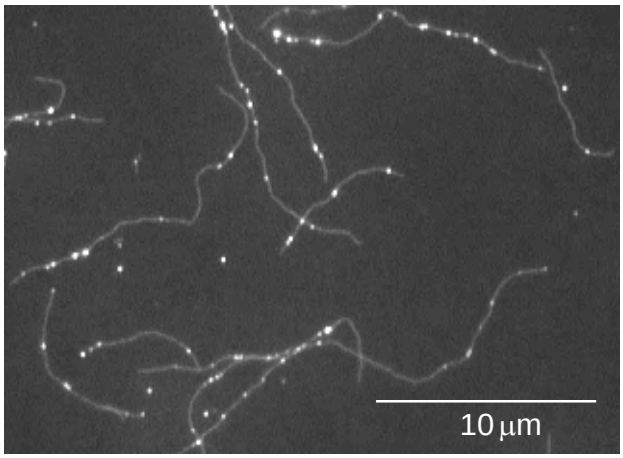

Figure 4.18: bead complexes bound to F-actin. There were much less nonspecific binding of the complexes after both the beads and nitrocellulose surface had been passivated with BSA. (100× objective)

4.3.2.3 Analysis of the motion of individual bead:

Some observations of the moving myosin V coated beads show that their motions are more complicated than expected. For instance, two moving beads are found to follow

each other and during which they change their positions (figure 4.18). In another example, one bead coated with myosin V moves such a long distance that it challenges the available explanation for bead movement supported by a single molecule. It seems that the myosin V molecules might cooperate and thus increase the affinity of the bead coated with myosin to the actin filament (figure 4.19).

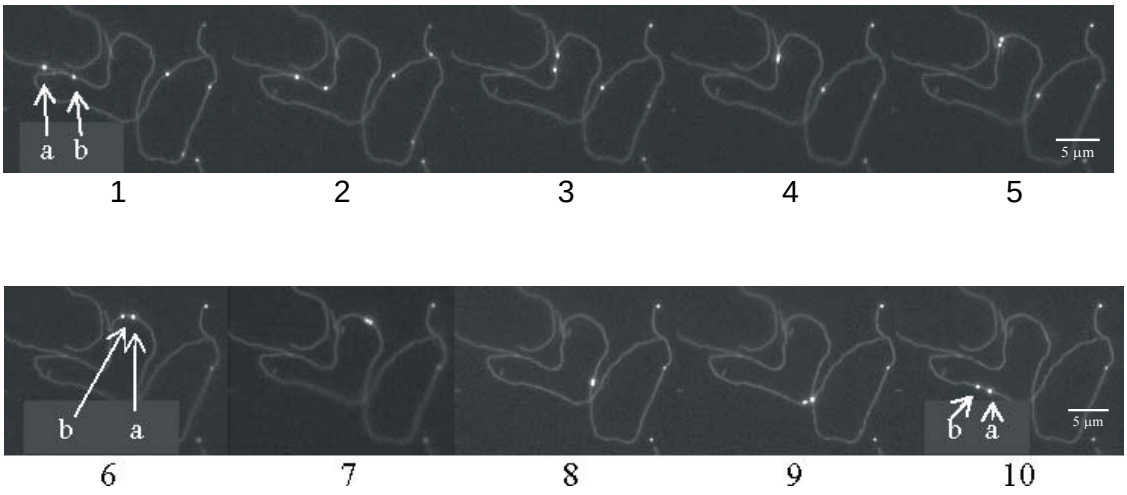

Figure 4.19: Two beads coated with myosin V are seen to move along actin filaments. They are seen to change their positions indicating that two motors bound to a single actin filament perhaps supports two myosin V molecules move in a coordinated way.

The curves of two crossed actin filaments are shown in figure 4.20. It seemed that there might be several crossing points formed by the two actin filaments. The motion of the leading bead complex was recorded and analyzed by using Igor. The trace of the leading bead is schematically shown in figure 4.20. It clearly resembles the curves in b, indicating that the leading bead moves along the filaments >30 µm.

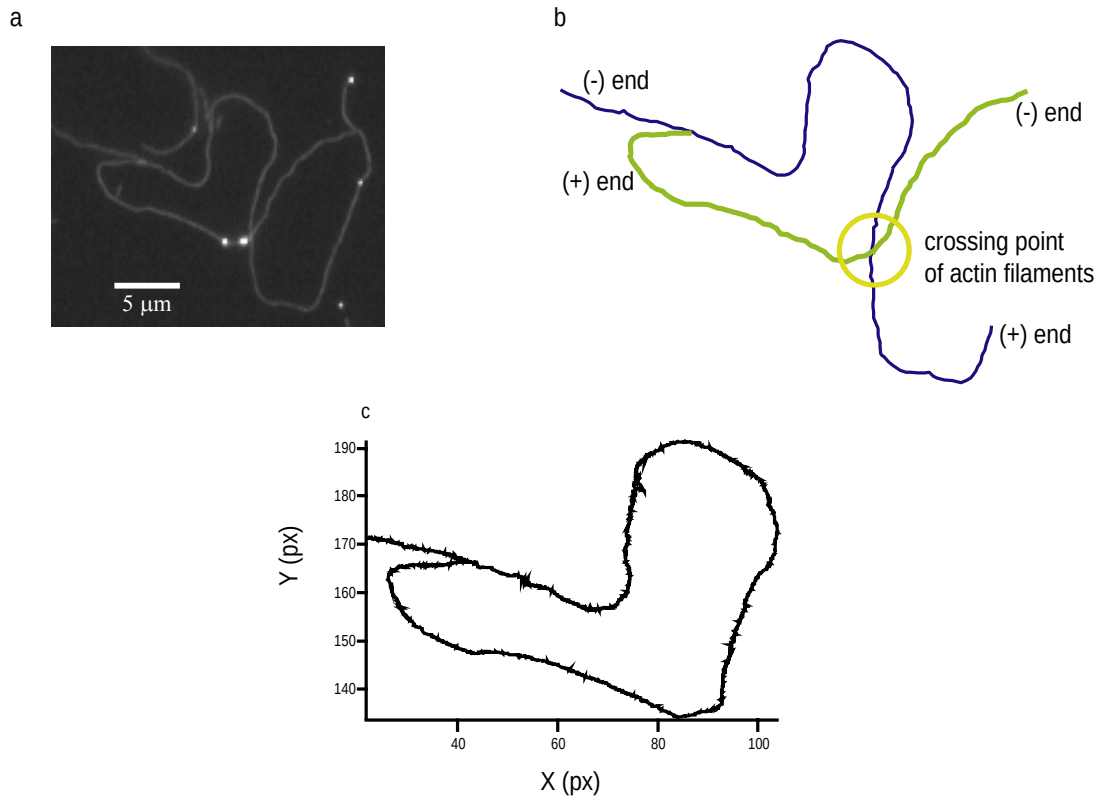

Figure 4.20: a) The tracks of the myosin coated beads agree with the curves formed by actin filaments, indicating that they move exactly along F-actins. b) The curves of actin filaments extracted from image. a) It shows two actin filaments crossing each other. c) Trace of an individual bead. The similarity of the tracks and the filament curves indicates that the motion follows the actin filament with high fidelity.

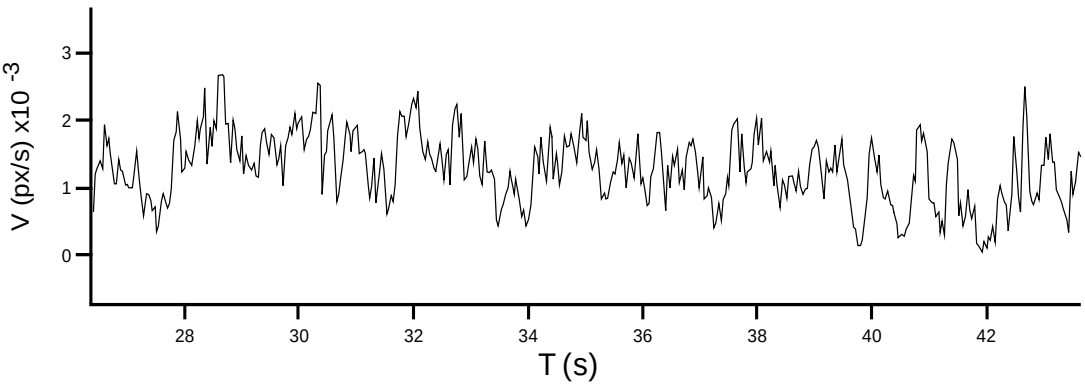

Figure 4.21: The motion of the leading bead in figure 4.20 is recorded and analyzed. This velocity versus time curve reveals a considerable variety of motion over a time range of

17s. The mean velocity over this time range is ~1.5 px/s or 0.3 μm/s which is indicated by the red line.

The velocity of the bead complex is analyzed and shown in figure 4.20. It seems that the mean value during the 18 seconds recorded is ~1.5 px/s or 300 nm/s.

An interesting finding is that of two beads moving along a filament, each behaves differently. In figure 4.22 two beads are seen moving counter-clockwise along a circular actin filament loop. This experiment again demonstrates the high processivity of myosin V motors. The track of the leading bead (the leading one) is compared with the filament loop.

Figure 4.22: Two beads are seen moving counter-clockwise along a circular actin filament loop in a motility test.

a

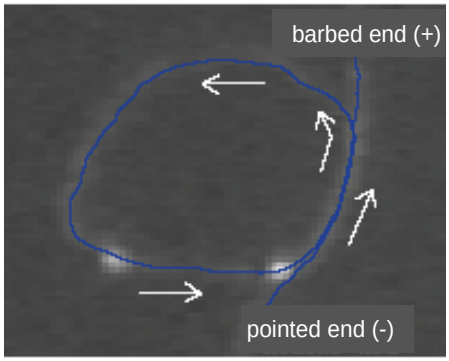

b

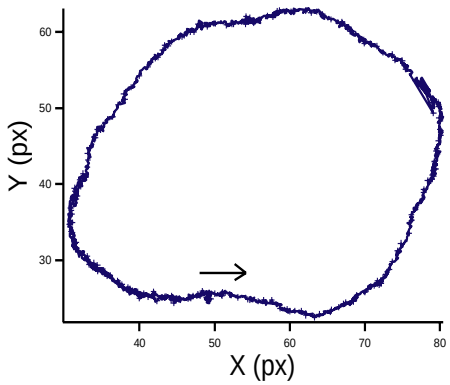

Figure 4.23: Analysis of the track shown in figure 4.22. a).The blue curve indicates the actin filament curve. From the moving direction of the two beads, the orientation of actin filament is indicated by arrows. b).The motion of the leading bead is recorded by using Openbox* and analyzed by Igor. The trace of the motion is illustrated and it agrees well with the circular part of the actin filament loop.

Another finding is the track changing that is explained in the figure 4.20. There are at least two different loop structures. To form the loop, the actin filament should contain one or more actin crossing point (Figure 4.24). If the bead moves along the same filament, it should move to the barbed end away from the circular loop. However, this did not occur which indicates that the bead most likely changes its track during its motion.

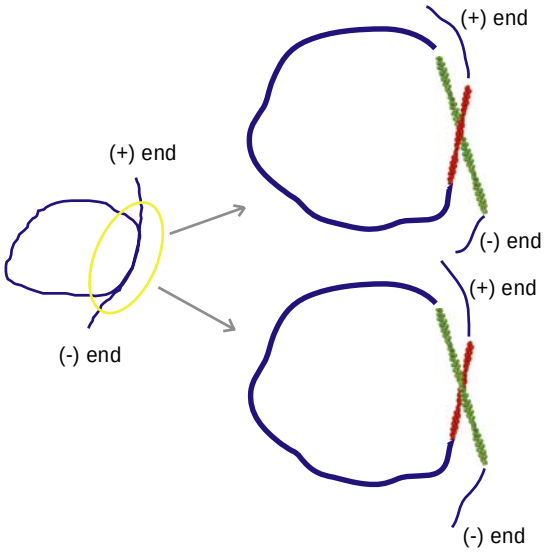

Figure 4.24: Two different crossing may explain the loop structure. The leading bead changes its track.

Similar track changing events are common in the motility assay studies. It seems that track changing is a reproducible behavior of the myosin-V-coated bead. For instance, in figure 4.25 two beads are found to change their tracks when they confront an actin filament crossing (similar events are also found in figure 4.17). In this event, two filaments form a sharp angle (~52 °) that is much larger than that in figure 4.20 (~0 °) and smaller than that in figure 4.17, which is ~135°. It is not clear that if it is forced to do so or not.

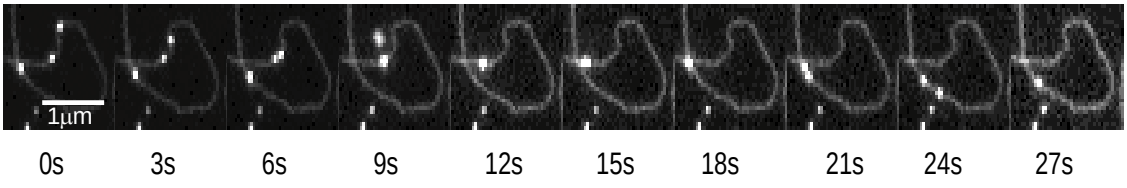

Figure 4.25: Two myosin-V-covered beads change track when they encounter a crossing of two filaments. This phenomenon demonstrates the high flexibility of the motor.

In figure 4.26, a group of beads are found to move along the same actin track in the presence of a high myosin V to bead ratio. If these myosin V molecules dwell a longer time than the myosin coated bead it will block the latter. This shows that the myosin V molecule either moves at similar velocity or dissociates from the track the moment ATP is provided. When the high processivity of myosin V is considered, it is more possible that the molecule moves in a similar way as those beads do.

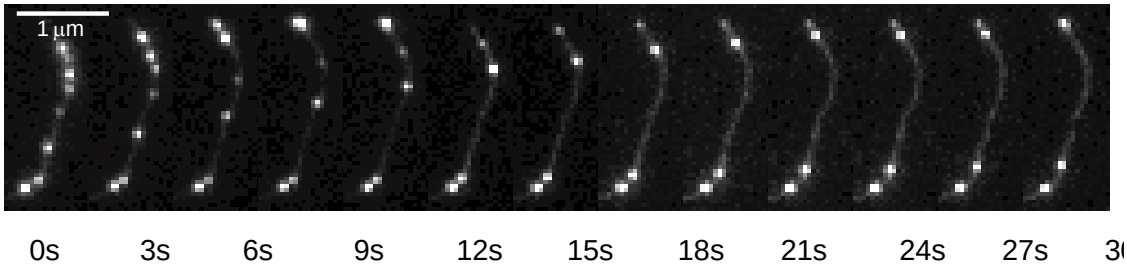

Figure 4.26: A group of myosin V covered beads move along an actin filament.

4.3.3 Motility assay supported by fluid bilayers

4.3.3.1 Demonstration of a filament breaking event on solid substrate

In the conventional motility assays where myosin bound to the nitrocellulose the filament tend to be shredded or broken as discussed in chapter 4.25. The reason is likely to be a combination of the *lp* (length of persistence) of F-actin and the interaction between actin filament and the prefixed myosin. Here the effect of the distribution of myosin is discussed.

In figure 4.27, an individual breaking event was recorded during motility assay on the surface of nitrocellulose. It seems that the actin filament bends in response to the propelling force of myosin V molecules. The myosin V molecules distribute randomly over the surface due to unspecific binding forces (hydrophobic forces).

The length of persistence of actin filaments is reported to the be of the order of 10 µm and the curve shown in the figure 4.27 agrees with this value. The figure suggests that once the curve reaches a minimal curving angle the actin filament breaks in order to release the curvature energy. (From the threshold curve angle the force could be determined.)

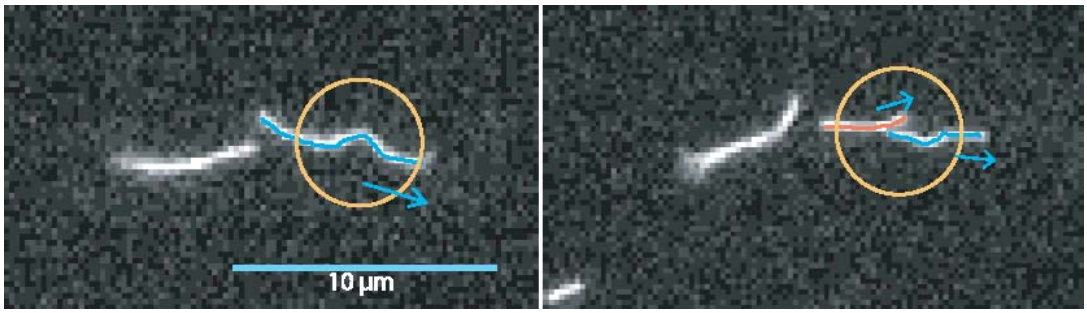

Figure 4.27: Breaking of the actin filament attached to nitrocellulose surface covered by myosins. Breakage occurs when curvature of small loop become too large. The arrow indicates the moving direction of the filament.

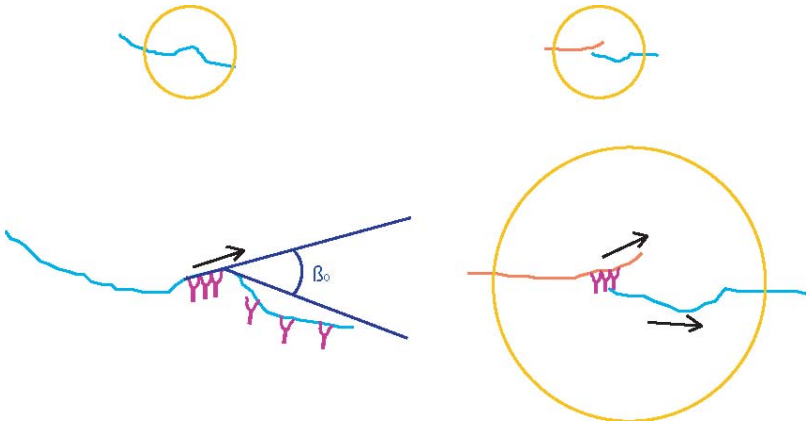

Figure 4.28: Shape of actin filament as obtained from the recorded pictures. ß₀ of Fig. 4.27 (ß₀ = ~36°) indicates the angle formed by adjacent filament segments. As breaking event occurs subsequently, this angle should be close to the threshold where actin filament could not resist the applied force.

4.3.3.2 Analysis of the flexibility of actin filament moving on a fluid surface

Other factors besides the myosin density are also responsible for the breakage of actin filaments, when the protein is able to diffuse in two dimensionals upon a fluid surface. The diffusion of myosin V molecule is limited to two dimensions. The diffusion rate of myosin over the membrane is between that in the solution and the nitrocellulose surface.

Here, the behavior of actin filament seems to be more flexible than that on a nitrocellulose surface. The tracks of actin filament during sliding over the bilayers are recorded. It shows that actin filament can be curved several times without breakage. The curves at such a high binding tension are observed only in case of lipid bilayers but not with nitrocellulose surface. This suggests that the diffusion potentiality of myosin V molecule prevents actin filament from breaking.

A lipid bilayer allows myosin molecules to be more flexible in two ways: first, myosin is able to diffuse over the surface alone or while it is bound to actin filament; second, myosin could perform self-rotation. The latter behavior is also possible for myosin molecules bound to nitrocellulose but it is expected to be restricted to a much smaller range.

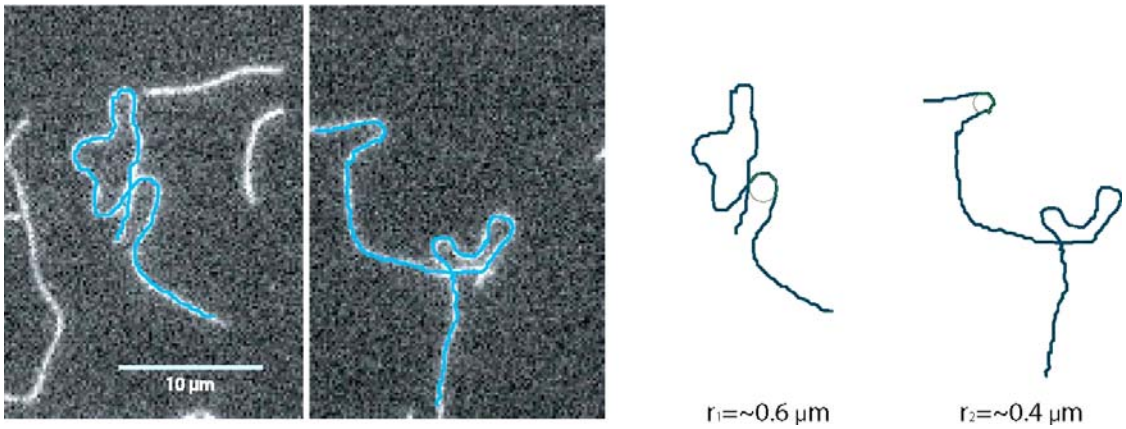

Figure 4.29: In the lipid-bilayer-supported motility assay, the long actin filament can undergo severe curving without breaking. In the two contours as illustrated, the radius is about ~0.4-0.6 μm.

Compared with the breaking events occurring with the nitrocellulose supported motility, the actin filament can survive high curvature deformation curving tension (Fig. 4.29). All the above observations show that actin filament releases the binding tension before it reaches a threshold where the breaking occurs. Or, to put it the other way, the force the myosin motor exerts will not act as strong as in the case where it is fast commeded to a mechanical resistance. This partially explains the existence of the extreme long actin filament, e.g. >30 μm after long sliding duration >10 min.

4.3.3.3 The impact of membrane fluidity on the sliding of actin filaments

The actin sliding assay over supported bilayer exhibits other advantages compared to motility test over nitrocellulose. First it seems to support a relative smooth sliding for long actin filaments. The filaments move in such a way that they can nearly overlap. It is clearly seen in video microscopy that the sliding is much smoother than that over nitrocellulose surface.

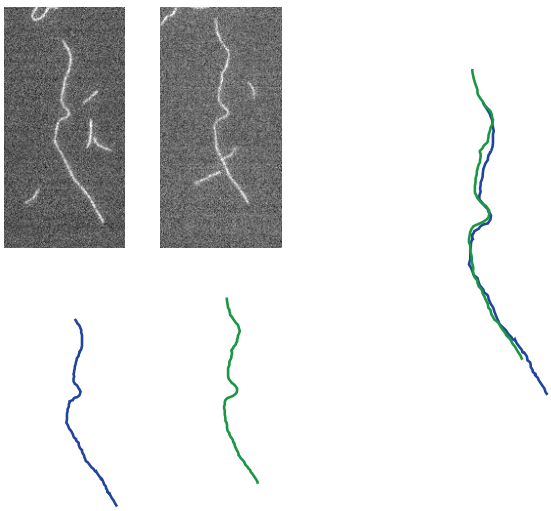

Figure 4.30: Overlaying different snapshot tracking of the track of an actin filament shows a smooth sliding way over the fluid lipid bilayers. The interval of picutures is ~10 seconds.

A further study focuses on the behavior of a defined segment within the contour of an actin filament. For this purpose, a short fragment with a length of 2 µm is studied which is locating 2 µm from the trailing end of the actin filament. The track of both ends of the segment are recorded and shown schematically.

For the primary evaluation of the actin filament sliding motion over bilayers, this length of the filament is chosen for two reasons. First we want to compare the motions of separated short filaments and that of the long filament. The minimal length of the filaments found over the lipid bilayers is close to ~2 µm. Second, the persistence length of the actin filament is well above this scale, so that we observed a relatively shift siding.

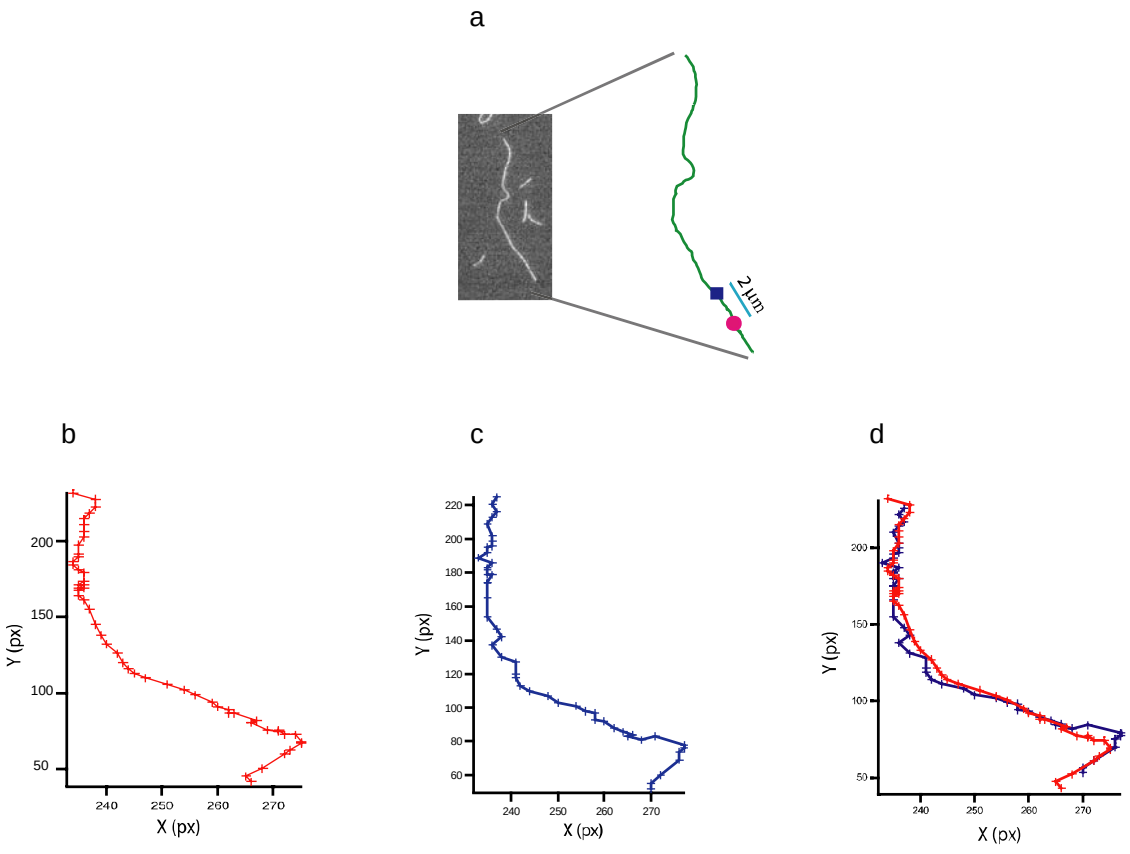

Figure 4.31: A segment of ~ 2 µm out of the complete length locating ~2 µm to the lagging end is marked with a blue and a red dot at both the ends (shown in figure a). Its motion is recorded and schemed as shown. The blue and red curves match the traces of the leading and the trailing point of the segment respectively. The traces of the trailing (figure c) and the leading ends (figure b) are shown. In figure d, the traces of both of the leading and trailing end are overlaid. Each of the position (Y, X) are obtained from the discrete digital picture at time intervals of 200 ms.

The separated scheme or overlaid tracks of the two points indicate a relative smooth motion of the long filament. The perpendicular amplitude of this segment is << 30% of its length. For comparison the tracks of both ends of a short actin fragment are recorded during sliding assay over HMM coated surface. The length of the fragment is close to 2 µm (figure 4.32).

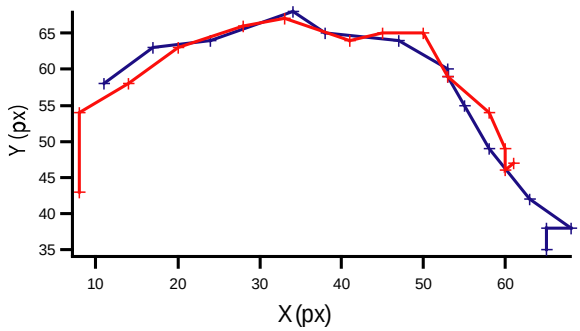

Figure 4.32: The traces of leading and trailing ends of a short actin filament of ~2 µm length during a nitrocellulose supported motility immobilized using HMM. The blue and red curves represent the trace of leading and lagging end of this filament respectively.

It is seen that the perpendicular amplitude of a long actin filament sliding over bilayers is smaller than that of a short actin filament sliding over the HMM coated nitrocellulose surface.

For another comparison a short actin filament with a length of 2 μm is observed in the same way. The track of the filament is shown in figure 4.31. The video shows a very dynamic behavior of the short filament which seems quite different from that obtained from long filament. The perpendicular amplitude of this segment is nearly close to ~100% of its length. It remains in the lipid bilayer surface indicating it is held by the pre-coupled myosin. For this reason, the motion of short filaments is a combination of the myosin powered sliding and the thermally driven diffusion.

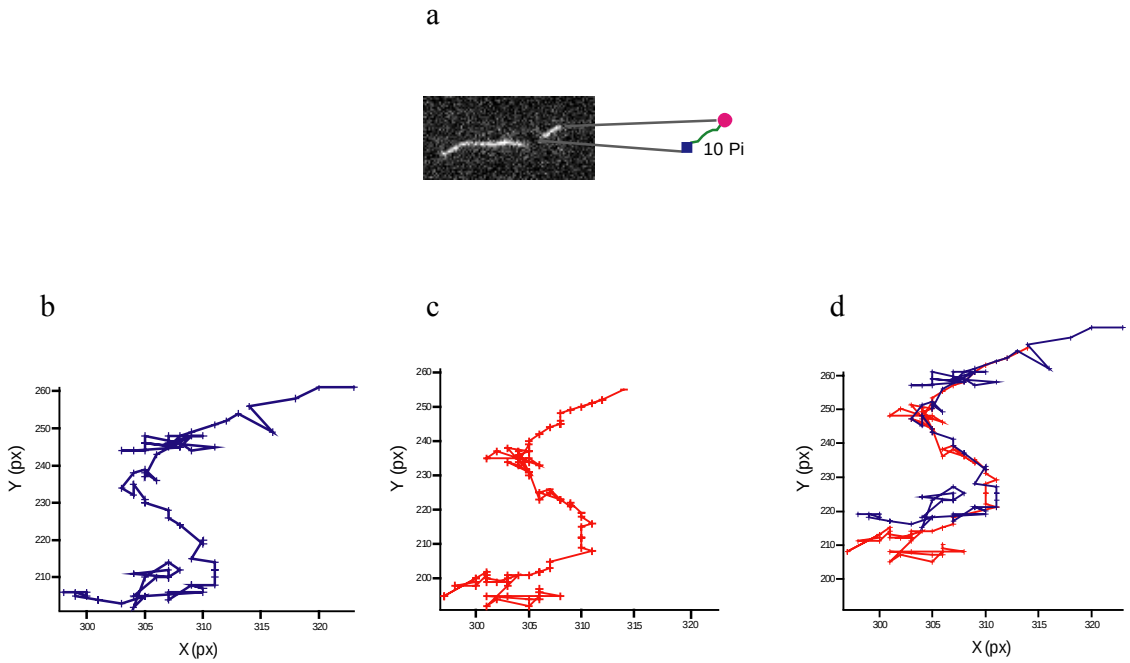

Figure 4.33: a) A short actin filament with a length of 2 μm is targeted. b). The track of the leading end (in blue) of the actin filament. c). The track of the trailing end (in red) of the filament. d) Both of the tracks of the leading and trailing ends are overlaid. Each of the position (Y, X) is extracted from the discrete digital picture at time interval of 200 ms.

4.3.3.4 Discussion of the effect of myosin diffusion in the motility assays

4.3.3.4.1 Diffusion theory

The diffusion constant for a particle in a free volume is described by the Stokes-Einstein formula:

$$D = \frac{kT}{6\pi\eta R}$$

Where D is the diffusion constant, *T* is the absolute temperature, *T* is the viscosity of the solution, k is the Boltzmann constant and R is the hydrodynamic radius of the particle. Because absolute temperature is usually constant, the most important factors underlying D are the size of a protein (or radius) and the viscosity of the medium within which it is diffusing. Membranes have a much higher viscosity than cytoplasm, so the lateral diffusion of a protein assembled within a membrane is considerably slower than that of a soluble protein, and this is reflected by a lower D value. When the viscosity is constant, the D value of a protein is mainly determined by its radius or size. For a soluble spherical protein, an eightfold increase in volume will lead to a twofold decrease in D. But this relationship does not hold for transmembrane/membrane binding proteins. Owing to the higher viscosity of membrane, the radius of the transmembrane segment dominates the D value of a membrane protein, whereas the aqueous portion usually does not significantly contribute to the D value.

Even though viscosity and size are key factors underlying the diffusion rate of a protein, other factors also have a role in determining protein diffusion rates inside cells. These include protein-protein interactions or binding to a matrix that might slow or immobilize a protein, and collisions with other molecules, which hinder free diffusion. Such factors often prevent proteins from diffusing at their theoretical limit.

In a summary, these deviations from predicted D include:

Increase in D

- Non-diffusive behavior such as flow-directed movement by motor proteins.
- Decrease in environment viscosity.

Decrease in D

- Formation of large aggregates or complexes (10-100-fold increase in molecule weight).
- Increase in environment viscosity.
- Transient interaction with large or fixed molecules, e.g. antibodies.

Though the diffusion constant of myosin V is limited by interaction with the prefixed antibody F_{ab} over the bilayers, the flexibility of the myosin molecule is compensated by the fluidity of lipid bilayers.

4.3.3.4.2 Explanation of the behavior of bead/myosin V complexes along the actin filament

The average run length of myosin V molecule along the actin filament depends on the ion strength (e.g. KCl, Mg^{2+}, et al). Recent studies on single Cy3-calmodulin labeled myosin V molecule show a mean run length of ~2.4 μm (~300 steps) at 150 mM KCl (Sakamoto et al., 2000).

The behavior of myosin decorated bead differs from that of labeled motor molecules by the much larger size as well as the different fluorescent labeling way. In our design, myosin V molecules are coupled to fluorescent beads via anti-myosin V antibody-protein A interaction. This lead to a strong reduction of the diffusion constant of myosin V. We assume that coupling of myosin to the bead increases the stability of the motor while it is stepping along the actin track. As a consequence, the observed run length of myosin covered bead exceeded the reported value. In some case, the run length reach up to ~⩾30 μm (figure 4.17-18).

4.3.4 Motility assay supported by gold array based on silicon

4.3.4.1 Structure of a gold array

The conventional motility assay supported by a nitrocellulose-coated solid substrate provides a convenient platform for the experimental study of myosin motor activities. But it also raises the likely modification of the motor activity by the non-specific binding to nitrocellulose. Due to various unspecific binding forces between the surface and target proteins (such as electrostatic or hydrophobic interaction) it is hard to control the density of active motors bound over the nitrocellulose surface. Therefore, the study of the actin filament sliding motion with a better defined motor density remains an important task . (Uyeda et al., 1990; Uyeda et al., 1991; Wang et al., 2000).

For this purpose we introduced a well-designed silicon supported array of nanometer - sized gold dots to generate a better controlled assay of immobilized myosin motors. These gold arrays were prepared in the laboratory of Prof. J.Spatz at the University of Heidelberg. To enable binding of only one motor molecule per dot the diameter of those gold dots was adjusted to 5nm .This is small compared to the size of myosin V (~90 nm), antibody (~10 nm), G-actin (~5 nm).

Moreover, the distance between discrete gold dots is adjusted to values much larger than the longest diameter of a single bound molecule. The overall distribution of gold dots is controlled by these parameters. Different arrays such as rings (figure 4.34) or a homogeneous dot pattern were generated. Obviously, by using the first strategy, a much smaller dot density could be obtained as by with homogenous dot distribution exhibiting the same spacing of dot.

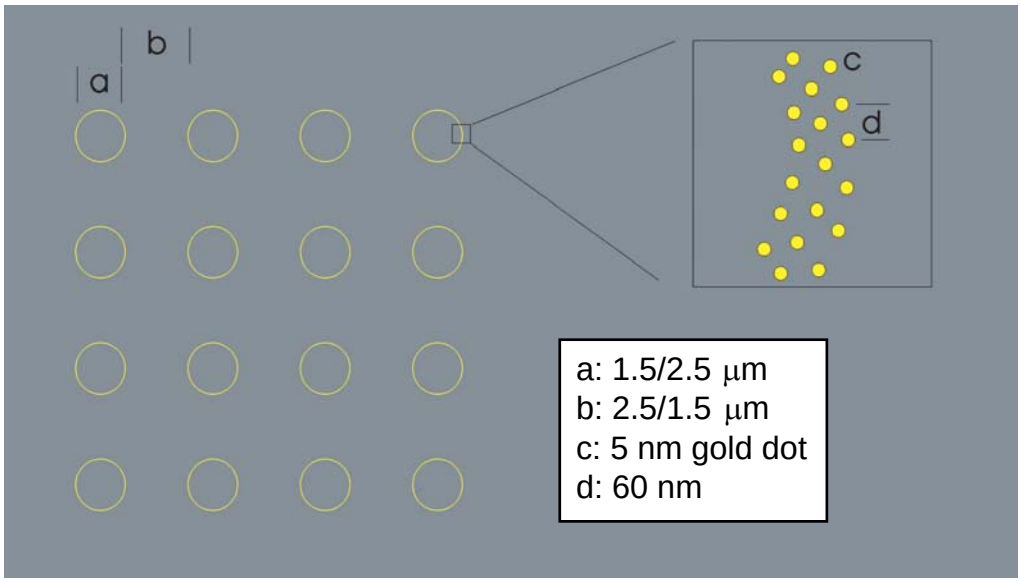

Figure 4.34: Schematic view of assay of 5 nm gold dot rings. a) the diameter of the gold dot ring; b) the space size between gold dot rings; c) the diameter of individual god dot; d) the distance between gold dots.

4.3.4.2 Specific activation of a gold array

The myosin V was coupled to the gold dots via anti-myosin antibodies-protein A. The binding of protein A is determined to be hydrophobic interaction and the specific interaction between thiolate group and gold (J. Gottschalck, 2002).

The distribution of the gold array could not be directly observed by optical microscopy. The observation of the gold dot array was done by means of AFM (atomic force microscopy) (figure 4.35).

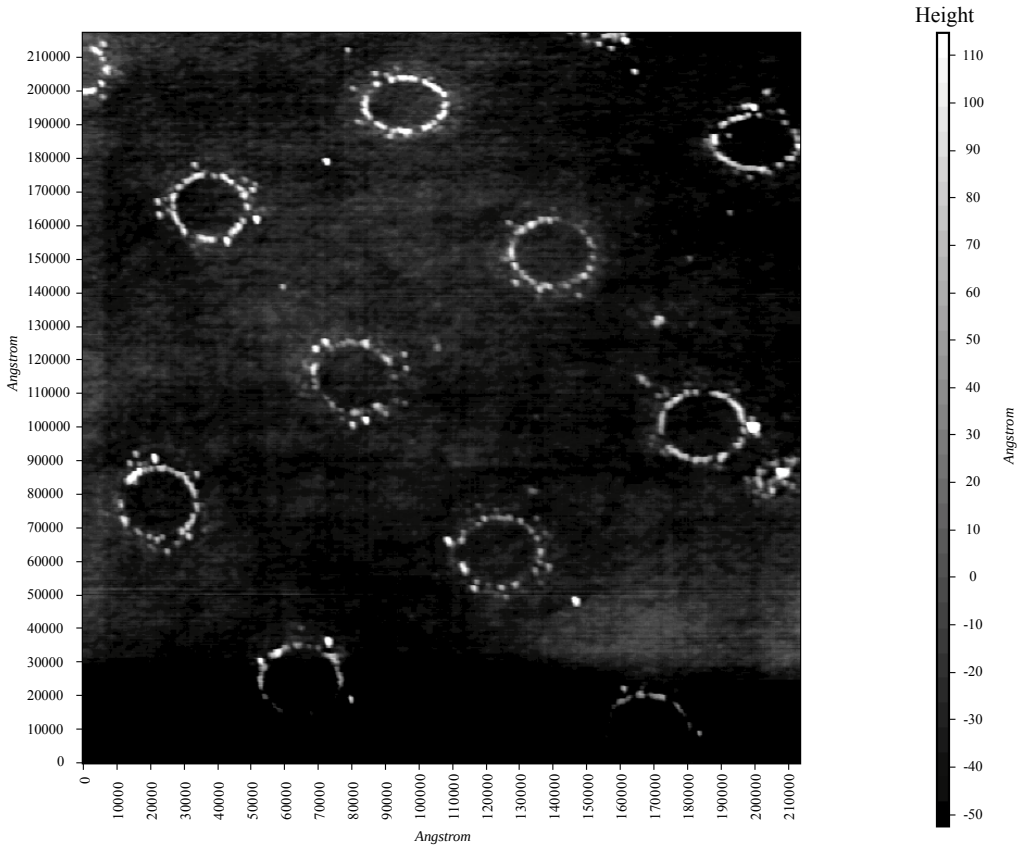

Figure 4.35: The gold dot array is illustrated by means of AFM. The height of the gold dots is indicated by a grayness gradient bar (right side).

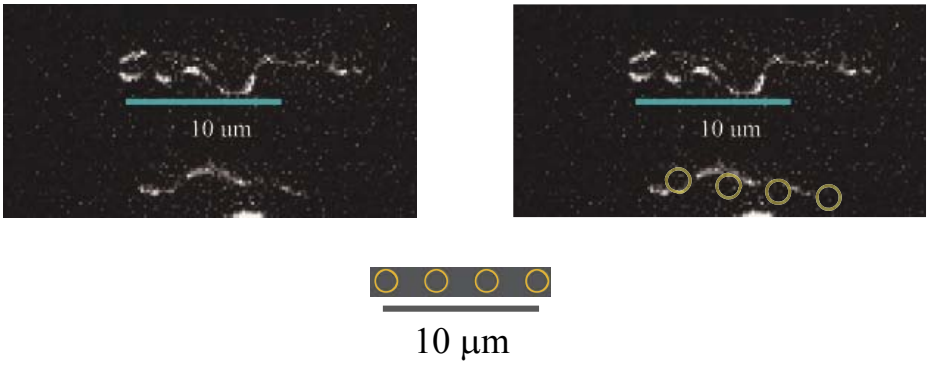

Figure 4.36: Fluorescent microscopic view of an actin filament bound to the gold dot ring (left). The fitting of gold dot array scheme to the actin filament shows that the distribution of the gold dots agrees with the quenching pattern.

The fluorescently labeled actin filaments are shown to bind over a gold array through the myosin covered beads. An interesting observation is that the actin filament seems to be fragmented into pieces. This, however, is due to the rhodamine labeling which stabilizes the actin filament in contact with gold for bleaching. The regular pattern of bleached sections along the filaments thus reveals the distribution of gold dots as shown in figure 4.34. After overlaying the fluorescent image and the image of the gold array, the dark sections and the circles fit well.

In the presence of ATP, these prefixed myosin V molecules are activated and actin filaments are found to be propelled to slide simultaneously, which is similar to that observed in motility assay performed on nitrocellulose. Characteristic differences are found which are summarized as follows:

1) Fragmentation of long actin filament by motor protein as in nitrocellulose based assay no longer occurs which might be due to the cooperative action of myosin V molecules. It could be due to fact that more motors are alive. On nitrocellulose more motors are in rigor state and fix filaments locally. This phenomenon is similar to that observed in fluid lipid bilayers supported motility assay but obviously bases on a different mechanism. Here the limited motor density more possibly accounts for such a difference.

2) The actin filament seems to be anchored by discrete sites. Between the binding sites, the filament demonstrates flexible motion similar to that of suspended filaments indicating those segments are partially free from the surface.

3) The sliding motion of actin filament driven by myosin V resembles those observations of single motor supported motility assays on a nitrocellulose surface. That means the major fraction of the actin filament slides over some fixed sites without dissociation. Also the motion is affected by the adjacent sites; therefore the track of actin filament sometimes could not overlap exactly. By comparing such tracks of an actin filament, the possible binding sites, or the distribution of motor protein could be determined (figure 4.37).

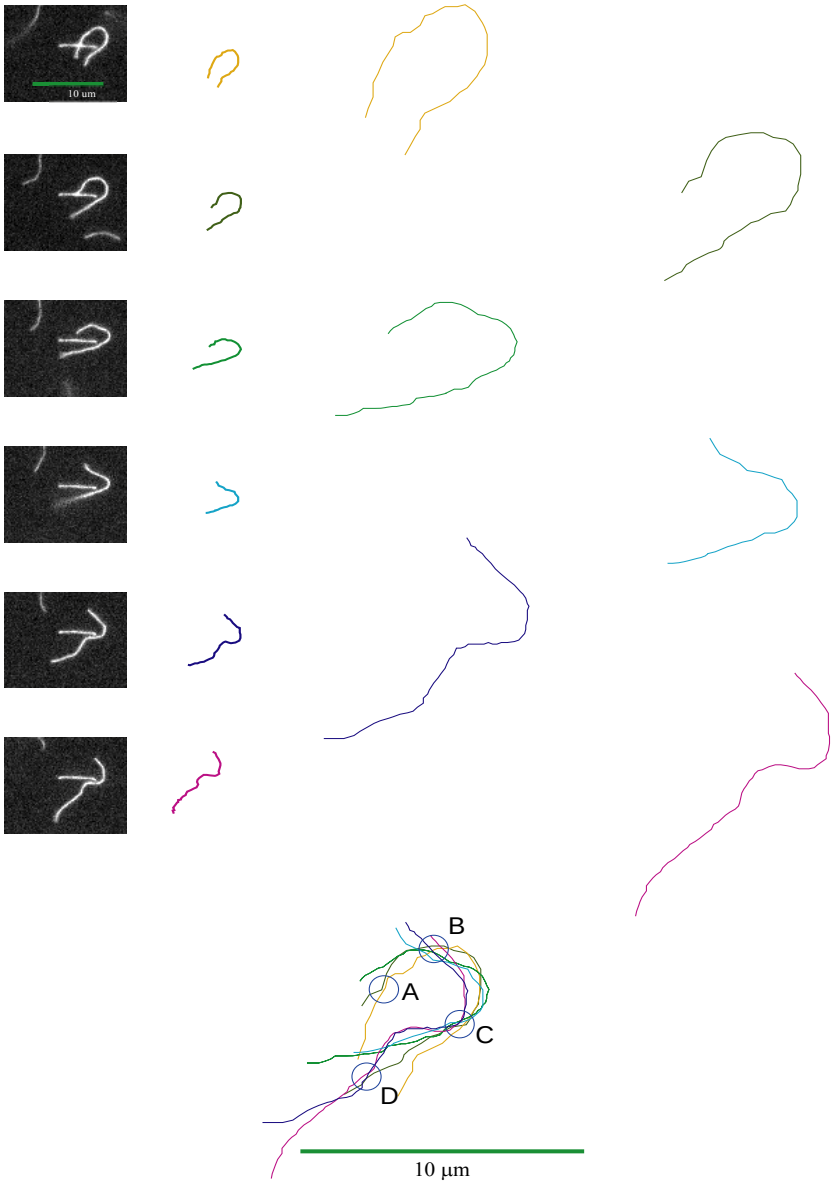

Figure 4.37: Overlaying of actin filament curves reveals the crossing points which indicate the possible sites of motor binding.

As shown in figure 4.35, an actin filament with a length of ~13 µm slides over a gold dot array. Despite of the simular behavior as in the assay on nitrocellulose, this new setup

allows us to relate the actin motion to the motor density. From the previous experiments done over myosin/BSA passivated surface, e.g. nitrocellulose, Triton X-100 et al, the motor density could only be calibrated indirectly (Howard J., 1989; Mehta et al., 1999a). The inaccuracy of estimation of motor density is a problem in understanding the distinct behavior of processive and nonprocessive motor proteins.

One difference between myosin II/HMM, and myosin V is that the threshold concentration required to support motility is much lowers. For myosin V, it could support actin filament sliding at a motor density varying from 1000 to 0.05 molecule/μm^2 (Mehta et al., 1999a), whereas it require at least ~23 myosin II molecule/μm^2. Another unexpected phenomenon is that myosin V could generate faster actin sliding velocity at 2.7 molecule/μm^2 than they did at 54 molecule/μm^2 (Moore et al., 2000). This shows that the motor density controls the motion in a very complex way. Since the motor densities in the experiments mentioned above are estimated, it is difficult to relate velocity to density. The gold-dot here is expected to the technique that provides a technique that makes a way out of this difficulty.

4.3.4.3 Motion analysis:

From the conventional motility assay supported by myosin V, the actin filament sliding shows unsmooth motion which could be interpreted in term of binding/unbinding equilibrium. By comparing the tracks of actin filaments, it is possible to detect these binding sites. We name this technique overlaying technique.

The motion of the actin sliding over the gold dot array is a mixture consisting of thermally exited and of myosin driven motion. By overlying the curves extracted from the track of actin filament, the binding sites represented by stationary points are detected, as shown in figure 4.35. The possible binding sites during the sliding are marked with A-D.
A-D demonstrates the major possible actin binding sites. The sliding motion is basically driven by myosin V molecules located at sites A-D.

4.3.4.4 Discussion of surface activation of gold array

From our experience, a disadvantage of gold arrays is that the evaluation of the efficiency of activation is difficult to measure. We implement fluorescent microscopy for this evaluation. However, a quick method is still expected to check the activation. Moreover, though the gold array could be reused for several times if it is recovered by plasma washing, it becomes useless after incubating with assay buffer that contains substrates consisting of –SH group. Due to this limit, treating a gold array with protein ligand still require much experiences. A possible solution is to store the functionalized gold array, e.g. with antibodies in compact.

In most of our experiments the incubation of the substrate occurs at a protein concentration of 500 µg/ml (for antibody and protein A). We expect that this saturates the gold surface after an incubation time of 12 hours at 4°C. Rinsing after incubation is routinely performed to ensure that the excess ligand is removed.

4.4 Track changing test and theory

4.4.1 Formation of well-defined actin filaments crossed

During the observation by the cargo transport assay, track changing events are frequently found. In some cases several myosin V coated beads are found to change the track one after another (figure 4.18), indicating that these beads react the same way when they encounter a barrier such as an actin filament. They are not able to move along the old filaments. This phenomenon is interesting for at least two reasons. First we want to investigate if the angle formed by the two filaments or by a single actin filament crossing itself could affect the track changing. Second we want to specify the relative position of the crossed filaments and bead complexes. Those behaviors might reflect the internal conformation change of myosin V molecule when performing its steps.

Up to now, myosin V is believed to perform steps in a hand-over-hand style (Figure 2.6). The trailing head detaches from the actin filament swapping over to the next binding site

which is ~72 nm from the initial position. The length of the myosin V head combined with the neck domain is estimated to be ~23 nm (Walker et al., 2000) with a diameter of ~6 nm (deduced form electron microscopy, figure 3.1c) while the diameter of an actin filament is ~6-8 nm. Judged from this consideration, myosin V could step over a crossed actin filament.

The distance between the myosin binding sites along the actin axis is ~2.5 nm (Rayment, I., 1993). If a myosin V molecule moves along a filament close to another actin filament the behavior depends upon whether the next binding site is on the same or the crossing filament. At this point the size of the head is an important factor and plays a role as well.

If the molecule has to step over a barrier of diameter of an actin filament, it has to find an optimal binding site to make a step. Considering the variability of the step width between 11-15 actin subunits, the distance between the barrier axis and the leading head is allowed to lie within ~0-24 nm.

To study the behavior of myosin coated bead upon confronting actin crossing, two layers of actin filament were bound to a nitrocellulose coated cover glass via NEM-HMM. One layer of actin filaments was labeled by rhodamine (TRITC), another layer labeled by FITC. Since the bead was also labeled by TRITC, the observation was performed at the extinction wave length of TRITC. In our experiment, the FITC labeled actin filament was always added after the TRITC labeled one. The following procedure was applied:

The flow cell was constructed by using a nitrocellulose coated cover glass, and then NEM-HMM was deposited to provide support sites for actin filament. Rhodamine-phalloidin labeled actin filaments were then applied in the flow cell. It was important to avoid breaking of the filament because the longer the filament were the larger chance was for the filament from the second layer to contact those from the first layer by crossing. The binding of the filament was monitored by FM to adjust the density of the filament to ~50% of the value used for the myosin coated bead motility assay. The excess filaments

were washed away by rinsing with assay buffer. To increase the probability of crossing of filaments it was appropriate to bind a higher density of the FITC labeled actin filament.

The extinction wave length of rhodamine was 550 nm and for FITC it is 405 nm. The two filaments could be observed by two different optical filters. Under the extinction with wave length of 550nm fluorescent FITC was invisible. Under the wave length of 405 nm, the rhodamine labeled filament was weakly visible. However the short wave length is unfavorable due to the accompanying rapid photo bleaching. The suspension of myosin coated bead suspension was injected into the chamber. After incubation for 5 minutes with the coating surface facing downward the excess beads were washed away from the flow cell by rinsing. The myosin coated beads could bind to both layers of actin filaments labeled by different dyes. By excitation with 550 nm, both the bead complex and the rhodamine labeled actin filaments were visible while filaments labeled by FITC was invisible. Wave length of 405 nm was used to observe FITC filament. But the myosin coated beads were invisible under this condition. The motion was always observed at 550 nm extinction. After the addition of ATP, the myosin coated beads moved simultaneously along the actin filament. The actin filament crossing was detected in two ways. One way was to determine the crossing by combining in the pictures observed by excitation with both wave lengths. But in this case many images did not exhibit a bead. Another way was to record first the motion of the beads and then record the tracks. By comparing the track of the bead with fluorescence images of filaments, it was possible to find out if the bead got through the actin filament crossing or not. In our experiment, we applied the second method that was to record the motion of individual beads and then chose the one performing track changing.

4.4.2 Track changing test with myosin V coated bead

Rhodamine labeled actin yields sharper images than the FITC labeled filament. Moreover, the longer wave length favors the photo stability of the dye. FITC labeled actin filament undergoes a faster bleaching (perhaps due to the shorter extinction wave-length) even in presence of oxygen scavengers (Glucose 2.3 mg/ml, Glucose Oxidase 1.8 mg/ml,

Catalase 0.018 mg/ml).The above described track changing by beads can be divided into two groups. The first group of beads moves along the same layer of actin filament; either in the lower or in the upper layer as shown in figure 4.23. Actin filament could form loops by self crossing and thus generate filament crossing points. The second group of beads changes the filament of different F-actin layers. In this case one can observe track change from the lower layer to the upper layer or in the reverse order.

Owing to the optimized condition of myosin V coated bead binding to the immobilized actin filaments, most of the beads bound specifically to the actin filament. After addition of ATP (1 mM), most of the beads started to move simultaneously. The percentage varies from test to test, normally it was >90%. The motions are then recorded and analyzed.

The track changing events are then collected and sorted according to the above classification. In Figure 4.38, the motion of the moving beads from a lower layer to an upper layer is shown. Closer inspection shows that the track changing events are a reproducible phenomenon. In the case of figure 4.39 one can see a myosin V coated bead that fails to step over an actin filament crossing the filament on which it moves.

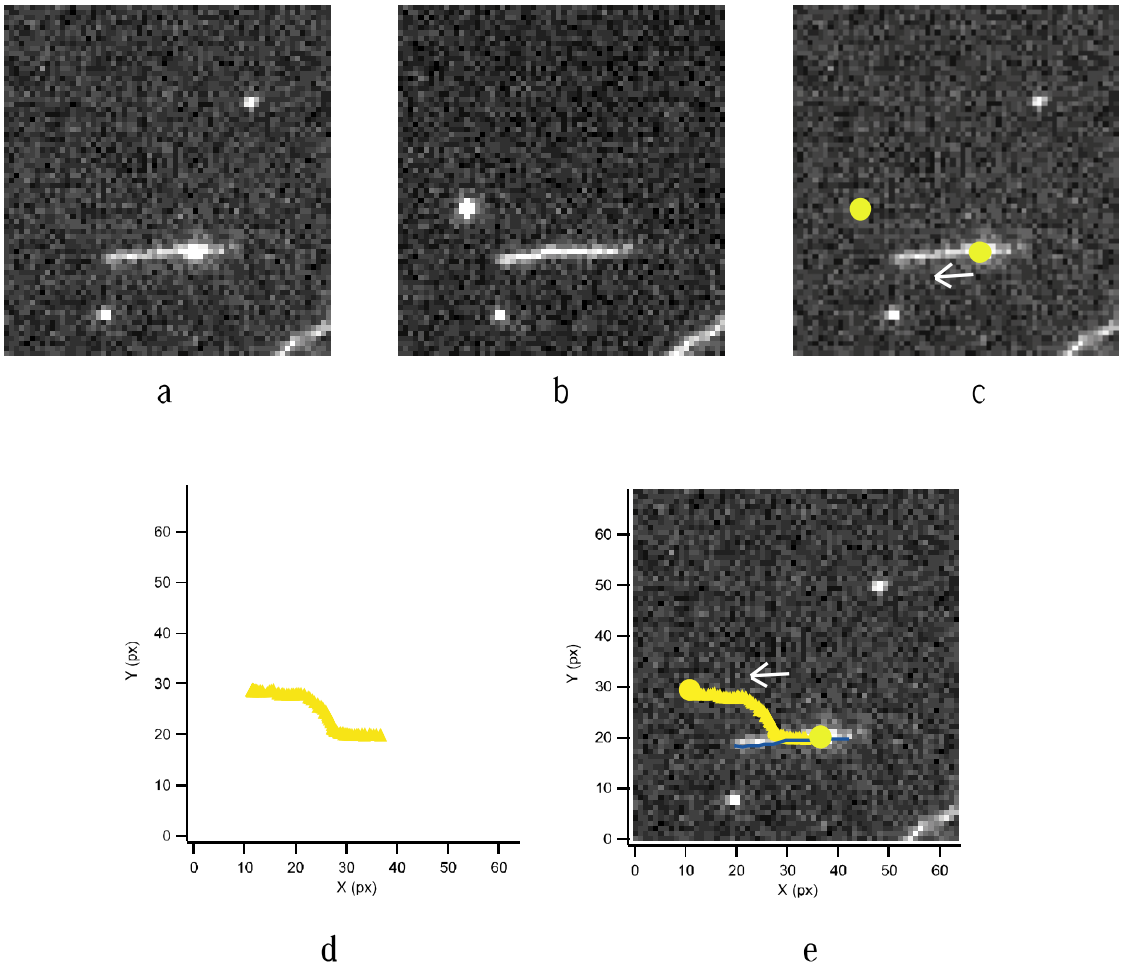

Figure 4.38: A myosin V coated bead moves along an actin filament and then changes its track (a-c). Only the filament labeled by rhodamine-phalloidin is visible while FITC labeled ones can not be seen by excitation with 550 nm. a) A myosin coated bead binds to the lower actin filament while in b), it has moved to the invisible filament in the upper layer. The motion of the bead was recorded and analyzed and the track is presended schematically in d. Fig e shows a superposition of the schematic track with the fluorescence image.

Myosin V carrying two beads was tested by means of optical tweezers (M. Yusuf Ali, 2002). It was shown that myosin does not walk exactly straight forward was but rotates slightly about the helical actin filament. This observation suggested that myosin V can easily contact actin filament lying in a lower layer. The present test was possible by

observing a large number of motor molecules changing to the track of a filament laying below the original track.

In figure 4.39, a typical actin filament crossing is illustrated showing a myosin V coated bead binding to the upper filament. The bead's motion was analyzed and the complete trajectory was superimposed on the fluorescent image recorded. Inspection of the pathway of the bead and the image of actin filament lying at the lower layer show that the bead moved over the crossing without being disturbed by the lower filament.

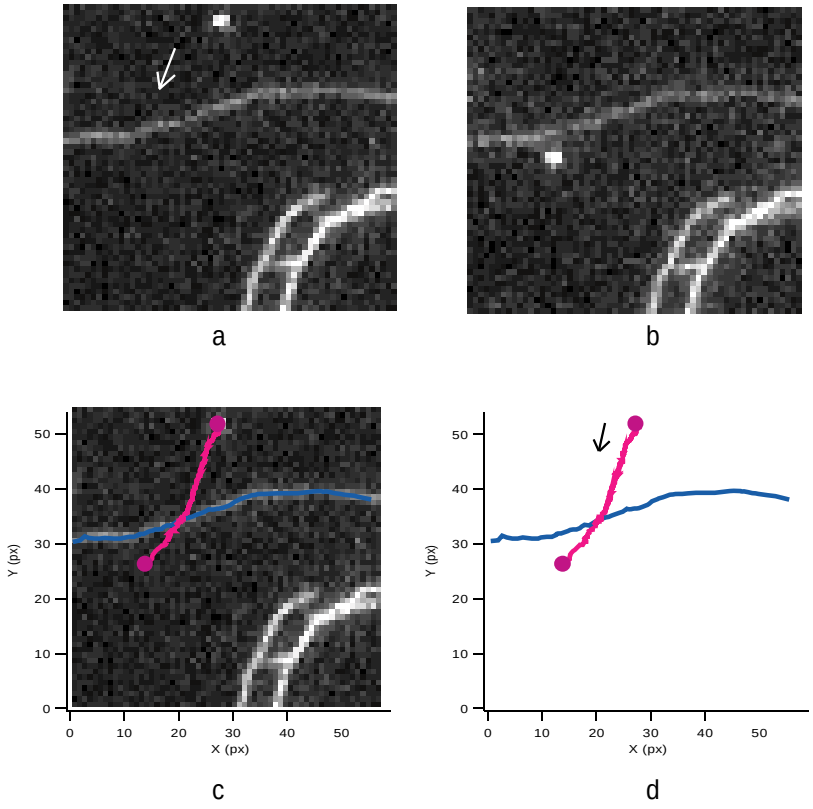

Figure 4.39: A myosin V coated bead moves along actin filament and a location where two actin filaments cross. In picture a, a myosin coated bead was shown binding to actin filament labeled by FITC. After the addition of ATP, the bead complex moves along the filament and crossed another actin filament that was labeled by Rhodamine-Phalloidin and was located at a lower layer (picture b). The motion of the bead was recorded,

analyzed and then superimposed on the original picture (picture c). The results show that the bead moves over the actin crossing without a problem.

Judged from this result a rotation of the myosin coated bead is not associated with the transport. In the earlier motility assay with myosin-bead as transporter, long transport distances have been observed on the NEM-HMM supported actin filament. If the rotation was necessary, the bead is expected to touch the NEM-HMM or the nitrocellulose surface which is likely to jeopardize or quench the movement. In this case the long transport distance would become nearly impossible.

In this test, the track changing was not observed which may be due to the small number of events studied or due to the fact that the lower actin was out of the reach of the myosin V molecule. On the other side, when the bead complex was attached on a lower actin filament, it was difficult for the myosin to bypass the crossing filament in order to continue its motion along the original filament. It shows that the new binding sites on the other actin filament should be close to the pathway of the actin binding site domain.

Information on the change of the conformation of myosin V was recently obtained through crystal structure studies by X-ray diffraction (Pierre-Damien Coureux1**,** 2003). The work shows how the subdomains of one head domain behave in responding to actin binding. The interface of myosin V and actin filament was estimated to be 1000 $Å^2$ or a circle area with radius of 2.5-3 nm, at the transition state and increases to 2000 $Å^2$ in a rigor state (Data from the result of myosin II; Pierre-Damien Coureux1**,** 2003). Compared with the step size of myosin V which is ~72 nm, this is a relatively small area. This comparison indicates a possible important role of the way the head domains behave during the motion. It is still not clear what happens between the stepping and binding of myosin V molecule. The pathway of the trailing head remains an interesting question.

An earlier study showed that the power stroke of myosin V consists of two phases (Claudia Viegel, 2002): the direct stroke generates a displacement of ~22 nm and the second phase is determined by diffusion. However, this result was obtained by optical

tweezers and does not seem to explain the behavior of an individual head which undergoes a 72 nm step during single catalytical cycle. The pathway of a head domain is schematically shown in figure 4.40.

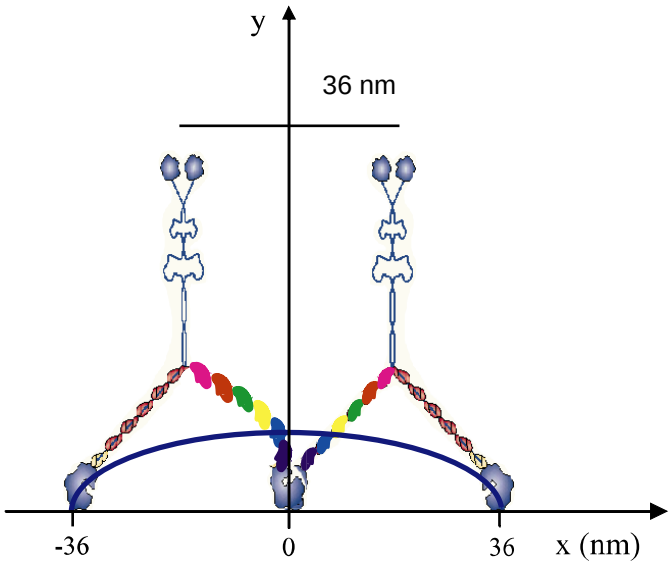

Figure 4.40: Schematic illustration of the stepping of a myosin V molecule.

In this schematic image several results are combined:
Firstly, electron microscopy (EM) shows the siding of the leading head domain which generates strain; secondly, the release of the trailing head is shown which swings to the next actin binding site. During this process the head domain undergoes a displacement of 72 nm while the tail domain or any cargo bound to the tail domain moves 36 nm.

In the image the two-headed binding state is taken as reference. The plane formed by the actin filament and myosin V contains the y direction and the horizontal axis X direction- the axis of actin filament.

Three parameters are introduced: h stands for the height of the pathway of the lagging head domain; α refer to the angle formed by the line linking the pathway of the trailing

head to current binding point and z axis. The distance between the trailing head and the leading heads is referred to r.

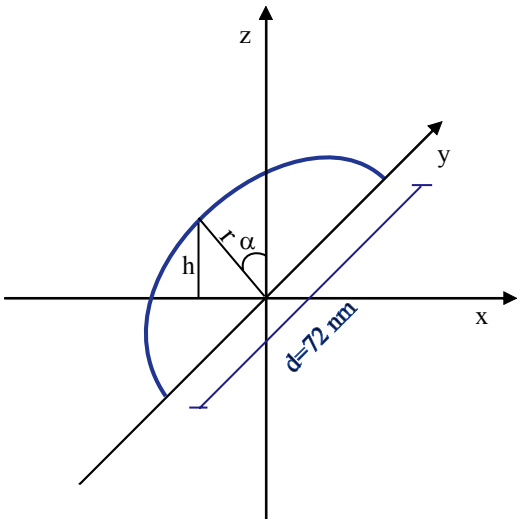

Figure 4.41: analysis of the pathway of the head domain of myosin V molecule.

Because the rod-like shape of the crossed filament, if the myosin V molecule conquers the actin filament barrier lying ahead of the leading head, it has to fit this condition: h>6 nm (the diameter of the actin filament). If h<6 nm, the lagging head domain would contact the crossed filament which also contains myosin V binding sites. Wether the head domain binds to the crossed filament or not, it would be disturbed in finding the subsequent binding site on the original filament. From most of the recorded track changing events, the bead complexes seem to move slower at the crossed point perhaps due to the blocking. As the result, a bead complex has to dwell longer on the original track.

Conclution

Myosin V is a processive motor molecule as has been found recently. In this work various techniques of biophysics together with biochemical techniques were applied to study the interaction between myosin V and actin.

Chicken brain myosin V was prepared from tissue and then its integrity and activity tested by SDS-PAGE, motility assays and an ATPase assay especially adapted to this purpose. Polyclonal anti-myosin V antibodies were prepared from rabbits. Subsequently anti-myosin V mouse monoclonal antibodies were prepared aiming at providing higher specifity. Five monoclonal antibodies producing hybridchamos were chosen out and characterized. The antibody binding site on the myosin V molecule was determinated by selective proteolysis and western-blotting. In the cases of monoclonal antibody no. 4 and 5, their binding sites on myosin V were determinated to locate between residues 1136 – 1472 which is part of the tail domain of myosin V molecule.

The ATPase assay makes use of an ATP recovery reaction system for continuously ATPase activity determination. The ATP turn over rate of myosin V was measured to be ~7 ATP/head.s^{-1} under steady state condition.

Fluid lipid bilayer was constructed to mimic the in vivo environment for myosin V. Myosin V was immobilized on the surface of lipid bilayers via F_{ab} fragment prepared from monoclonal anti-myosin antibodies. The sliding motion of actin filament over fluid lipid bilayer differed from that observed in conventional motility assay. These differences comprised: a) improved stability of long actin filaments (>10 μm); b) higher flexibility of short actin filaments (<2 μm). These results indicate that the fluidity of bilayer provided higher flexibility to myosin V bound to the surface.

To study the sliding motion of F-actin over a well-defined myosin density, a gold dot array based on silicon was introduced. The well-defined density of gold dots in the array allows the actin filament to be bound by myosin controlled in regulary spaced and at a number of molecule. By analyzing the sliding motion of the actin filament the binding sites of actin filaments during the sliding were determinated.

To test the myosin molecule as a transporter, a 40 nm fluorescent polystyrene bead coated with myosin V was used in motility assay. In this study, actin filaments were used

as tracks for myosin V coated beads. Under a favorable ratios of myosin V, antibodies, protein A and beads was made possible to observe bead movement supported by single myosin V motor. It provides direct evaluation from microscopic observation. The velocity of the bead was determinated to be ~0.3 μm/s. In the motility test, beads coated with myosin V were observed to perform 'track-changing' when encountering an actin filament crossing point. To clarify this phenomenon crossed actin filaments were set up in a defined order to test the behaviors of beads coated with myosin V. The results showed: a) a bead changed tracks from the lower actin filament to an upper one at the crossing point; b) if a bead coated with myosin moved along an upper filament it did not change its track. These results indicate apossible intermediate stepping state of the myosin V which did not allow the molecule to step over a crossing actin filament.

Outlook:

Instead of several speculations about future development of motor protein research I would like to suggest a few experiments that could clarify open questions:

1. For a deeper understanding of structure/function relations, it is necessary to determinate the antibody epitopes on the myosin V molecular surface. Two alternative techniques, mass spectroscopy and scanning atomic force microscopy could be applied.

(a) After the selective proteolysis of myosin V the fragments could be assayed by western blotting. The peptides are then tested by mass spectroscopy and sequenced by the first 5 amino acids. From the accurate molecular weight and the sequence the fragment could be located.

(b) Scanning atomic force microscopy (AFM) provides the possibility to test the antibody binding site under conditions where the myosin V molecule is kept intact. Considerring the molecular size of myosin V which is ~ 6 × 90 (diameter × length in nm) and that of antibody ~ 5 × 4 × 9 (in nm), it is possible to map the antibody molecule bound to a

myosin V. Compared with the above method AFM requires much less sample and provides the binding information in real environment.

2. For the artificial barrier test an alternative barrier – NEM-S1 domain derived from HMM could be used. Compared with previous actin filament barrier this NEM-S1 domain has the following advantages: a) it binds directly to the same actin filament where myosin V binds. b) the NEM-S1 domain (~6 nm in diameter) is almost the thickness of an actin filament (7-8 nm) that is smaller than the myosin V head domain (~23 nm in length) but larger than G-actin (~4 nm in diameter). c) the NEM-S1 domain is globular so that the blocking is only affected by its size. d) this domain does not contain any myosin V binding sites as actin filament does.

This blocking test could be performed by means of the motility assay based on a gold dot array. It can be performed as follows. The actin filament used for motility assay is decorated with NEM-S1. In the motility assay, the actin filament sliding rate was motor density dependent but weakly. Previous study has shown that under saturating ATP concentration, the actin filament velocity was ~300 nm/s at myosin V densities from 1000 moleules/μm^2 to 2.7 molecules/μm^2 or even less. There are at least two possible roles for NEM-S1 in this experiment. One should be simply to just occupy the myosin binding site on the actin filament which should result in an effect as if the myosin density was relatively decreased. The other possibility would be that if the NEM-S1 was an unconquerable barrier, the filament should be either shredded or released so that the processive propelling was stopped.

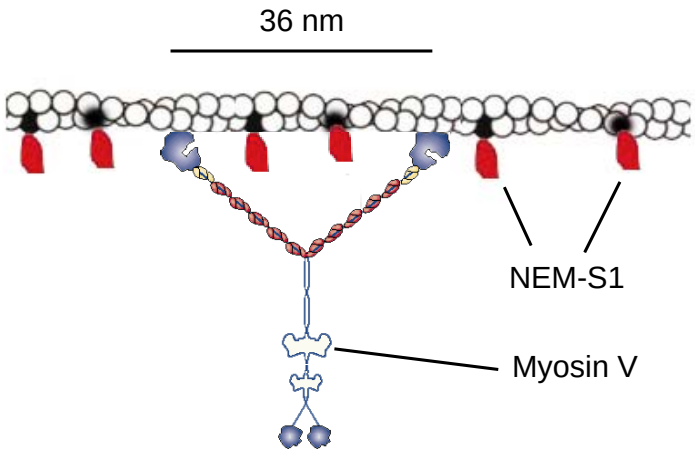

Figure 4.42: Schematic illustration of a single myosin V molecule walking along an actin filament decorated by barriers (NEM-S1).

This barrier test is expected to provide more information about the intermediate conformation change of the myosin V molecule.

References

Ahmet Yildiz, Joseph N. Forkey, Sean A. McKinney, Taekjip Ha, Yale E. Goldman, Paul R. Selvin. (2003) Myosin V Walks Hand-Over-Hand: Single Fluorophore Imaging with 1.5-nm Localization. *Science* 300, 2061-2065

Anson, M., Geeves, M. A., Kurzawa, S. E. and Manstein, D. J. (1996). Myosin motors with artificial lever arms. *EMBO J.* **15**, 6069-6074.

Arn, E.A. and Macdonald, P.M. (1998). Motors driving mRNA localization: new insights from in vivo imaging. *Cell* **95**, 151-154.

Bagshaw, C.R. (1993) Muscle Contraction. 2nd edition Chapman & Hall, London & New York, 155 pp.3520.

Block, S. M., Goldstein, L. S. and Schnapp, B. J. (1990). Bead movement by single kinesin molecules studied with optical tweezers. *Nature* **348**, 348352.

Brown, S. S. (1997) Myosins in yeast. *Curr.Opin.Cell Biol.* **9**, 44-48.

Burgess, S., Walker, M., Schmitz, S., Wang, F., Seller, J. R., Knight, P. J. and Trinick, J. (2001). Direct visualization of gross conformational changes in the heads of myosin V between different nucleotide states. *Biophys. J.* **80**, 341a

Charles L. Asbury, Adrian N. Fehr, and Steven M. Block Kinesin Moves by an Asymmetric Hand-Over-Hand Mechanism. *Science* Published online December 4 2003.

Cheney, R. E., O'Shea, M. K., Heuser, J. E., Coelho, M. V., Wolenski, J. S., Espreafico, E. M., Forscher, P., Larson, R. E. and Mooseker, M. S. (1993). Brain myosin-V is a two-headed unconventional myosin with motor activity. *Cell* **75**, 13-23.

Cheney, R. E. (1998). Purification and assay of myosin-V. *Methods Enzymol*. **298**, 3-18.

Chung, J., Hua, W. and Gelles, J. (2001). Evidence against the kinesin symmetric hand-over-hand model. (2001). *Biophys. J*. **80**, 570a.

Claudia Veigel1, Fei Wang2, Marc L. Bartoo1, James R. Sellers2 and Justin E. Molloy1. (2001). The gated gait of the processive molecular motor, myosin V. *nature cell biology* 4. 59-65

Conibear, P. B. and Geeves, M. A. (1998). Cooperativity between the two heads of rabbit skeletal muscle heavy meromyosin in binding to actin. *Biophys. J*. **75**, 926-937.

Corrie, J. E. T., Brandmeier, B. D., Ferguson, R. E., Trentham, D. R., Kendrick-Jones, J., Hopkins, S. C., Van der Heide, U. A., Goldman, Y. E., Sabido-David, C., Dale, R. E., Criddle, S. and Irving, M. (1999). Dynamic measurement of myosin light-chain-domain tilt and twist in muscle contraction. *Nature* **200**, 425-430.

Coy, D. L., Wagenbach, M. and Howard, J. (1999a). Kinesin takes one 8nm step for each ATP that it hydrolyzes. *J. Biol. Chem*. **274**, 3667-3671.

Coy, D. L., Hancock, W. O., Wagenbach, M. and Howard, J. (1999b). Kinesin's tail domain is an inhibitory regulator of the motor domain. *Nat. Cell Biol.* **1**, 288-292.

Crevel, I., Carter, N., Schliwa, M. and Cross, R. (1999). Coupled chemical and mechanical reaction steps in a processive Neurospora kinesin. *EMBO J.* **18**, 5863-5872.

De La Cruz, E. M., Wells, A. L., Rosenfeld, S. S., Ostap, E. M. and Sweeney, H. L. (1999). The kinetic mechanism of myosin V. *Proc. Natl. Acad. Sci. USA* **96**, 13726-13731.

De La Cruz, E. M., Wells, A. L., Sweeney, H. L. and Ostap, E. M. (2000a). Actin and light chain isoform dependence of myosin V kinetics. *Biochemistry* **39**, 14196-14202.

De La Cruz, E. M., Sweeney, H. L. and Ostap, E. M. (2000b). ADP inhibition of myosin V ATPase activity. *Biophys. J.* **79**, 1524-1529.

Dominguez, R., Freyzon, Y., Trybus, K. M. and Cohen, C. (1998). Crystal structure of a vertebrate smooth muscle myosin motor domain and its complex with the essential light chain: visualization of the pre-power stroke state. *Cell* **94**, 559-571.

Egelman, E. H. and DeRosier, D. J. (1992). Image analysis shows that variations in actin crossover spacings are random, not compensatory. *Biophys. J.* **63**, 1299-1305.

Ellis, R. J. (2001). Macromolecular crowding: an important but neglected aspect of the intracellular environment. *Curr. Opin. Struct. Biol.* **11**, 114119.

Espindola, F. S., Suter, D. M., Partata, L. B., Cao, T., Wolenski, J. S., Cheney, R. E., King, S. M. and Mooseker, M. S. (2000). The light chain composition of chicken brain myosin-Va: calmodulin, myosin-II essential light chains, and 8-kDa dynein light chain/PIN. *Cell Motil. Cytoskel.* **47**, 269-281.

Espreafico, E. M., Cheney, R. E., Matteoli, M., Nascimento, A. A., De Camilli, P. V., Larson, R. E. and Mooseker, M. S. (1992). Primary structure and cellular localization of chicken brain myosin-V (p190), an unconventional myosin with calmodulin light chains. *J. Cell Biol.* **119**, 1541-1557.

Evans, L. L., Lee, A. J., Bridgman, P. C. and Mooseker, M. S. (1998). Vesicle-associated brain myosin-V can be activated to catalyze actin-based transport. *J. Cell Sci.* **111**, 2055-2066.

Finer, J. T., Simmons, R. M. and Spudich, J. A. (1994). Single myosin molecule mechanics: piconewton forces and nanometre steps. *Nature* **368**, 113-119.

Friedman D. S. and Vale, R. D. (1999). Single-molecule analysis of kinesin motility reveals regulation by the cargo-binding tail domain. *Nat. Cell Biol.* **1**, 293-297.

Hancock, W. O. and Howard, J. (1998). Processivity of the motor protein kinesin requires two heads. *J. Cell Biol*. **140**, 1395-1405.

William O. Hancock and Howard, J. (1999). Kinesin's processivity results from mechanical and chemical coordination between the ATP hydrolysis cycles of the two motor domains. *Proc. Natl. Acad. Sci. USA* **23**, 13147-13152.

Hibberd, M. G. and Trentham, D. R. (1986). Relationships between chemical and mechanical events during muscular contraction. *Annu. Rev. Biophys. Chem*. **15**, 119-161.

Homma, K., Saito, J., Ikege, R. and Ikege, M. (2000). Ca^{2+}-dependent regulation of the motor activity of myosin V. *J. Biol. Chem*. **275**, 3476634771.

Howard, J. (1997). Molecular motors: structural adaptations to cellular functions. *Nature* **389**, 561-567.

Hua, W., Young, E. C., Fleming, M. L. and Gelles, J. (1997). Coupling of kinesin steps to ATP hydrolysis. *Nature* **388**, 390-393.

Hua, W., Chung, J and Gelles, J. (2001). Kinesin does not rotate during stepping. *Biophys. J*. **80**, 512a.

Huang, J. D., Brady, S. T., Richards, B. W., Stenoien, D., Resau, J. H., Copeland, N. G. and Jenkins, N. A. (1999). Direct interaction of microtubule- and actin-based transport motors. *Nature* **397**, 267-270.

Hunt, A. J. and Howard, J. (1993). Kinesin swivels to permit microtubule movement in any direction. *Proc. Natl. Acad. Sci. USA* **90**, 11653-11657.

Hunt, A. J., Gittes, F. and Howard, J. (1994). The force exerted by a single kinesin molecule against a viscous load. *Biophys. J*. 67, 766-781.

Howard, J., Hudspeth, A. J. & Vale, R. D. Movement of microtubules by single kinesin molecules. *Nature* 342, 154-158 (1989).

Ito, K., Liu, X., Katayama, E. and Uyeda, T. Q. (1999). Cooperativity between two heads of dictyostelium myosin II in in vitro motility and ATP hydrolysis. *Biophys. J.* **76**, 985-992.

Jontes, J. D., Milligan, R. A., Pollard, T. D. and Ostep, E. M. (1997). Kinetic characterization of brush border myosin-I ATPase. *Proc. Natl. Acad. Sci. USA* **94**, 14332-14337.

J. Käs, H. Stey, J.X. Tang, D. Finger, R. Ezzel, E. Sackmann, P.A. Janmey, *Biophys. J*. **70**, 602-625 (1996).

J. Gottschalck and B. Hammer, *J. Chem. Phys*. 116, 784 (2002).

Joseph N. Forkey, Margot E. Quinlan, M. Alexander Shaw, John E. T. Corrie & Yale E. Goldman. (2003) Three-dimensional structural dynamics of myosin V by single-molecule fluorescence polarization. *Nature* 422. 399-405

Kitamura, K., Tokunaga, M., Iwane, A. H. and Yanagida, T. (1999). A single myosin head moves along an actin filament with regular steps of 5.3 nanometres. *Nature* **397**, 129-134.

Kron, S. J. and Spudich, J. A. (1986). Fluorescent actin filaments move on

myosin fixed to a glass surface. *Proc. Natl. Acad. Sci. USA* **83**, 6272-6276.

Kuo, S. C. and Sheetz, M. P. (1993). Force of single kinesin molecules measured with optical tweezers. *Science* **260**, 232-234.

Lang, M. F., Asbury, C. L., Shaevitz, J. W. and Block, S. M. (2001). A 2D force clamp for kinesin with fluorescence capability. *Biophys. J.* **80**, 571a.

Margossian S.S. and Lowey S.(1982) Preparation of myosin and its subfragments from rabbit skeletal muscle. *Meth. Enzym*., 85 (Pt B) 55-72

Mehta, A. D., Rock, R. S., Rief, M., Spudich, J. A., Mooseker, M. S. and Cheney, R. E. (1999a). Myosin-V is a processive actin-based motor. *Nature* **400**, 590-593.

Mehta, A. D., Rief, M., Spudich, J. A., Smith, D. A. and Simmons, R. M. (1999b). Single-molecule biomechanics with optical methods. *Science* **283**, 1689-1695.

Mermall, V., Post, P. L. and Mooseker, M. S. (1998). Unconventional myosins in cell movement, membrane traffic and signal transduction. *Science* **279**, 527-533.

M. Yusuf Ali, Sotaro Uemura, Kengo Adachi, Hiroyasu Itoh, Kazuhiko Kinosita Jr.' & Shin'ichi Ishiwata. (2002) Myosin V is a left-handed spiral motor on the right-handed actin helix**.** *Nature structural biology* **9:** 464 – 467.

Moore, J. R., Krementsova, E., Trybus, K. M. and Warshaw, D. M. (2000). Myosin V exhibits a high duty cycle and large unitary displacement at zero load. *Biophys. J*. **78**, 272a.

Nascimento, A. A. C., Cheney, R. E., Tauhata, S. B. F., Larson, R. E. and Mooseker, M. S. (1996). Enzymatic characterization and functional domain mapping of brain myosin-V. *J. Biol. Chem*. **271**, 17561-17569.

Pastural E, Barrat FJ, Dufourcq-Lagelouse R, Certain S, Sanal O, Jabado N, Seger R, Griscelli C, Fischer A, de Saint Basile G (1997) Griscelli disease maps to chromosome 15q21 and is associated with mutations in the myosin-Va gene. *Nat. Genet*. **16**: 289-292.

Pierre-Damien Coureux1, Amber L. Wells2, Julie Me´ne´ trey1, Christopher M. Yengo2, Carl A. Morris2, H. Lee Sweeney2 & Anne Houdusse1. (2003). A structural state of the myosin V motor without bound nucleotide. *Nature* 425, 419-427

Rayment, I. et al. Structure of the actin-myosin complex and its implications for muscle contraction. *Science* 261, 58–61 (1993).

Reck-Peterson, S. L., Novick, P. J. and Mooseker, M. S. (1999). The tail of a yeast class V myosin, myo2p, functions as a localization domain. *Mol*. *Biol*. *Cell* **10**, 1001-1017.

Reck-Peterson, S. L., Tyska, M. J., Novick, P. J. and Mooseker, M. S. (2000b). The yeast class V myosins, Myo2p and Myo4p, are non-processive actin-based motors. *Mol. Biol. Cell* **11**, 373a.

Ronald D. Vale1 and Ronald A. Milligan. (2000)The Way Things Move: Looking Under the Hood of Molecular Motor Proteins. *Science* 288. 88-95

Rice, S., Lin, A. W., Safer, D., Hart, C. L., Naber, N., Carragher, B. O., Cain, S. M., Pechatnikova, E., Wilson-Kubalek, E. M., Whittaker, M. et al. (1999). A structural change in the kinesin motor protein that drives motility. *Nature* **402**, 778-784.

Rief, M., Rock, R. S., Mehta, A. D., Mooseker, M. S., Cheney, R. E. and Spudich, J. A. (2000). Myosin V stepping kinetics: a molecular model for processivity. *Proc*. *Natl*. *Acad*. *Sci*. *USA* **97**, 9482-9486.

Rock, R. S., Rief, M., Mehta, A. D. and Spudich, J. A. (2000). In vitro assays of processive myosin motors. *Methods Enzymol*.

Spudich, J. A. (1994). How molecular motors work. *Nature* **372**, 515-518.

Spudich, J. A. (2001). The myosin swinging cross-bridge model *Nature Reviews Molecular Cell Biology* **2** 387-392

Schilling J., Ph.D thesis 2003

Uyeda, T. Q., Kron, S. J. and Spudich, J. A. (1990). Myosin step size estimation from slow sliding movement of actin over low densities of heavy meromyosin. *J. Mol. Biol.* **214**, 699-710.

Uyeda, T. Q., Warrick, H. M., Kron, S. J. and Spudich, J. A. (1991). Quantized velocities at low myosin densities in an in vitro motility assay. *Nature* **352**, 307-311.

Vale, R. D. and Milligan, R. A. (2000). The way things move: looking under the hood of molecular motor proteins. *Science* **288**, 88-95.

Visscher, K. and Block, S. M. (1998). Versatile optical traps with fedback control. *Methods Enzymol*. **298**, 460-489.

Visscher, K., Schnitzer, M. J. and Block, S. M. (1999). Single kinesin molecules studied with a molecular force clamp. *Nature* **400**, 184-189.

Wang, F., Chen, L., Arcucci, O., Harvey, E. V., Bowers, B., Xu, Y., Hammer, J. A., III and Sellers, J. R. (2000). Effect of ADP and ionic strength on the kinetic and motile properties of recombinant mouse myosin V. *J. Biol. Chem.* **275**, 4329-4335.

Wu X, Bowers B, Wei Q, Kocher B, Hammer JA 3rd (1997) Myosin V associates with melanosomes in mouse melanocytes: evidence that myosin V is an organelle motor. *J Cell Sci* **110**: 847-59.

Acknowledgement

The first I want to express my thanks to **Prof. Erich Sackmann** for this opportunity of my Ph.D study and supervisory. And thanks to **Prof**. **Matthias Rief** for giving me chance doing some work in his interesting GFP project and being my examinator. The help from **Michael Bärmann** in discussion and revising my thesis is appreciated very much. Many thanks to the cooperation partners **Prof. Kaspers, Markus Fischer** in the myosin project and Prof. **Andreas Bausch** for valuable discussions. The help in preparation of materials used in this work from Frau **Kirpal**, **Monika**, **Claudia**, **Karin** and **Gabi** are very helpful and appreciated. Thanks to the former coworkers **Manfred Keller, Jörg Schilling Alex Roth**, **Jörg Uhde** and **Rainer Tharmann** for their cooperation and discussions. Great help from the postdoc including Dr. **Khenya, Laurent Vonna**, **Laurent Limozin** are also much appreciated. It was nice time for me to spend some time with the new E22 members from Matthias group: **Anabel**,**Hendrik Dientz**, **Michael Schlierf** for their great help either in cooperation, discussion and many other aspects. The last I want to express my appreciation specially to my Chinese friends-Miss **Zheng Yi**, Dr. **Shi Wei** who strongly supported me in the past years.